TÉCNICO LISBOA

Modelling of Gas and Slurry Phase Polyolefin Production: The importance of thermodynamics

Duarte Morais Cecílio

Thesis to obtain the Master of Science Degree in

Chemical Engineering

Supervisor(s): Prof. Maria do Rosário Gomes Ribeiro
Dr. Timothy F. L. McKenna
Prof. Carla Isabel Costa Pinheiro

Examination Committee

Chairperson: Prof. Carlos Manuel Faria de Barros Henriques
Supervisor: Prof. Maria do Rosário Gomes Ribeiro
Member of the Committee: Prof. Henrique Anibal Santos de Matos

October 2015

Dedicated to my family.

Acknowledgments

This thesis is the result of a five month experience working at the Laboratory for the Chemistry and Processes of Polymerization (LCPP) in Lyon. It was an extraordinary experience that allowed me to grow both as a professional and as a person. New challenges were faced, new relationships were forged and, for that, I have many people to thank.

First and foremost, I would like to thank Dr. Timothy F. L. McKenna, Professor Maria do Rosário Gomes Ribeiro and Professor Carla Isabel Costa Pinheiro, without whom this experience would not have been possible. Their support and guidance helped me develop a more focused work, with greater quality. It has been a pleasure working with such seasoned professionals.

I would also like to thank Mr. Muhammad Ahsan Bashir from the LCPP for helping me with my work and providing me with crucial thermodynamic data for the developed models. His guidance and opinions also proved invaluable to the result.

On another note, I would like to thank everyone at the LCPP, particularly Dr. Christophe Boisson, Mrs Nathalie Jouglard and Mr. Olivier Boyron for helping us ease into the laboratory and creating a friendly work environment. I would like to thank Mr. Mathieu Fuentes, Mr. Matthieu Humbert, Mr. Anderson Medeiros and Ms. Andreia Nunes for their friendship, helping me and my compatriots find a home away from home.

I would like to thank my compatriots as well, Ms. Ana Rita Cruz, Ms. Ana Rita Martins, Mr. André Pereira, Mr. Ricardo Luís and Mr. Rodolfo Ribeiro for the good moments that we spent together and a friendship forged that will not be forgotten.

On a more personal note, I would especially like to thank Ms. Rita Alves, whose support, companionship and love made me arrive where I am today. You have been with me since the beginning, pushing me, helping me and driving me to improve myself as a professional and as a person. You have helped me with my work. You have been my best friend and my girlfriend. I would not be where I am without you.

I would also like to thank Ms. Ana Rita, Mr. Diogo Pedro, Mr. Pedro Rio, Mr. Renato Wong and Mr. Ricardo Marques for their invaluable friendship over the years.

Last, but not least, I would like to thank my family. My father Fernando, my mother Leonor and my grandparents Lúcia, Manuela, Manuel and Rui. Their education, their support and their love made me who I am today and none of this would be possible were it not for them.

Resumo

Esta tese estuda o efeito do *swelling* de um polímero na produção de polietileno. O trabalho incluiu o desenvolvimento de dois modelos diferentes. O primeiro calcula a Distribuição de Tamanho de Partículas (PSD) de polietileno produzido em fase de lama e estuda o impacto do *swelling* do polímero na PSD. O segundo descreve o funcionamento de um reactor em fase gasosa em modo seco e investiga o efeito da adição de um alcano inerte, no inchaço do polímero e na produção de polietileno.

O primeiro modelo desenvolvido prevê a PSD do polietileno produzido num processo de n CSTRs. As simulações realizadas calculam a PSD do polímero que sai do segundo reactor e analisam a influência do tamanho de catalisador e tipo de diluente. Os resultados mostram que o tipo de diluente influencia muito a concentração do monómero e o swelling do polímero.

Na segunda parte do trabalho, estuda-se o processo de produção de polietileno em reactores de leito fluidizado operados em modo seco. O modelo prevê a produção de polietileno em estado estacionário e as condições de funcionamento do reactor. A concentração de etileno no centro ativo é determinada utilizando o equação de Sanchez-Lacombe. O modelo é validado com dados da Patente US 6864332 B2. Para a mesma pressão parcial a adição de n-hexano conduz a uma maior produção comparativamente ao isobutano. Contudo, em virtude da possibilidade de adicionar maiores quantidades de isobutano mantendo o modo de operação seca, este diluente permite atingir valores produção global superiores.

Palavras-chave: Distribuição de Tamanho de Partícula, Inchaço de Polímero, Produção de Polietileno em fase gasosa, Modelação de Reactor FBR, Solubilidade de Etileno, Modo Seco

Abstract

This thesis studies the effect of polymer swelling in polyethylene production by slurry and gas-phase processes.

The work comprises the development of two different models. The first one calculates the Particle Size Distribution (PSD) of polyethylene produced in slurry phase, and studies the impact of polymer swelling on the corresponding PSD. The second model describes the operation of a gas-phase HDPE reactor in dry mode and investigates the influence of the addition of an inert alkane, on polymer swelling and on HDPE production.

The first developed model predicts the PSD of a polyethylene for a reactor train of n CSTRs. The simulations performed calculate the PSD of the polymer exiting the 2nd reactor. Parameters like, catalyst size and diluent type were analyzed. From the results it is possible to conclude that diluent type greatly affects monomer concentration and therefore polymer swelling.

In the second part of the work, a gas-phase polyethylene process is studied in dry mode operated fluidized bed reactors. The developed model predicts the steady-state polyethylene production and the reactor operating conditions. Effective ethylene concentrations near the catalyst active sites were predicted using the Sanchez-Lacombe EOS thermodynamic model.

The model was validated with data gathered from Patent US 6864332 B2. From the results it is possible to conclude that, for the same partial pressure, adding n-hexane yields higher productions over adding isobutane. However, component vapor pressure indicates that it is possible to add greater quantities of isobutane while maintaining dry mode operation, thus achieving higher overall productions.

Keywords: Polyethylene PSD, Diluent, Polymer swelling, Gas-phase Polyethylene Production, FBR Reactor Modelling, Ethylene Solubility, Dry Mode

Contents

List of Tables

List of Figures

Nomenclature

Greek symbols

α	Combined kinetic parameter.
Δ	Expresses variation.
ρ	Density.
τ	Average residence time in the reactor.
ε	Porosity.

Roman symbols

A	Heat transfer area.
b	Reactor cross section area.
$\overline{C_p}$	Component heat capacity at constant pressure.
C	Concentration.
$Conversion$	Monomer conversion per pass.
D, d	Diameter.
E	Energy.
$E(t)$	Residence Time Distribution.
F	Total gaseous inlet molar flowrate.
$F(D_p)$	Numerical Particle Size Distribution.
H	Enthalpy.
h	Convective heat transfer coefficient.
k	kinetic rate constant.
$[M]$	Monomer concentration at the active sites.
M	Molar Mass.

m Average monomer concentration over all co-monomers.

N Number of particles.

n Number of CSTR reactors in the battery;number of moles.

P Pressure.

$Productivity$ Catalyst productivity.

Q Component mass flowrate.

R Perfect Gas Constant.

R_p Rate of polymerization.

T Temperature.

t Polymerization time.

u Superficial velocity.

V Volume.

Subscripts

a Activation.

b Refers to the bulk phase in the reactor.

bed, b Refers to the catalyst/polymer bed.

c Refers to the catalyst or catalyst particle.

d Dissolved in the polymer phase; catalyst deactivation.

Et Ethylene.

g Refers to the gas-phase.

hex Refers to n-hexane.

$ibut, isobut$ Refers to isobutane.

ICA Inert Alkane.

in Entering the reactor.

N_2 Nitrogen.

out Exiting the reactor.

p Refers to the polymer particle.

PE Polyethylene.

pol Refers to the polymer.

$polym$ Polymerization.

ref Reference.

s Refers to the solids in the reactor.

v Volumetric.

Superscripts

0 Initial condition.

i Reactor position in the battery.

P Refers to the polymer phase.

$\star$ Concerns the catalyst active sites.

Glossary

CSTR	Continuous Stirred Tank Reactor
EOS	Equation of State
FBR	Fluidized Bed Reactor
HDPE	High Density Polyethylene
ICA	Inert/Induced Condensing Agent
LDPE	Low Density Polyethylene
LLDPE	Linear Low Density Polyethylene
MGM	Multigrain Model
MWD	Molecular Weight Distribution
MW	Molecular Weight
PC-SAFT	Perturbed Chain Statistical Association Fluid Theory
PSD	Particle Size Distribution
RTD	Residence Time Distribution
SAFT	Statistical Association Fluid Theory
SPM	Single Particle Model
UHMWPE	Ultra High Molecular Weight Polyethylene
ULMWPE	Ultra Low Molecular Weight Polyethylene
VLMWPE	Very Low Molecular Weight Polyethylene
XLPE	Cross-Linked Polyethylene

Chapter 0

Thesis Outline

This thesis is divided into the following chapters: **Introduction**, **Literature Review**, **Model Implementation**, **Results** and **Conclusions**.

The **Introduction** contains some general information about polyethylene, such as a brief description of the main types of polyethylene, their properties and applications. A short overview of polyethylene integrated in the polyolefin industry will also be mentioned, including a short-term prediction of demand and production. Afterwards the objective of the thesis will also be clarified. The **Literature Review** chapter will provide the necessary context for the reader to be able to understand the subjects that serve as base for the development of the two models presented in this thesis. In accordance with the rest of the work, this chapter will be divided into 3 sections:

- The first will contain a common background, describing the general processes for the industrial production of polyethylene.
- The second will focus on specific background for the slurry phase model. It will contain a detailed explanation of the slurry phase LLDPE production process and the parameters that affect the particle size distribution of a polymer.
- The third and final part will focus on considerations necessary for the development of the gas phase reactor model. This will include a description of the *Sanchez-Lacombe* equation of state to obtain co-solubility predictions of a given induced condensing agent/inert alkane on ethylene/ICA/polyethylene ternary systems.

The chapter **Model Implementation** will be divided into two subchapters, each one pertaining to the developed models. Each subchapter will explain the development of the respective model, with particular emphasis on the assumptions taken into account (and their justifications) and the necessary equations. The following chapter, **Results** will be divided according to the previous one and will include not only the results obtained from the models but also a sensitivity analysis, so as to determine which are the parameters that influence the result to a greater degree. The sensitivity analysis parameters will be chosen according to the objectives of the work.

The final chapter, **Conclusions** will contain the main conclusions to be taken out of the studies conducted and suggestions on further improvements regarding both models.

Chapter 1

Introduction

1.1 Quick Overview on Polyethylene

1.1.1 Polyethylene Molecular Structure

In the family of polyolefins, polyethylene is one of its most important members. In its simplest form it consists of a long backbone with an even number of carbon atoms (covalently linked) and two hydrogen atoms attached to each carbon, ending in methyl groups [1].

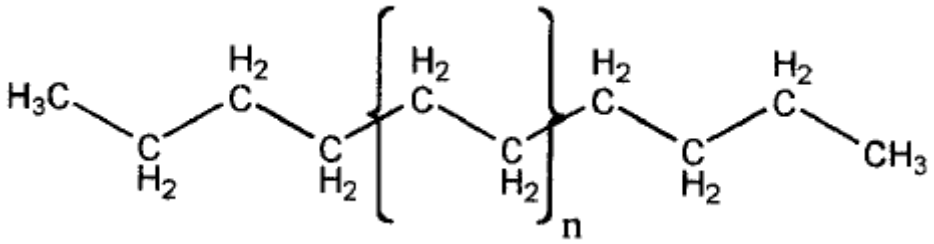

Figure 1.1: Chemical structure of pure polyethylene (adapted from [1]).

Chemically pure polyethylene resins present the chemical formula $C_{2n}H_{4n+2}$, where n is the degree of polymerization. As opposed to conventional organic materials, polyethylene consists of molecules of different sizes (and occasionally composition), wherein the degree of polymerization can vary and go as high as 250000. This means that its molecular weight varies from 1400 to 3500000 grams per mole or more, which means that the resulting polymer presents a particle size distribution (PSD). Some degree of branching and unsaturation can also be observed in the polymer molecules [1].

1.1.2 Different Types of Polyethylene

Different types of polyethylene exist. While they retain essentially the same backbone, the variations arise from branching that modifies the nature of the polymer. There are different types of branches, such as alkyl groups or ester (only for free radical processes) functional groups. Variations in polyethylene

structure can also arise - albeit less frequently - from defects in the backbone. Such defects are typically vinyl groups, which often end the growing polymer chain.

While in solid state, branches and defects in the polymer structure change the polymer's crystallinity. Chains with fewer defects present higher crystallinity, and vice-versa. A polyethylene sample that presents 0% crystallinity is referred to as amorphous.

With changing crystallinity there is an important aspect to mention: chain packing. Samples with higher crystallinity present better packing than samples with lower crystallinity. As such, polymer density increases with crystallinity.

Polyethylene is divided into different categories:

By **density**:

- High Density Polyethylene (HDPE)
- Low Density Polyethylene (LDPE)
- Linear Low Density Polyethylene (LLDPE)

By **molecular weight**:

- Very/Ultra Low Molecular Weight Polyethylene (VLMWPE/ULMWPE)
- Ultra High Molecular Weight Polyethylene (UHMWPE)

And by **composition/structure**:

- Ethylene-Vinyl Ester Copolymers
- Ionomers
- Cross-Linked Polyethylene (XLPE)

High Density, Low Density and Linear Low Density Polyethylenes

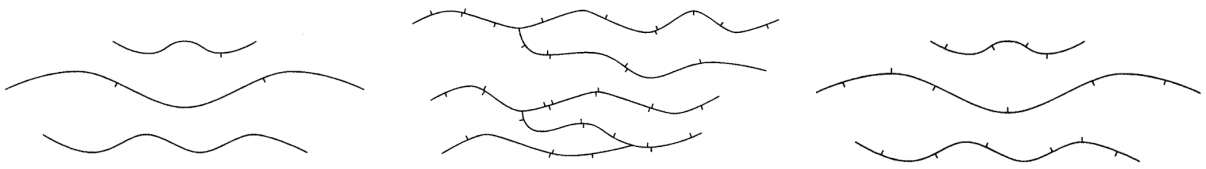

(a) Schematic representation of HDPE (b) Schematic representation of LDPE (c) Schematic representation of LLDPE

Figure 1.2: Schematic representation of HDPE, LDPE and LLDPE [1].

High Density Polyethylene is made of highly linear unbranched molecules and minimal defects in the backbone. HDPE consists of highly crystalline samples with higher densities, when comparing to other types of polyethylene. Some resins of this type are copolymerized with small concentrations of 1-alkenes, in order to reduce the crystallinity. Density can vary between 0.94 g/cm^3 and 0.97 g/cm^3 [1].

As opposed to HDPE, **Low Density Polyethylene** is so named due to its very low crystallinity. The low crystallinity is caused by the high concentration of branching. Branches are mainly ethyl and butyl groups, but there is also a significant number of long chain branches. These hinder the crystallization process, resulting in lower densities and defining the rheological properties of the final polymer. Due to the high pressure processes by which LDPE is produced, the ethyl and butyl groups are clustered together in the molecule, while the long chain branches can present some branching themselves. Density varies typically between 0.90 g/cm^3 and 0.94 g/cm^3 [1].

Linear Low Density Polyethylene resins are obtained through the copolymerization of ethylene with 1-alkenes. The result is a long linear backbone with short alkyl groups attached at random intervals, wherein the most commonly present branches are ethyl, butyl or hexyl groups. LLDPE can also present small ammounts of long chain branching, although its complexity is considerably simpler than in LDPE. The branches somewhat hinder crystallization, as in the previous case, but these resins can be thought of as a compromise between high density and low density polyethylenes. Its density range is 0.90 - 0.94 g/cm^3 [1].

The following table summarizes the characteristics of these three main types of polyethylene, as well as their applications:

Table 1.1: Comparison of the properties and applications of different Polyethylenes [2].

Compound	Density (g/cm^3)	Properties	Applications
HDPE	0.94-0.97	90% + Crystallinity Strong and more rigid than LDPE Easily extruded or pressed Resists abrasion/corrosion	Food/Chemical Containers Chemical resistant piping systems Wood plastic composites Insulation and extrusion coating
LDPE	0.90-0.94	50 - 60% Crystallinity More flexible than HDPE High degree of LCB Retains toughness over a wide temperature range	Food packaging (films) Molded laboratory equipment Disposable thermoformed products Corrosion resistant work surfaces
LLDPE	0.90-0.94	Small degree of LCB Better tear/impact film resistance than LDPE High degree of SCB Retains shape	Food packaging (films) Rotomolding of toys and tanks Heavy-duty shipping sacks Thin-wall lids

1.1.3 Polyethylene Worldwide

Polyethylene is the most widely produced polymer in the world. The following figure 1.3 illustrates the demand for each main type of polyethylene in 2012, out of a total commodity polymer demand of 211 Million tonnes:

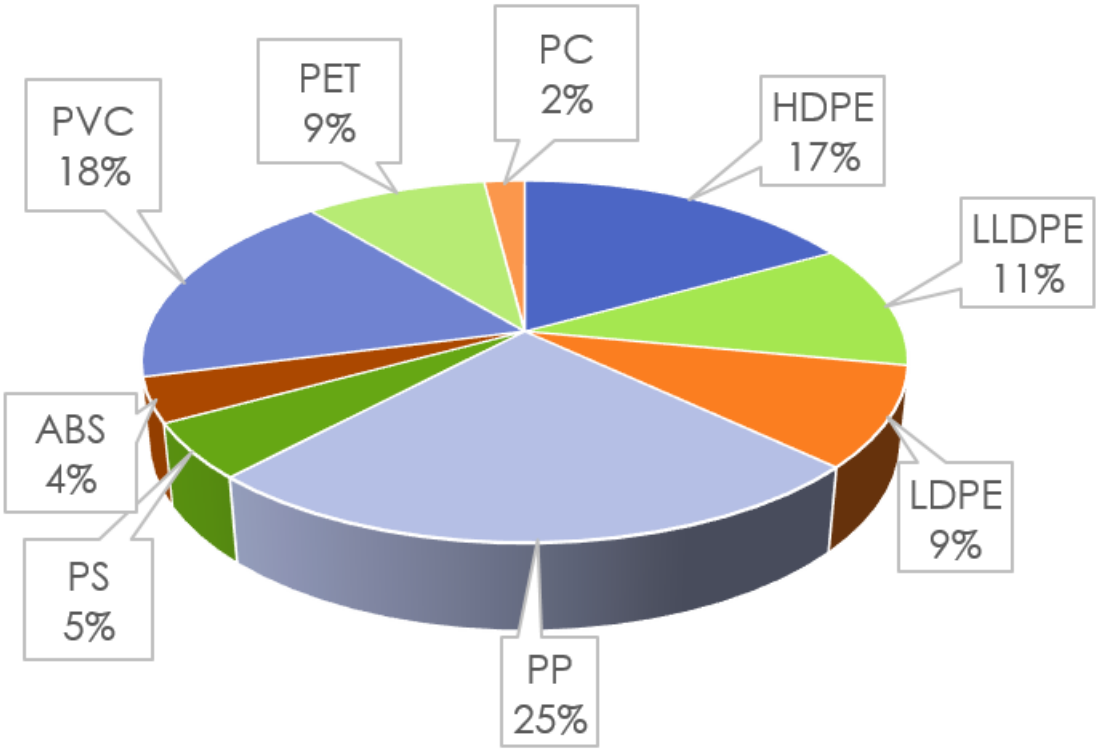

Figure 1.3: Total worldwide polymer demand in 2012. Plot was made in *Microsoft Excel*® and the data was extracted from IHS (adapted from [3]).

Figure 1.3 shows that polyethylene is the most demanded polymer in the world with a significant 37% of total polymer demand (78 million tonnes). After this is polypropylene with 25%. As such, the weight of polyethylene in the global polymer industry is evident, its research and continuous advancement are of paramount importance for the success of this industry as well as the creation of a more sustainable environment, resulting from the development of cleaner and more energy-efficient industrial polymerization processes.

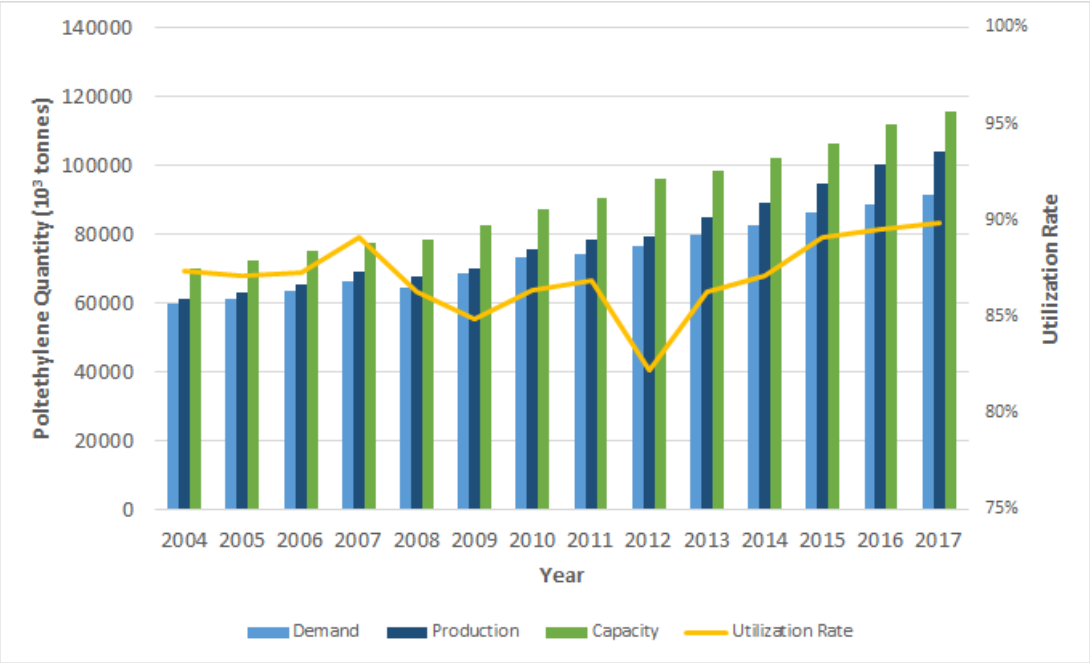

Figure 1.4: Global Polyethylene plant utilization rate predictions from the year 2004 to the year 2017. Plot was made in *Microsoft Excel*® and the data was extracted from (adapted from [4]).

From figure 1.4, predictions indicate that global polyethylene demand will at least increase until 2017, without signs of slowing down. As such, it is necessary for the installed capacity (worldwide) to be able to satisfy this growing demand. These predictions indicate that the global installed capacity will also grow accordingly and with production values estimated for each year, global utilization rate for polyethylene plants can also be estimated. In summary, significant growth is expected for demand, production and capacity and the utilization rate is expected to remain fairly constant [4].

1.2 Motivation

All the subjects presented in this last section highlight the importance of polyethylene as a commodity in the modern world. It is part of a high volume market and a major part of the polymer industry. Since the available predictions point to an undisputed growth of the demand for this product, further development is of the utmost interest.

It is in such context that this work comes into light.

Chapter 2

Literature Review

It is not possible to discuss polyolefin production reactors without first discussing the existing processes. Since there are so many different polymers each with its own molecular weight distribution, composition and even branching distributions, it is clear that a wide range of polymerization conditions and different types of catalyst are used to tune these differences in the polymers. In other words a great number of polymerization processes and reactors exist.

The reactor has a strong connection with the chosen catalyst in such a way that developments achieved in one of these aspects often spur the need for developments in the other. The output of polymerization processes has been drastically increased since the beginning, in the 1960s. Values have changed from 80 ktonnes per year to 750 ktonnes per year in modern plants. The changes from the earliest process design are mostly in terms of operation efficiency, higher throughput and lower capital investments [5].

2.1 General Information on Industrial Polyethylene Processes

While LDPE is an important polymer and form of polyethylene, it is produced through free radical processes. However, since the main interests of the work developed focus on Ziegler-Natta/metallocenes heterogeneous catalysis systems, such processes as the free radical process will not be described.

The catalytic polymerization of olefins can be achieved by different processes, depending on the continuous medium phase in the reactor. These processes are: **solution**, **slurry** or **gas-phase**.

In **solution** processes both the catalyst and polymer are soluble in the reaction medium. They are used to produce commercial EPDM rubbers (EPDM stands for Ethylene Propylene Diene Monomers) and some polyethylene resins. The types of reactors used in these kinds of processes are usually **stirred autoclaves**, operating at temperatures in the range of **150-250° C**. However, solution processes will not be considered in this work.

Gas-phase and **slurry** reactors have one important similarity, which is that the polymer is formed around heterogeneous catalyst particles. **Slurry** processes are subdivided into **diluent** and **bulk**. In the **diluent** slurry processes a liquid heavy alkane (usually C_4 to C_6) is introduced into the reactor in order to suspend the particles, while gaseous and/or liquid monomers are fed. The **bulk** process, on the other hand uses liquid propylene,so it is only possible to produce polypropylene and its copolymers. Using diluent processes one is able to obtain either polyethylene or polypropylene.

Slurry processes use autoclave, loop reactors or CSTR (Continuous Stirred Tank Reactor). Gas-phase processes use Fluidized Bed Reactors (FBRs) or stirred bed reactors. Industrially, polyethylene is produced exclusively in FBR and polypropylene is produced in both types of reactors. The FBR will be explained in detail in section 2.3.2.

In this work **only polyethylene** will be considered.

A general schematic description of an industrial polymerization process can be shown in figure 2.1.

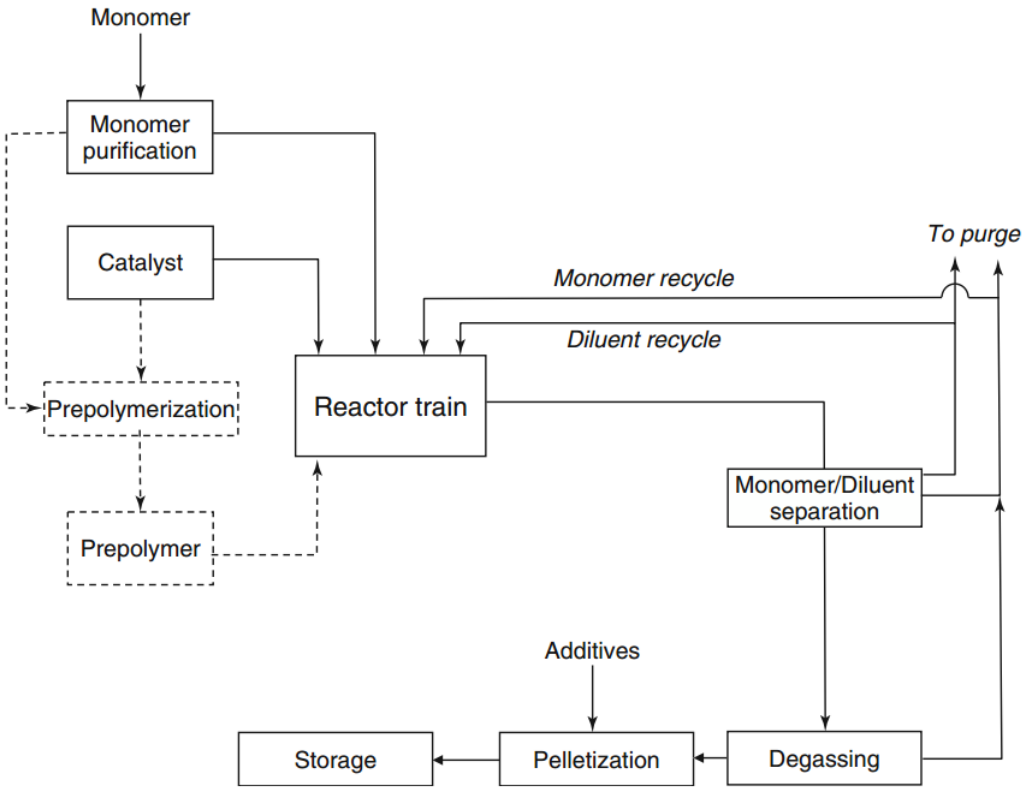

Figure 2.1: Scheme of a polyolefin plant using post-4th *Ziegler-Natta* catalysts (adapted from [5]).

Monomer, catalyst, make-up and other process fluids are fed to the reactor train. Ocassionaly the catalyst and part of the monomer are fed to a **prepolymeriser** in order to help develop better particle morphology before being fed to the main reactor. The resulting polyolefin exits the train and undergoes Monomer and diluent separation before degassing. The recovered diluent and monomer are recycled to the reactor train after a purge and the purified polymer undergoes the necessary operations before its storage. One very important aspect to take into account is that, although the nature of the operations

varies according to the components, the main difference between the various processes arises from the type of reactor chosen and the medium in which the particles are suspended.

In the following sections two production processes are going to be explained in detail: the slurry process using a CSTR reactor and the gas-phase process using a FBR reactor. Understanding these two processes' is crucial for understanding the development of the models, as they are the foundations for the assumptions made throughout the work.

2.2 Particle Size Distribution Model

The **Particle Size Distribution** of a polyolefin refers to the variation of polymer particle sizes in a polymer sample. This variable is instrumental in the design and operation of polymer recovery, treatment and processing units [6].

2.2.1 Particle Fragmentation and Growth

Supported catalyst particles have a diameter of 10-100 µm, depending on the polymerization process. Ideally, the resulting polymer particle after polymerization should present a diameter ranging from several hundred µm to 1 or 2 mm [5]. A large number of industrial processes for polyoefin production use heterogeneous Ziegler-Natta catalysts. These catalysts consist of highly porous secondary particles formed by aggregated primary particles.

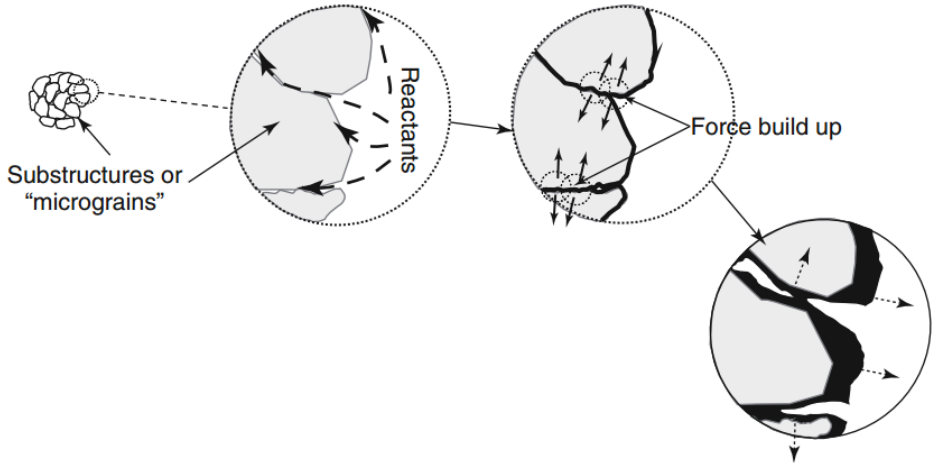

Figure 2.2: Particle growth evolution (adapted from [5]).

During polymerization the particle's inorganic phase suffers a buildup of stress at the weak points where primary particles (micrograins) are in contact (figure 2.2). The secondary particles then fragment due to the growth of polymer chains, resulting in expanding polymer particles (consisting of primary particles, living chains and dead chains).

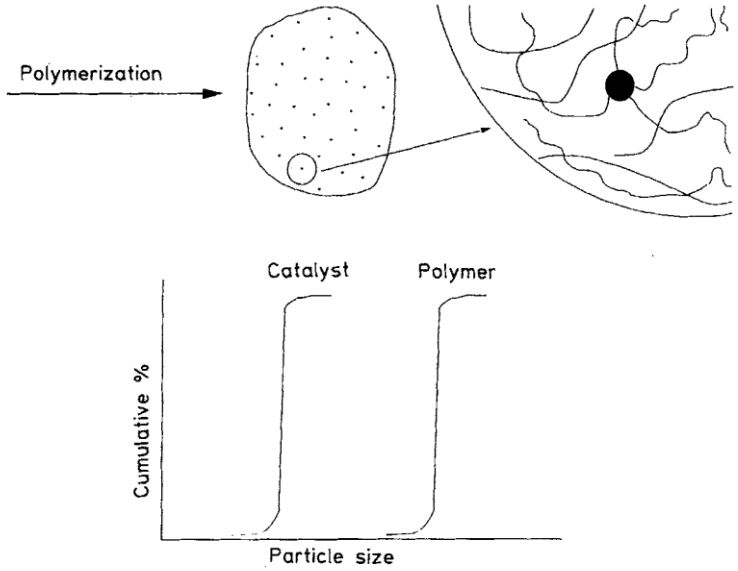

Figure 2.3: Growth of heterogeneous catalysts (adapted from [6]).

If no problems occur, the fragmentation process results in a particular phenomenon: the particle size distribution (**PSD**) of the polymer after polymerization is similar to the PSD of the catalyst before undergoing polymerization [6].

This is called the **replication** phenomenon (shown in figure 2.3) and it is a crucial step in establishing a relationship between the catalyst PSD and the polymer PSD.

A balance must be observed between the mechanical strength of a particle and the catalyst activity. If the particles are weak and high reactivity is observed, the particles breal up into pieces reffered to as fines. Fines are thus polymer powder, which is detrimental to good reactor operation and product quality. Conversely, if the particle is too strong, fragmentation will not occur and the growing polymer chains will block the catalyst pores, rendering the internal active sites inaccessible due to great diffusion resistance and the reactor shuts down[6].

Once fragmentation occurs, polymer formed at the active sites will displace previously formed polymer and, as a result, the particle size increases.

Similarities exist between particle fragmentation and growth. The polymerization reaction creates forces inside the particles that cause fragmentation and, afterwards, expansion. It is also possible to observe the generation of fine particles or the agglomeration of particles, depending on the polymerization conditions and on the polymer's mechanical properties.

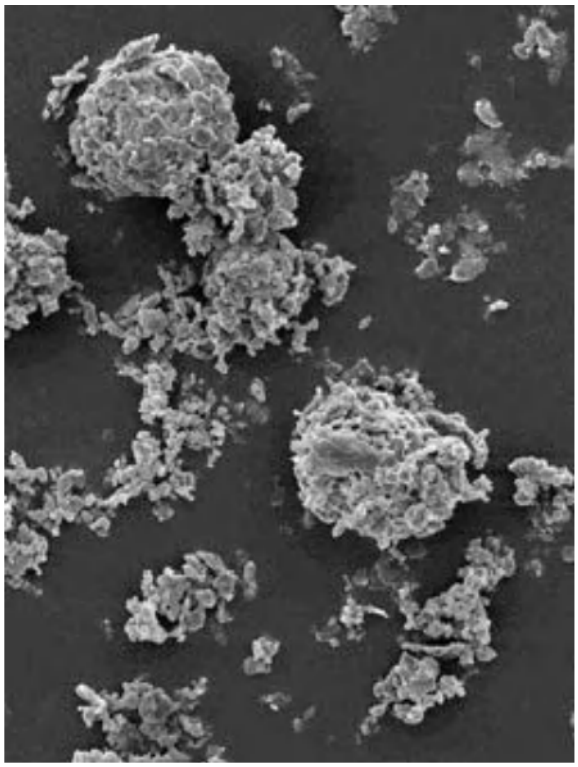

Figure 2.4: Portion of fine HDPE Particles produced in a gas-phase reactor with Ziegler-Natta catalyst (adapted from [5]).

One crucial aspect related to polymerization in heterogeneous catalysts is that the **rate of polymerization** depends on the **concentration of active sites** on the surface of the micrograins and on the **monomer concentration at the active sites**. Therefore the monomer must solubilize and diffuse through the growing polymer phase to reach the active sites located on the surface of the micrograins. However, it can only solubilize in the amorphous phase of the polymer, as opposed to the crystalline phase.

2.2.2 Slurry Phase Processes

Slurry phase processes include 3 phases inside the reactor: a gas-phase, containing the ethylene, hydrogen and possibly comonomer, and a slurry containing solid catalyst and polymer particles and the liquid diluent. The reason for adding the liquid diluent is that operating with liquid ethylene would be impractical.

The simplest slurry phase polymerization process includes a series of CSTRs with the polymerization ocurring inside a heterogeneous catalyst suspended in an inert medium (the diluent). In the first commercial processes a CSTR series was needed to compensate for the low Ziegler-Natta catalyst activity. A *deashing* operation was also necessary to remove catalyst residue, which greatly increased the capital costs associated with such processes.

The arrival of high activity catalysts brought with it significant improval to the established processes and nowadays it is possible to produce the polymer in two reactors without deashing [5].

The slurry phase process was the first developed process for ethylene polymerization and it remains to this day an economically viable and competitive alternative.

The following table 2.1 summarizes the differences between the three dominant licensed processes worldwide:

Table 2.1: Typical reactor conditions for slurry phase HDPE processes (adapted from [5]).

Process	**Reactor Type**	**Diluent**	**Reactor Temperature (° C)**	**Reactor Pressure (bar)**	**Residence Time (hour per reactor)**
Mitsui CX	2 stirred autoclaves	Hexane	80 - 85	<8	3/4
LyondellBasell (Hostalen Process)	2-3 stirred autoclaves	Hexane	75-85	5-10	1-5
Equistar-Maruzen-Nissan	1-2 stirred autoclaves	Hexane	75-90	10-14	3/4-2

It is also important to mention processes such as **Chevron Phillips** and **Innovene S** use isobutane as diluent and loop reactors. The **Borealis - Borstar** process, on the other hand, uses supercritical propane as diluent [5].

These main processes shown in table 2.1 are not adequate for the production of LLDPE since, by using hexane as a diluent, the amorphous fraction of the polymer will solubilize in the diluent and result in reactor fouling.

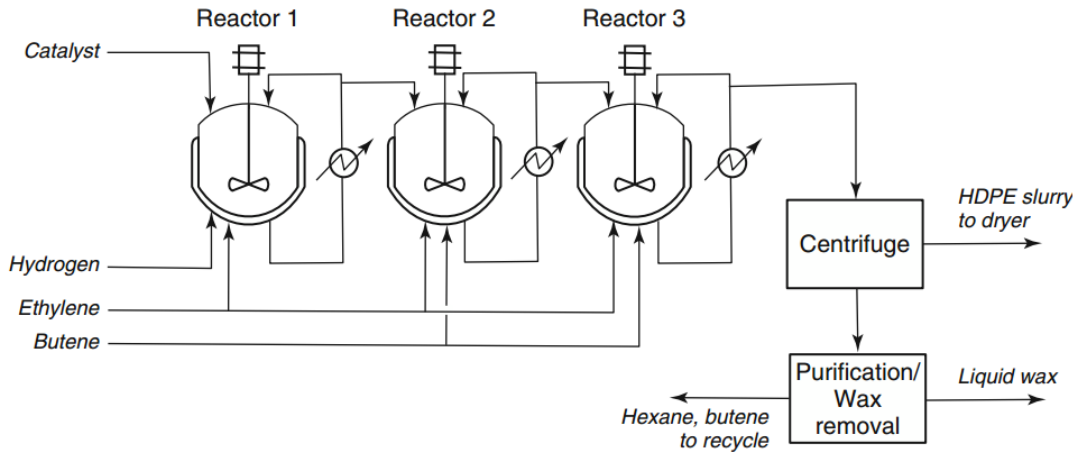

Figure 2.5: Simplified scheme of the new Hostalen process from LyondellBasell (adapted from [5]).

Figure 2.5 makes use of the three reactor configuration and serves as a good base to explain slurry processes in more detail.

The stirred autoclave reactors can be operated in series or in parallel. When operated in **series** the catalyst is only fed to the first reactor and the result is an increase in plant output. However, if operated in **parallel** the advantage is the ability to produce different polymers [5].

On the **first** reactor a catalyst with a decay profile is added, producing a low molecular weight homopolymer. Since hydrogen (controls molecular weight as a chain transfer agent) causes a decrease in polymerization rate, it must be added when the catalyst shows its highest intrinsic activity (hence, the first reactor).

In the **second** and sometimes **third** reactors a small amount of an α -olefin comonomer is introduced. This increases the rate of reaction, regarding homopolymerization, and maintaining good productivity. This is referred to as the **co-monomer kick** [5].

Regardless of the polymerization being conducted in slurry, gas or liquid phase this order of addition (catalyst, hydrogen and comonomer) is often employed to achieve better results.

The **Phillips** process is also an important mention. As opposed to the Hostalen process, this one resorts to **loop** reactors instead of autoclaves/CSTRs, although the Residence Time Distribution of a loop reactor is similar to that of a CSTR.

The advantage of loop reactors is that they have a specific surface area 20 times higher than that of a CSTR and higher overall heat transfer coefficient. Therefore it is possible to remove significantly more heat and polymerize faster.

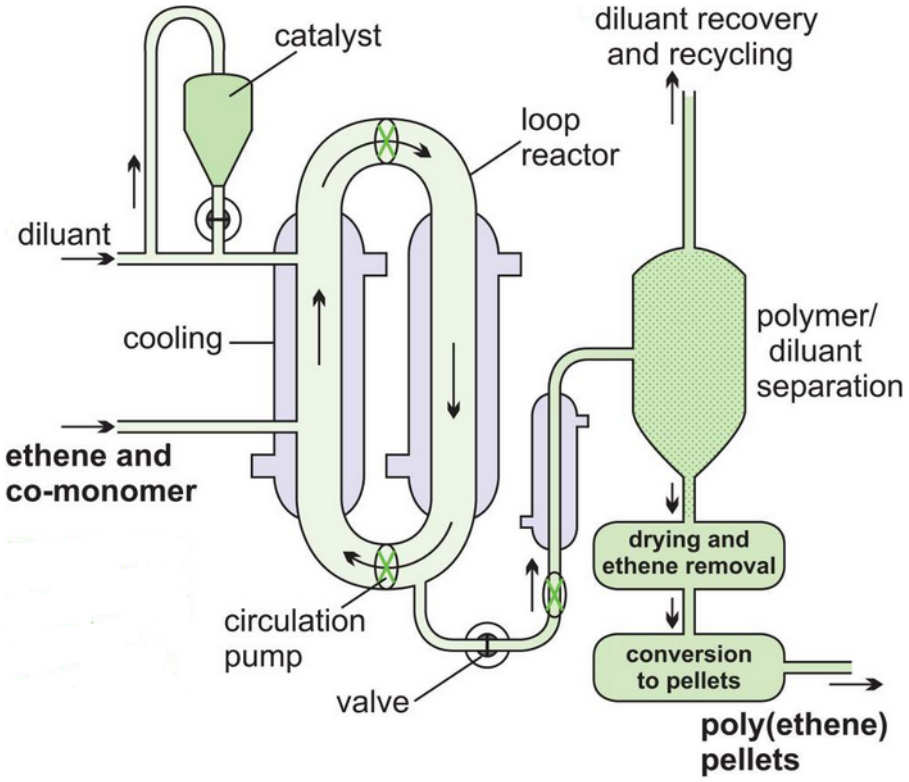

Figure 2.6: Diagram showing a loop reactor used for polyethylene production (adapted from [7]).

In a **loop reactor**, ethylene and the catalyst are mixed with the diluent, heated and afterwards circulated around the loop(s). The stirring on this reactor is maintained by an axial pump. The produced polymer exits the loop through a valve and the diluent is evaporated. Afterwards water vapour with

nitrogen are passed through the polymer in order to fully deactivate the active sites [7].

The diluent used in the Phillips process is isobutane, which has a lower boiling point than hexane. As such, the centrifuge and drying steps of the Mitsui CX process are not necessary and it has the added effect of a lower amorphous material solubility, thus making it easier to produce lower density polymers [5].

There are claims that certain grades of LLDPE can be produced using supported metallocene catalysts [8]. These catalysts produce the comonomer (usually hexene) *in situ*. This is advantageous because, since hexene increases the polymer's solubility in the diluent, the fact that it is consumed and produced simultaneously, hexene concentration is kept on relatively low levels [5].

Another process that uses a loop reactor is Borealis' Borstar process. The unique features, however, are the use of a gas-phase fluidized bed reactor after the initial loop reactor and the use of supercritical propane as a diluent. This propane solubilizes less amorphous polyethylene compared to isobutane, resulting in less reactor fouling. The catalyst is prepolymerized in a smaller loop reactor that operates under less severe conditions. The high operating pressures in the main reactor allow for the production of polymers with lower average molecular weights but have the downside of requiring greater capital investment [5].

2.3 Gas-Phase Reactor Model

2.3.1 Gas-Phase Processes

Gas-phase polyethylene production processes rely solely on fluidized bed reactors (**FBR**). This technology was first commercialized by Union Carbide and its main advantage compared to slurry processes is that, due to the fact that the polymerization medium is gaseous, the unreacted monomer is separated simply by flash. The low molecular weight polymer formed remains attached to the polymer particles, effectively rendering further separations unnecessary. As such, gas-phase processes are true **swing** processes [5]. In other words, they can be used to produce resins from the LLDPE grade to the HDPE grade in the same process.

Swing processes can be used to make products with a range of 0.90-0.96 g/cm^3 densities and are, for that reason, able to produce all types of polyethylene resins, from linear low density to high density.

The following figure 2.7 represents a simplified scheme of a polymerization plant with a fluidized bed reactor.

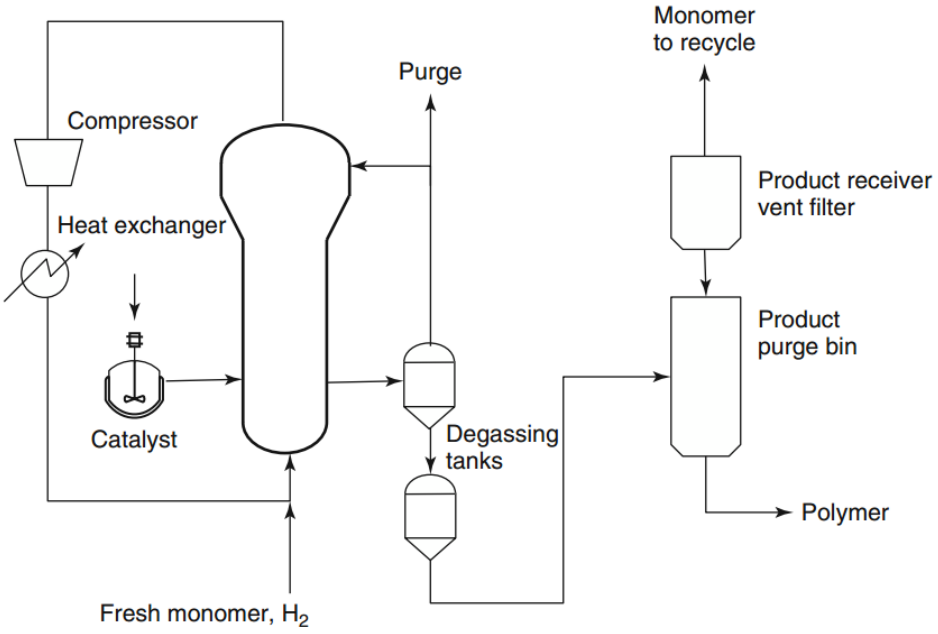

Figure 2.7: Unipol process for polyethylene production (adapted from [5]).

The traditional gas-phase polyethylene production processes present a structure similar to the first generation Unipol process (figure 2.7). Fresh monomer and hydrogen are fed to the reactor as well as fresh catalyst. There is a product discharge valve to remove the polymer, degassing tanks to separate the unreacted monomer and a purge column to remove any residual monomer and deactivate the catalyst. The recovered unreacted monomer is compressed, heated and afterwards mixed with the fresh monomer and recycled to the reactor.

These first generation plants presented frequent reactor runaway issues but improvements in catalyst

technology and process control systems rendered these issues almost nonexistent. Modern plants can also be operated in condensed mode, increasing throughput. Condensed mode operation refers to the partial condensation of the gaseous reactor outlet and will be explained in detail in section 2.3.2.

It is possible to produce both HDPE and LLDPE through the Unipol process but most plants focus on LLDPE production, although some can be operated in *swing mode* and produce both resins. Other gas-phase polyethylene production processes include:

- The **Innovene G** process from INEOS;
- The **Spherilene** process from Basell;

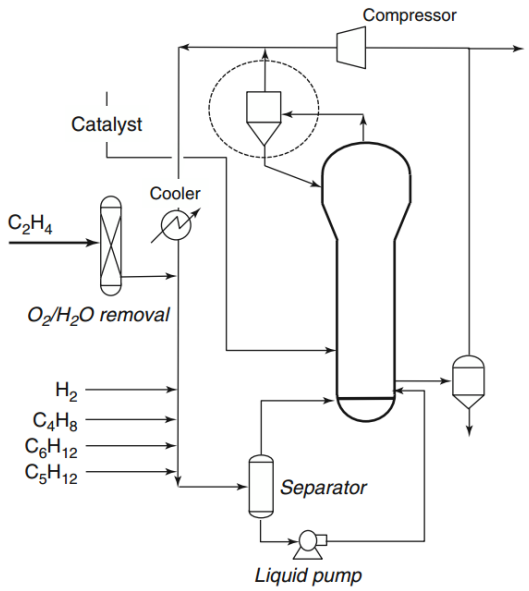

Figure 2.8: Innovene G reactor block diagram (adapted from [5]).

The **Innovene G** process differs from the traditional ones for having a cyclone (shown in figure 2.8) at the gaseous outlet stream designed to eliminate fines from the recycled stream. There is also a separation loop beneath the reactor, recovering condensable material from the recycled stream.

There are 2 **Spherilene** processes: the **S** process and the **C** process. While the Spherilene S process employs one FBR and Ziegler/Chromium catalysts, its C counterpart employs a two FBR cascade and Ziegler catalysts; both offer only dry mode cooling. The inert cooling gas used is propane rather than the common nitrogen due to its significantly higher heat capacity and to easier downstream gas purification operations, according to LyondellBasell [5].

In gas-phase processes for polyethylene production, FBRs are the only type of reactor used. This is due to the fact that the only mechanism available to remove the polymerization heat is to pass a gaseous stream through the reaction mixture.

It is also important to mention that Ziegler-Natta catalysts or metallocenes require previous **prepolymerization**. This step serves two purposes: the first is that it maintains particle morphology but the second, and most important one, is that it prevents particle overheating and therefore, melted polymer production.

Particle overheating can happen because of the catalysts very high initial activity and the high exothermicity of the polymerization. Ziegler-Natta and metallocene catalysts present very high initial activities but chromium catalysts, on the other hand, present a slower buildup rate, which is to say

the buildup in catalyst activity happens at a slower pace and the polymer accumulates on the catalyst particles in a more controlled manner.

Table 2.2 summarizes the characteristics of the main commercial gas-phase processes:

Table 2.2: Typical reactor conditions for gas-phase HDPE processes (adapted from [5]).

Process	Reactor Type	Mode of Operation	Reactor Temperature (° C)	Reactor Pressure (bar)	Residence Time (hour per reactor)
Unipol	1-2 FBR	Condensed	90 - 110	20-25	2
Spheriline Chrome	FBR	Condensed	90-110	20-25	2
Spherilene C/S	1-2 FBR	Dry	70-90	20-25	1.5
Innovene	1 FBR	Condensed	90-110	20-25	2

2.3.2 Fluidized Bed Reactors

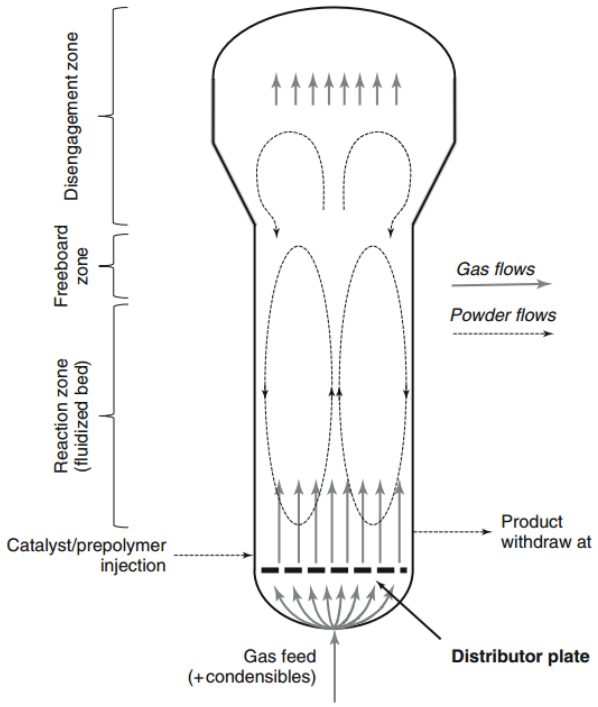

Figure 2.9: Polyolefin production FBR schema (adapted from [5]).

The **Fluidized Bed Reactor** consists of an empty cylinder with a distributor plate on the bottom and a disengagement zone at the top and it is divided into three zones: the **distributor plate**, the **reaction zone** and the **disengagement zone**.

The disengagement zone at the top is usually two times wider than the reaction zone.

The **distributor plate** is a crucial aspect in reactor operation. It is designed to appropriately distribute the components in the powder bed. Its design is of the utmost importance; The holes in the plate allow the passage of the gases (and possibly liquid droplets) to promote fluidization but, simultaneously, it

must prevent the settling of reactor particles in the injection zone and, therefore, blocking the passage of gases.

The **reaction zone** begins above the distributor plate and ends at the freeboard zone. Typically its **height** varies from **10** to **15** meters and the ratio of **height/diameter** varies from **2.5** to **5**.

Catalyst or prepolymerized catalyst is injected in pulses above the distributor plate and the polymer is removed at a similar bed height, also in pulses. The injectors design is a very important detail, since it must avoid blocking of the feed lines and monomer backflow after each pulse.

The discharge of the polymer powder is made through a series of two chambers or more and the frequency of the opening and closing of the valves is controlled to maintain a certain bed height in those chambers, while also preventing plugging due to unwanted polymer formation [5].

The gas flow rate in the reactor zone is important to guarantee particle fluidization. To that effect, a **superficial gas velocity** of **0.5-1** m/s is needed and the **relative gas-particle velocity** should vary between **2** and **8**. In order to achieve this a **recycle ratio** of more than **50** is needed, which entails a low per pass **conversion**: **2-30%**. The reactor outlet gas is compressed, cooled and recycled to the reactor [5].

Another important aspect in FBR operation is the **fluidization** of the powder bed. The **Residence Time Distribution (RTD)** of the powder phase inside the reactor is similar to that of a **CSTR**, which means that the PSD can present a significant range, from some tens of microns (fresh catalyst particles) to several hundred microns or even millimeters (final polymer particles). Proper gas flow rates and catalyst particle design are needed to induce the necessary fluidization but still prevent the presence of too many fine particles that can be dragged out of the reactor. To this effect a prepolymerization step is often employed [5].

The reaction zone and the disengagement zone are separated by the **freeboard zone**. Here, the void fraction is close to 1 and the particles' velocity decreases below minimum fluidization velocity, causing them to fall back into the powder bed. To account for some fines generation the diameter of the **disengagement zone** is doubled, so as to further decrease the superficial gas velocity and minimize the amount of fine particles dragged out of the reactor. Ideally the fine particles would fall back down into the powder bed but, on occasion, they deposit on the reactor wall and form chunks or sheets that sometimes fall back into the bed.

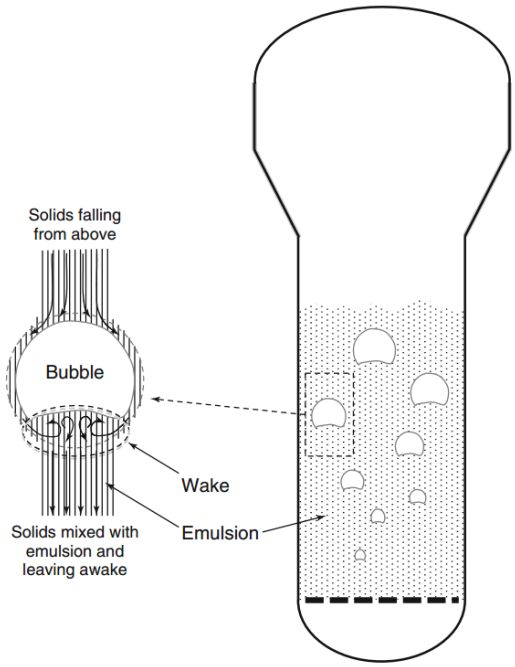

Figure 2.10: Gas and solid flows in an FBR (adapted from [5]).

The gas and powder phases present different RTDs, as is often the case in gas-phase reactors. The gas inside the reactor assumes a plug flow-like RTD. The powder is typically blown up in the middle of the reactor bed and falls back down the reactor walls. This creates a recirculation zone that takes 30 to 60 seconds to complete a cycle. Due to the fact that the **average residence time** of the powder phase is **60-180** minutes, the RTD of the powder phase is similar to that of a CSTR (it is highly back-mixed).

In reality FBRs tend to operate in a bubbling regime as shown in **figure 2.10**. The gas is distributed between two phases: a **bubble** phase, containing only gaseous components, and an **emulsion** phase that presents fluid-like behaviour and contains the solid particles, mixing in the wake of the rising gas bubbles. Due to the difference in velocity of the emulsion phase and the bubbles, the gas-phase is not exactly in plug flow.

There is also tendency for particle segregation in the bed, with the presence of smaller particles higher and bigger particles lower in the bed. This happens due to the fact that smaller particles have lower minimum fluidization velocities and it means that the smaller particles polymerize longer than larger particles and the result is a slightly narrower PSD, comparing to the one expected with ideal CSTR behaviour [5].

Operating conditions inside the reactor, such as pressure and temperature, are set depending on which product is desired. Upper temperature limits are defined based on polymerization kinetics, molecular weight distribution and the softening point of the polymer (around 90° C for LLDPE and higher than 110° C for HDPE).

While per pass conversions in FBRs are typically around 5%, overall conversion is greater than 95%. Nevertheless there are numerous issues associated with FBR operation.

One such issue is temperature control to minimize localised hot spots formation. Hot spots cause the polymer to form chunks by melting and sticking to other particles. These chunks can lead to severe problems downstream, including reactor shutdown, if necessary. Thus, heat removal is a critical aspect of FBR operation and can be achieved by different means.

The amount of heat lost through the reactor walls is insignificant, so the energy generated by the polymerization reaction needs to be removed by the flowing gaseous stream. Two different methods of reactor operation can be used to achieve this goal: **dry mode operation** and **condensed mode operation**, as mentioned before.

In **dry mode** operation heat removal is achieved by transferring heat to the gas phase. Increasing the gas flow rate increases the convective heat transfer coefficient, which leads to higher heat removal rate. There are, of course, limits to the increase in gas flow rate, since higher values mean a decrease in per pass conversion and an increase in both recycle rate and risk of particles being dragged out through the top of the reactor. In addition to increasing the gas flow rate, it is also common to introduce an inert gas with high heat capacity. Such gases include alkanes like propane, butane, pentane or hexane. Due to their higher heat capacities, some dry mode processes use these components as a process gas, in detriment of nitrogen [5].

$$\Delta H_g = Q_m \cdot C_p \left(T_{out} - t_{in}\right) \tag{2.1}$$

Equation 2.1 is a good example to illustrate what was mentioned. The amount of heat that a certain gaseous stream is able to remove (ΔH_g) is given by the product of its mass flowrate (Q_m), its heat capacity (C_p) and the temperature gradient. As such, by increasing the heat capacity of the stream it is possible to remove more heat without increasing reactor throughput. The increase of the C_p is achieved with the addition of the inert heavy alkane. The resulting C_p will also depend on the alkane chosen. A heavier alkane will result in a greater heat capacity increase. Typically C_4 to C_6 alkanes are preferred.

In **condensed mode**, however, the principle is to include condensable material in the recycle stream and cooling it below the dew point of said condensable. As it is introduced into the reactor it vaporizes and absorbs more polymerization heat. This condensable material can be a monomer, in the case of propylene, a comonomer or an inert alkane. This component is called **Induced Condensing Agent** or **Inert Condensing Agent** and, although its benefits are clear, it also significantly increases the load in downstream purification operations due to the increased levels of residual hydrocarbons in the effluents of the reactor, although that is also the case for dry mode operation, when a vapor phase ICA is used.

Table 2.3: Process and Reactor operating conditions for FBR Polyethylene production [5, 9, 10].

Pressure (atm)	20-30	**Temperature $^\circ$C**	75-110
MW Control	H_2	**MWD,** $\bar{M}_w/\bar{M}_n$	4-30
Catalyst size (µm)	30-50	**Polymer particle size (µm)**	300-1300
Density (g/cm^3)	0.91-097	**Superficial Gas Velocity (m/s)**	0.5-1
Per pass conversion (%)	5-30	**Overall conversion (%)**	$>$95
Reaction bed height (m)	10-15	**Bed height/diameter ration**	2.5-5

Table 2.3 summarizes representative process and operating conditions for gas-phase FBRs.

2.3.3 Thermodynamic Considerations

As it was mentioned in section 2.2.1, during polymerization the polymer forms in the catalyst's active sites and expands around the catalyst particles.

The polymerization rate depends on various factors, such as: the temperature at the active sites, the kinetic propagation constant, the active sites concentration in the catalyst and the monomer concentration.

The **monomer concentration at the active sites** is not to be confused with the concentration in the bulk phase due to the fact that this (and other) compound is partitioned between the continuous phase and the amorphous fraction of the polymer. Since the polymer is growing around the catalyst particle, the monomer has to absorb and diffuse through the growing polymer phase to reach the active sites. It is the concentration of monomer at the active sites that directly determines the rate of reaction.

In industrial gas-phase polymerization processes for the production of polyethylene a multi-component mixture exists inside the reactor, out of which the most significant components are: the **monomer**, the **inert alkane** and **polyethylene**.

Due to the high non-ideality of polymer penetrant thermodynamics, it is necessary to employ a thermodynamic model that is able to give accurate predictions of not only the monomer(s) solubility and concentration in the polymer phase under reaction conditions, but also hydrogen and eventually inert alkanes. As it will be discussed, linear models, such as Henry's Law are not enough to even approximately describe the complex phenomena taking place due to the fact that there are interactions between penetrants that models such as Henry's Law are not able to describe.

The challenge of non ideality is the need for complex semi-empirical models, for which it is often difficult to obtain parameters, due to the facts that the necessary experiments are both difficult and expensive to conduct.

There are two different types of thermodynamic equation of state models that have suffered significant improvements over the years and that are currently widely applied in the polymer industry:

- Perturbation theory models, such as the recent **Perturbed Chain Statistical Association Fluid Theory (PC-SAFT)**;
- Lattice models like **Sanchez-Lacombe EOS**;

The main assumption in perturbation theory is that the residual part of the Helmholtz energy of a system that establishes its difference from an ideal gas can be expressed as the summation of different contributions.

One of the first models derived from the perturbation theory was the **Statistical Associating Fluid Theory**, or SAFT, whereas a widely applied model resulting from this theory is the **Perturbed Chain SAFT**, which has been modified to suit polymeric systems' modelling. In the polyolefin industry these models have been implemented to study the phase diagrams in polymer-solvent systems related to

slurry polymerization. In gas-phase polymerization, PC-SAFT has been employed in the study of sorption behaviour of gas as a mixture of ethylene and 1-hexene in LLDPE [11].

Lattice models assume that a molecule can assume various configurations arranged in hypothetical cells that resemble the crystal lattice of a solid. This lattice can be compressible or incompressible and the thermodynamic properties of the system are obtained through statistical mechanics.

The incompressible lattices are used to model liquids at low pressures while compressible lattices result in equations of state, such as Sanchez-Lacombe [11].

Sanchez-Lacombe EOS can be considered an extension of the Flory-Huggins theory, with the significant improvement of considering holes in the hypothetical lattice to account for variations in compressibility and, therefore, density [11].

In the polyolefin industry, Sanchez-Lacombe has been applied to predict the solubility of different single solutes in polymer. Bashir et al. extended the Sanchez-Lacombe EOS to predict the solubility of a mixture of two solutes in the polymer. According to their findings, Sanchez-Lacombe is able to predict the effect in the different analyzed systems [12].

2.3.4 Sanchez-Lacombe EOS for prediction of co-solubility effect

The Sanchez-Lacombe Equation of State is written in the following form:

$$\bar{\rho}^2 + \bar{P} + \bar{T}\left[ln(1-\bar{\rho}) + \left(1 - \frac{1}{r}\right)\bar{\rho}\right] = 0 \tag{2.2}$$

where $\bar{T}, \bar{P}, \bar{\rho}$ are the reduced temperature, pressure and density, respectively, and are defined as follows:

$$\bar{T} = T/T^* \tag{2.3}$$

$$\bar{P} = P/P^* \tag{2.4}$$

$$\bar{\rho} = \rho/\rho^* = 1/\bar{V} = V^*/V \tag{2.5}$$

where $\bar{V}$ and V^* are the reduced and characteristic volumes and T^*, P^*, ρ^* are, respectively, the characteristic temperature, pressure and close-packed mass density.

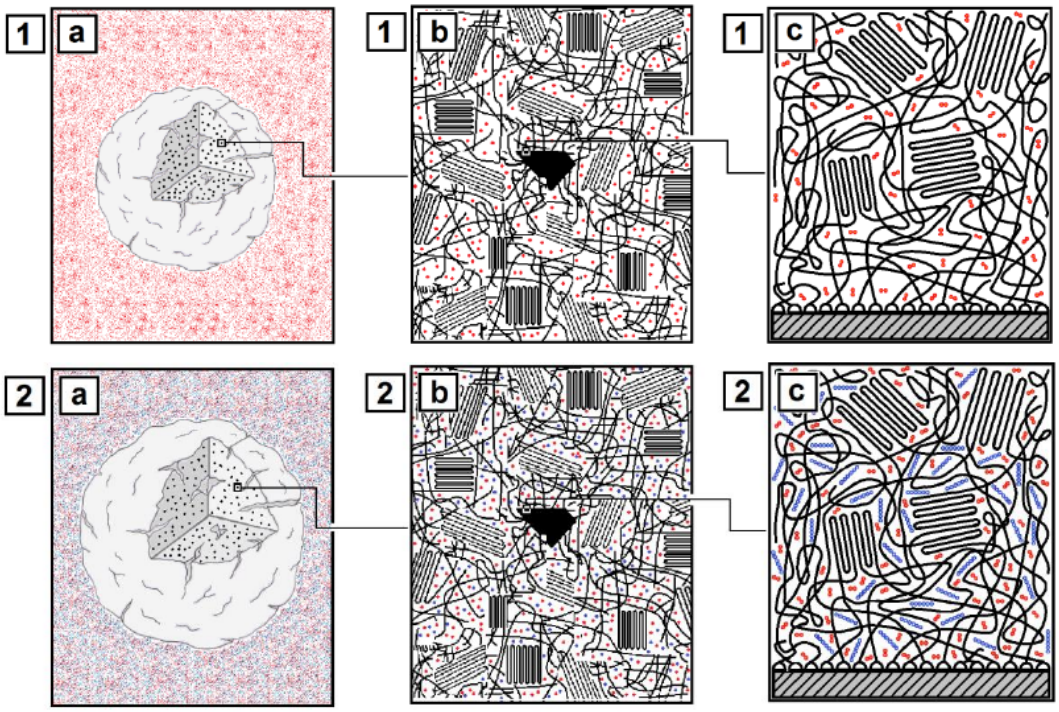

Figure 2.11: Schematic representation of ethylene-polyethylene binary system (1) and ethylene-n-hexane-polyethylene ternary system (2) at different magnifications (adapted from [11]).

Figure 2.11 shows a simplified schema of a polymer particle in two distinct systems: a binary one (1) and a ternary one (2). Each schema is divided into three subfigures:

- **a:** Polymer structure surrounded by a gas phase;
- **b:** Catalyst fragment (black) surrounded by semi-crystalline polyethylene;
- **c:** Polymer chains immobilized on the surface of the catalyst fragment

In schema 1 there is only ethylene present with the polymer (in red) and in schema 2 there is both ethylene (in red) and n-hexane (in blue). The addition of n-hexane causes a phenomenon called **co-solubility effect**. The local concentration of ethylene in the polymer phase, that is to say, its **solubility** in the polymer phase increases when n-hexane is added. To adequately model such effect and predict the ethylene solubility, Sanchez-Lacombe thermodynamic model was chosen.

The model's predictive abilities rely on **binary interaction parameters** and it has been observed that some parameters are temperature-dependent. Through the study of binary systems such as ethylene-polyethylene and hexane-polyethylene the binary parameters can be adjusted and then employed in a ternary system simulation to predict the necessary concentration [11]. It is important to mention that ethylene is an anti-solvent for the heavier component.

A thermodynamic model that predicts equilibrium monomer concentration at the catalyst sites from bulk gas-phase monomer concentration is present in [13]. In [14] the advantages of steady-state modelling and the possibility of dependence of temperature and concentrations (inside the particles) on model parameters were analysed.

In systems for which the heat and mass transfer resistances do not influence monomer concentration and temperature within the particles, it was observed that the **monomer concentration at the active sites** is determined by the **equilibrium sorption** of the monomer in the polymer particles.

Yang et al. [15] measured the solubility of ethylene/isopentane and ethylene/n-hexane in polyethylene of 48.6% crystallinity at the temperatures of 70, 80 and 90° C, total pressure of 2 MPa, varying partial pressures of 80-190 kPa for isopentane and 20-90 kPa for n-hexane. The conclusion was that both **isopentane** and **n-hexane increase the solubility** of ethylene in the ternary systems and that **varying ethylene partial pressure does not alter** the solubility of either alkane.

Bashir et al.[12] used Sanchez-Lacombe to predict solubility data in the system ethylene/1-hexene/LLDPE at 70, 90 and 150° C and found that the predictions were in agreement with experimental data. It was also observed that the solubility improvement depends on the co-monomer.

Alizadeh [11] applied the Sanchez-Lacombe model to the ternary system of ethylene/n-hexane/Polyethylene to predict the change in ethylene solubility in the amorphous phase of the polymer. The predictions were made by fitting the model to the experimental data presented in [15] and adjusting the binary interaction parameters. It was found that the application of Sanchez-Lacombe to a ternary system using binary interaction parameters overestimates the ethylene solubility. The exception was the prediction made for 90° C and 5 bar total pressure, in which case the solubility was not overestimated. It was also observed that the degree of overestimation decreases with the increase in equilibrium temperature.

2.4 Modelling of Industrial Olefin Polymerization Reactors

To discuss the development of models for polyolefin production reactors it is necessary to discuss the scale at which the intended phenomena takes place. In the heart of the polymerization process the supported catalyst particle possesses a crucial role. It serves as a filter between macroscopic events (mixing, bulk heat transfer, liquid injections and particle interactions) and molecular level events that control the architecture of the polymer particle(reaction, crystallization).

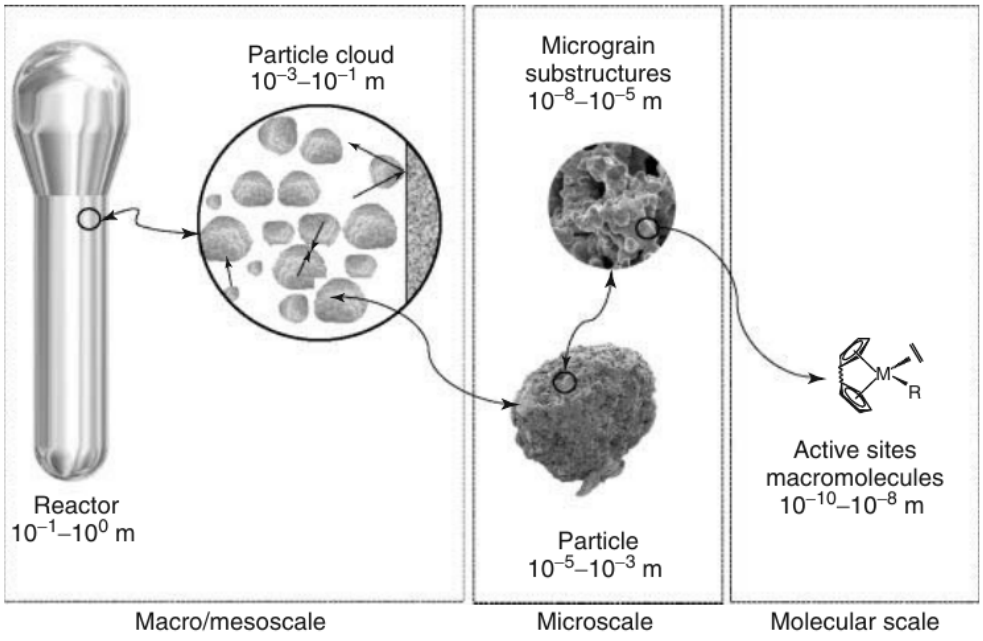

Figure 2.12: Different length scales in an olefin polymerization process (adapted from [5].

Figure 2.12 shows the connections between the different length scales of the phenomena occurring inside the polymerization reactor.

Taking the case of an FBR as example, the injection of gas and possibly liquids causes the particle bed to fluidize. It also causes the development of a complex flow field and the complications that it entails. Particles are subjected to different gas velocities and thus, heat transfer conditions. This can lead to local hotspots formation that affects polymerization rate. In turn it can possibly lead to polymer softening, agglomeration and chunks formation. On a serious scale, bed operation can be compromised.

Bearing this in mind, it is clear that the phenomenological mathematical modelling of olefin polymerization reactors should include a treatment of phenomena occurring from the molecular level to the macroscopic level. In terms of particle growth (mesoscale), there are models that combine energy and mass balances, coupled with the reaction term that, once solved, are able to calculate the temperature and concentration of reactants in every point inside the reactor. These are called **Single Particle Models (SPM)**. This information can then be used to predict polymerization rate, for instance.

Other models, called **Multigrain Models (MGM)** account for the two levels of structural organization mentioned in section 2.2.1: micrograins and macrograins. While these models allow for a more comprehensive representation of the real phenomena they are not without shortcomings, the most relevant

of which is that an assumption is made considering that the internal structure of the polymer particle replicates that of the catalyst particle, which may not be the case with supported olefin polymerization catalysts [5].

In terms of molecular level events (microscale) thermodynamic models like the Sanchez-Lacombe model discussed previously are employed to predict molecular properties and kinetic models are employed to predict rate of polymerization.

Considering macroscale, models pertaining to the reactor configuration are introduced, such as the residence time distribution (RTD).

All these models combined result in a simplified but efficient mathematical treatment of the olefin polymerization reactor system and it is possible to extract meaningful information from it. While it is possible to further develop and arrive at a more complex situation, a cost-benefit analysis must be considered so that the additional information that is gained outweighs the various costs associated with the model's continuation. Sometimes simpler models that use adjustable parameters and reasonable approximations are able to give a more robust picture of the phenomena occurring inside the reactor [5].

2.5 Topic Overview

The amorphous phase of the polymer is a parameter closely related to polymer swelling. This is due to the fact that the monomer is only able to solubilize in the amorphous phase of the polymer. This thesis studies polymer swelling in polyethylene production slurry processes and gas-phase processes. Different processes present different swelling of the polymer, which in turn yields different effects. Thus, two models were developed, the first for the slurry process and the second for the gas-phase process.

2.6 Objectives

The objective of this thesis is to develop two different models, in order to study different aspects of the polyolefin industry. There are different objectives for each developed model. The slurry phase model's objective is to calculate the PSD of a polyethylene produced in slurry phase and discuss the parameters that affect polymer swelling.

The objective for the gas-phase reactor model is the study of the impact of polymer swelling, through the addition of an inert alkane agent, on HDPE production through two distinct mechanisms:

- Polymerization Heat Absorption
- Co-solubility effect

Different alkanes will be analyzed and their effects discussed with regards to achieving higher production. Reactor behaviour will also be one of the analysis objectives.

Chapter 3

Model Implementation

In this chapter the assumptions and implementation of both models will be discussed. The equations will be presented and briefly explained along with significant data necessary for the simulations. An example for the code of both models is present in appendix C, as well as the tables containing variable grouping for the gas-phase reactor model equations.

3.1 Particle Size Distribution Model

The model presented in this section is a generic mathematical model that calculates the PSD of polymer particles produced with heterogeneous Ziegler-Natta and supported metallocene catalysts, taking into account the RTD of ideal or non-ideal polymerization reactors.

3.1.1 Model Assumptions

The following assumptions were made when developing this model:

1. All active sites on the catalyst have the same propagation constant;
2. The concentration of active sites is uniform throughout the catalyst and polymer particles;
3. The catalyst possesses only stable active sites that do not suffer deactivation;
4. The catalyst particle shape is considered to be a sphere;
5. Each catalyst particle is followed individually throughout the reactor;
6. The reactors in the battery behave as ideal CSTRs, as shown by their RTD;

Nowadays it is known that Ziegler-Natta catalysts have more than one type of active sites, each with its characteristic kinetic rate propagation constant, chain transfer and deactivation. These different types of active sites are the main reason for the broad molecular weight and chemical composition distributions. In this model, however, it is sufficient to employ an average propagation constant because only particle growth is of interest.

The second assumption is supported by the fact that good replication would not occur unless the active sites are uniformly distributed on the catalyst particle.

The third assumption, while unrealistic, is made to simplify the model while also allowing to obtain significant conclusions regarding the model's objective, which is to analyse the effect of polymer swelling on the PSD.

The fourth assumption, while admittedly an oversimplification, it constitutes a very decent first approximation and is very frequently employed.

The fifth assumption essentially means that each catalyst particle's growth is calculated individually, meaning that a single catalyst particle gives a single polymer particle. In order to obtain an accurate representation of the PSD of a polymer produced with an industrial catalyst, the model must consider different catalyst diameters.

The last assumption is made also for the sake of simplifying the model. By assuming ideal CSTR RTD instead of a real reactor RTD it is still possible to take out meaningful conclusions regarding polymer swelling.

3.1.2 Model Equations

The following equation calculates the volume of the polymer particle exiting the reactor:

$$V_p = V_p^0 + \Delta V_p \tag{3.1}$$

In terms of particle diameter this can be translated as:

$$\frac{\pi D_p^3}{6} = \frac{\pi D_p^{0^3}}{6} + \frac{\pi D_p^{0^3}}{6} \frac{k_p[M][C_0^*]\, t\, m}{\rho_{pol}} \tag{3.2}$$

Equation 3.2 can be rearranged into into a simpler and more convenient form, as follows:

$$D_p = D_p^0 \sqrt[3]{1 + \alpha t} \tag{3.3}$$

where α constitutes a combined kinetic parameter and its expression is:

$$\alpha = \frac{k_p[M][C_0^*]\, m}{\rho_{pol}} \tag{3.4}$$

Equation 3.3 can be derived, resulting in the following expression:

$$\frac{dD_p}{dt} = \frac{D_p^0}{3} (1 + \alpha t)^{-2/3}\, \alpha \tag{3.5}$$

The number-based PSD $F(D_p)$ can be related to the reactor RTD $E(t)$ through the expression:

$$F(D_p)\,dD_p = E(t)\,dt \tag{3.6}$$

Rearranging,

$$F(D_p) = E(t)\left(\frac{dD_p}{dt}\right)^{-1} \tag{3.7}$$

Substituting equation 3.5 in equation 3.7, $F(D_p)$ can be related to $E(t)$ through a more developed expression:

$$F(D_p) = \frac{3(1+\alpha\,t)^{2/3}}{\alpha\,D_p^0}E(t) \tag{3.8}$$

A well know expression for the residence time distribution of a series of n CSTRs of equal mean residence times is presented in the following equation 3.9:

$$E(t) = \frac{t^{n-1}}{(n-1)!\,\tau^n}\exp(-t/\tau) \tag{3.9}$$

Rearranging equation 3.3 it is possible to arrive at the following expression:

$$t = \left[\left(\frac{D_p}{D_p^0}\right)^3 - 1\right]\frac{1}{\alpha} \tag{3.10}$$

Combining equations 3.8 and 3.9, the following expression is obtained:

$$F(D_p) = \frac{3(1+\alpha t)^{2/3}}{\alpha D_p^0}\frac{t^{n-1}}{(n-1)!\,\tau^n}\exp(-t/\tau) \tag{3.11}$$

which can only be used if α and τ do not vary between reactors. Otherwise, if the reactors do not have the same τ or if the polymerization conditions differ, equations 3.11 and 3.10 can be employed for the first reactor in the series but the subsequent reactors are described with the following equation:

$$\frac{\pi D_p^{i^3}}{6} = \frac{\pi D_p^{i-1^3}}{6} + \frac{D_p^{0^3}}{6}\frac{k_p^i[M^i][C_0^*]\,t^i\,m^i}{\rho_{pol}^i} \tag{3.12}$$

Equation 3.12 can be rearranged into a simpler form, shown in equation 3.13:

$$D_p^i = D_p^0\sqrt[3]{\left(\frac{D_p^{i-1}}{D_p^0}\right) + \alpha^i t^i} \tag{3.13}$$

and equation 3.12 can be arranged into:

$$F(D_p) = \frac{3\left[\left(\frac{D_p^{i-1}}{D_p^0}\right) + \alpha t\right]^{2/3}}{\alpha D_p^0}\frac{t^{n-1}}{(n-1)!\,\tau^n}\exp(-t/\tau) \tag{3.14}$$

The number of moles of active sites in the catalyst particle is described in the following equation:

$$C^* = V_p^0[C_0^*] = \frac{\pi D_p^{0^3}}{6}[C_0^*] \tag{3.15}$$

3.2 Gas-Phase Reactor Model

The model presented in the following section describes the operation of a gas-phase HDPE production reactor in dry mode through a series of mass and heat balances, which will be explained in the following subsections.

3.2.1 Model Assumptions

The following assumptions were made during the development of the following model:

- A single-phase CSTR approach is considered, operating in **Steady-State**;
- The reactor is approximated to a cylinder;
- 1 gaseous inlet consisting of **ethylene**, an **inert heavy alkane** and **nitrogen**;
- 1 solid inlet consisting of **catalyst** particles;
- 1 gaseous outlet containing **non-reacted ethylene**, **inert heavy alkane** and **nitrogen**;
- 1 solid outlet containing the **polymer phase**, consisting of the **polymer and catalyst** particles with **dissolved ethylene and alkane**;
- The catalyst particles are considered **spherical** and **mono-dispersed**;
- Catalyst activation is considered to be **instantaneous**;
- Elutriation of solids is neglected;
- The thermodynamic equilibrium is achieved instantaneously and the polymer particles are considered fully mature;
- The polymer is considered fully amorphous;
- Ethylene and ICA solubility dependence on temperature is neglected;
- Nitrogen solubility in the polymer phase and impact on ethylene solubility are neglected;
- Convective heat transfer is considered between the catalyst/polymer particles and the bulk gaseous phase;
- Due to the heat transfer, **2 different outlet temperatures** are considered, one for the **gaseous outlet** and another for the **polymer phase outlet**;
- No difference in **Pressure** is considered between reactor inlet and outlets;

As it was discussed in chapter 2 approximating an FBR to a CSTR is a reasonable first approximation, since the RTD of the powder phase in an FBR is similar to that of a CSTR. This implies a great number of assumption associated with CSTR reactors. The restraining of the components present in the inlet and

outlet flows is due to the constraints of the Sanchez-Lacombe thermodynamic model, since it can only give reasonable predictions for a ternary system, including the polymer. Related to this is the assumption that the produced polymer is amorphous. While this is not desirable, the monomer and alkane can only diffuse in the amorphous part of a polymer. Thus, for simplification's sake, this assumption is made. Considering that the equilibrium is established instantaneously translates into neglecting mass diffusion resistances.

The catalyst is considered to be mono-dispersed, meaning that a single constant diameter is assumed for the catalyst, instead of the usual particle size distribution. A mean value is considered based on the standard range of catalyst particle sizes and the assumption is also made for simplification purposes. The same is true for the mature polymer particles' size.

3.2.2 Model Equations

Similarly to what was done in section 3.1.2, the following section presents and discusses the equations contained in the gas-phase polymerization reactor model.

The equations intend to be able to calculate essentially the production of polyethylene and the temperature of the bulk and polymer phases inside said reactor. These equations can be summarized into:

- Ethylene Mass Balance;
- ICA Mass Balance;
- Nitrogen Mass Balance;
- Catalyst Active Sites Mass Balance;
- Polyethylene Mass Balance;
- Heat Balance;

Ethylene Mass Balance

The ethylene mass balance in its most general form is written as

$$Q_{Et,in} - Q_{Et,out} - R_p(T,P)\,V_c - Q_{Et,d} = 0 \tag{3.16}$$

where one important term is the mass flowrate of ethylene dissolved in the polymer phase ($Q_{Et,d}$), defined as:

$$Q_{Et,d} = \frac{C_{Et}^{P}\,M_{Et}}{\rho_{pol}}\,Q_{PE} \tag{3.17}$$

ICA Mass Balance

Similarly to the case of ethylene, the heavy alkane's mass balance is written according to the following equation:

$$Q_{ICA,in} - Q_{ICA,out} - Q_{ICA,d} = 0 \tag{3.18}$$

$$Q_{ICA,d} = \frac{C^P_{ICA}\, M_{ICA}}{\rho_{pol}}\, Q_{PE} \tag{3.19}$$

Nitrogen Mass Balance

The nitrogen mass balance considered is described according to equation 3.20:

$$Q_{N_2,in} = Q_{N_2,out} \tag{3.20}$$

Catalyst Active Sites Mass Balance

The mass balance concerning the active sites concentration in the catalyst is essential in accounting for catalyst deactivation. Its main calculated variable is the concentration of active sites after the deactivation has taken place.

This balance can be written in the general form

$$Q_c\, C^*_0 - Q_c\, C^* - k_d(T)\, C^*\, V_c = 0 \tag{3.21}$$

Rearranging equation 3.21 it is possible to directly calculate the concentration of active sites C^*:

$$C^* = C^*_0\, \frac{1}{1 + k_d(T)\, \frac{V_c}{Q_c/\rho_{bed}}} \tag{3.22}$$

where the deactivation constant k_d depends on the temperature through the Arrhenius law:

$$k_d^{T_s} = k_d^{T_{ref}}\, \exp\left[\frac{E_a}{R}\left(\frac{1}{T_{ref}} - \frac{1}{T_s}\right)\right] \tag{3.23}$$

Polyethylene Mass Balance

The polyethylene mass balance starts, of course, with the presentation of the kinetic rate equation assumed. The assumed rate law was proposed by Floyd[16] and is written as follows

$$R_p = k_p\, C^*\, C^P_{Et} \tag{3.24}$$

It is a **first order** reaction rate law considering a **single-site** catalyst and takes into account the monomer concentration dissolved in the polymer phase.

As for the case of catalyst deactivation, the kinetic rate constant k_p also presents an Arrhenius temperature dependence:

$$k_p^{T_s} = k_p^{T_{ref}} \exp\left[\frac{E_a}{R}\left(\frac{1}{T_{ref}} - \frac{1}{T_s}\right)\right] \tag{3.25}$$

The polyethylene mass balance is then written through the following expression

$$Q_{PE} = R_p V_c M_{Et} \tag{3.26}$$

The reason why the ethylene molar mass M_{Et} is used in equation 3.26 is because the rate of polymerization R_p describes the ethylene that is consumed in the polymerization reactor and, therefore, the mass of polyethylene generated.

Catalyst Heat Balance

A simple catalyst heat balance was included in this work to account for the temperature gradient between the polymer particles and the bulk gas phase in the reactor. The conductive heat transfer inside the particles was considered to be instantaneous and convective heat transfer was assumed as the main mechanism between the polymer phase and the gas phase.

The following equation describes the relationship between the solids' temperature T_s and the bulk gas phase temperature T_b:

$$\Delta H_{polym} = h \cdot A_p \cdot (T_b - T_s) \tag{3.27}$$

where h represents the convective heat transfer coefficient, admitted by Wong[17] and the heat transfer area A_p is described by the expression

$$A_p = N_p \cdot \pi \cdot D_p^2 \tag{3.28}$$

Equation 3.27 is used to calculate the bulk phase temperature from the assumed value for the solids temperature.

Reactor Heat Balance

The general heat balance is described by the following equation:

$$\Delta H_{In} - \Delta H_{Out} + \Delta H_{Generated} = \Delta H_{Accumulation} \tag{3.29}$$

Since steady-state operation was assumed, this means that accumulation is neglected. Also, the reference state is an essential parameter of the heat balance.

Reference State

- Reference Temperature - Inlet Flow Temperature T_{in}
- Reference Pressure - Reactor working pressure
- Gaseous ethylene, nitrogen and alkane
- Solid Catalyst
- Amorphous Polyethylene

Considering this reference state, equation 3.29 can be simplified into equation 3.30.

$$-\Delta H_{Out} + \Delta H_{Generated} = 0 \tag{3.30}$$

Replacing the necessary parameters the complete expression for equation 3.30 takes the following form:

$$\begin{aligned} &Q_{Et,out} \cdot \overline{C_{p,Et}} \cdot (T_b - T_{in}) + Q_{ICA,out} \cdot \overline{C_{p,ICA}} \cdot (T_b - T_{in}) \\ &+ Q_{N_2,out} \cdot \overline{C_{p,N_2}} \cdot (T_b - T_{in}) + Q_{PE} \cdot \overline{C_{p,PE}} \cdot (T_s - T_{in}) \\ &+ Q_c \cdot \overline{C_{p,c}} \cdot (T_s - T_{in}) + Q_{Et,reacts} \cdot \Delta H_{polym} = 0 \end{aligned} \tag{3.31}$$

where $Q_{Et,reacts}$ represents the mass flow rate of ethylene that is consumed as reactant described by equation 3.32:

$$Q_{Et,reacts} = \frac{Q_{PE}}{M_{Et}} \tag{3.32}$$

To solve the model the software *Microsoft Excel*® was used. An initial assumption is made for the solids temperature T_s and the equations are introduced leading to the heat balance where T_s is calculated rearranging equation 3.31.

$$\begin{aligned} T_s = &T_{in} \cdot \frac{Q_{Et,out} \cdot \overline{C_{p,Et}} + Q_{ICA,out} \cdot \overline{C_{p,ICA}} + Q_{N_2,out} \cdot \overline{C_{p,N_2}} + Q_{PE} \cdot \overline{C_{p,PE}} + Q_c \cdot \overline{C_{p,c}}}{Q_{PE} \cdot \overline{C_{p,PE}} + Q_c \cdot \overline{C_{p,c}}} \\ &- T_b \cdot \frac{Q_{Et,out} \cdot \overline{C_{p,Et}} + Q_{ICA,out} \cdot \overline{C_{p,ICA}} + Q_{N_2,out} \cdot \overline{C_{p,N_2}}}{Q_{PE} \cdot \overline{C_{p,PE}} + Q_c \cdot \overline{C_{p,c}}} + \frac{|\Delta H_{polym}| \cdot Q_{Et,reacts}}{Q_{PE} \cdot \overline{C_{p,PE}} + Q_c \cdot \overline{C_{p,c}}} \end{aligned} \tag{3.33}$$

Afterwards the tool *Solver* is used to minimize the difference between the calculated and assumed T_s by changing the assumed value. GRG Nonlinear is the adopted solver, available by default in *Excel*'s Solver Add-in. Alternatively a *Matlab*® script was developed, using the Optimization Toolbox's *fsolve* function. This function is able to simultaneously solve a system of non-linear equations by considering initial values for each variable.

Diagnostic Parameters

In order to better evaluate the results of a model a small set of diagnostic parameters were chosen. These parameters were:

- **Catalyst Productivity**;
- **Ethylene Per Pass Conversion**;
- **Superficial Gas Velocity**;

The objective of these parameters is to guarantee that, despite the results of the model (namely HDPE production and reactor temperature) appear as expected, the chosen parameters are included within the operating ranges for FBRs, thus guaranteeing good reactor operation.

Catalyst Productivity is a simple parameter defined by equation 3.34:

$$Productivity = \frac{Q_{PE}}{Q_c} \tag{3.34}$$

This parameter can vary from 3000 to 50000 $g_{Polymer}/g_{Catalyst}$ [18] or more, depending on catalyst activity and translates to the amount of polymer that the catalyst is able to produce, per unit of mass.

Monomer **Per Pass Conversion** usually varies from 5-30% [5] and is defined according to equation 3.35:

$$Conversion = \frac{Q_{Et,reacts}}{Q_{Et,in}} \cdot 100 \tag{3.35}$$

This parameters describes the amount of monomer that reacts per cycle of the gas stream.

The **superficial gas velocity** (0.5 - 1 m/s [5]) is a very important parameter in terms of reactor operation. It maintains correct bed fluidization, which has serious impact on heat transfer. It is defined according to equation 3.36:

$$u_g = \frac{Q_{v,in}}{\frac{\pi}{4} \cdot d^2} \tag{3.36}$$

$$Q_{v,in} = \frac{(n_{Et,in} + n_{ICA,in} + n_{N_2,in}) \cdot R \cdot T_b}{P} \tag{3.37}$$

Additional Calculations

Another important calculation is presented here to obtain the volume of catalyst inside the reactor. Firstly, a reactor bed height h_b and diameter d are assumed. According to usual value ranges present in the literature ([5]) the values assumed were 13.3 m and 4.75 m respectively. Thus, the cross-section of the reactor is calculated with the expression

$$b = \frac{\pi}{4} \cdot d^2 \tag{3.38}$$

And the volume of the bed is calculated using equation 3.39

$$V_b = b \times h_b = \frac{\pi}{4} \cdot d^2 \cdot h_b \tag{3.39}$$

Assuming a common value for fluidized bed porosity, the volume of particles in the bed is calculated.

$$V_p = V_b \cdot (1 - \varepsilon) \tag{3.40}$$

The value assumed for ε was 0.55, above the minimum fluidization bed porosity present in the literature ([19]). Afterwards the number of polymer particles is calculated assuming that each particle is a **sphere**.

$$V_p = N_p \cdot \frac{\pi}{6} \cdot d_p^3 <=> N_p = \frac{6 \cdot V_p}{\pi \cdot d_p^3} \tag{3.41}$$

Assuming that each catalyst particle is going to originate a polymer particle ($N_p = N_c$) then the volume of catalyst V_c can be calculated using equation 3.42

$$V_c = N_c \cdot \frac{\pi}{6} \cdot d_c^3 \tag{3.42}$$

According to the typical ranges consulted in the literature ([5]) the values assumed for d_c and d_p were 50 and 500 µm respectively.

Other calculations in this work include:

- Gaseous component Heat Capacity
- Component Vapor Pressure
- Ethylene and ICA Solubility Correlations;
- Polymer Density Correlations;

They will be briefly present and discussed in appendix A.

Chapter 4

Results

In this chapter the results regarding both models will be presented and discussed. A sensitivity analysis will also be analyzed, regarding the gas-phase reactor model.

4.1 Slurry Phase Particle Size Distribution Model

In the following section the results of the slurry phase PSD model are discussed.

4.1.1 Summary of Data used in Simulation and Model Validation

As a means of testing the validity of the implemented model, the data used for running the simulations is taken out of the example shown in Fig. 4 of reference [6].

The following table 4.1 summarizes the data used for the model validation:

Table 4.1: Data used for PSD model validation (taken from [6]).

i	2	D_p^0	30 µm
τ_1	60 min	k_p^1	1.2×10^4 L/(mol.min)
τ_2	120 min	k_p^2	2.4×10^5 L/(mol.min)
$[M]$	4.0 mol/L	$[C_0^*]$	1.0×10^{-3} mol/L
m	42 g/mol	ρ_{pol}	900 g/L

Data in table 4.1 describes a system consisting of a series of 2 CSTR reactors in a row, each with different polymerization conditions and mean residence times. The concentration of active sites in the catalyst is constant in both reactors, as is the monomer concentration. The catalyst consists of only 30 µm particles.

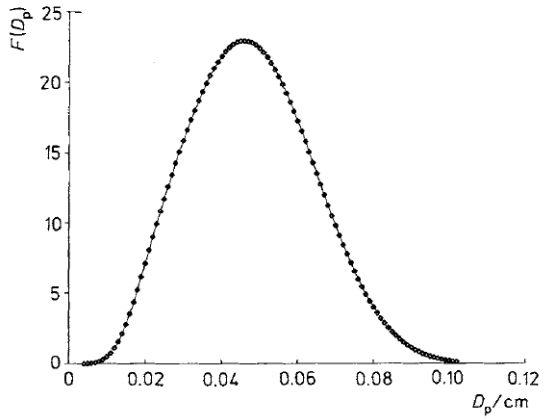

Figure 4.1: Solution for the PSD model present in Figure 4 of [6].

Figure 4.1 shows a Particle Size Distribution of a polyethylene resin with 900 g/L density (LLDPE) considering no catalyst deactivation. The distribution itself assumes the shape of a standard bell curve with a mean particle diameter of approximately 500 µm. Afterwards the simulation was ran and the results were compared to the previous figure.

The following figure 4.2 shows the comparison between the developed model and the solution present in the literature, using the same data. The simulation was ran using *Matlab*® software and exporting the results to *Microsoft Excel*® where the graph was constructed. Figure 4.1 was digitized using *Plot Digitizer* software and the results were also exported to *Microsoft Excel*®. It is important to mention that due to the fact that the plot is digitized by calibrating the image and manually selecting coordinates a deviation to what is presented in the literature[6], however small, is to be expected.

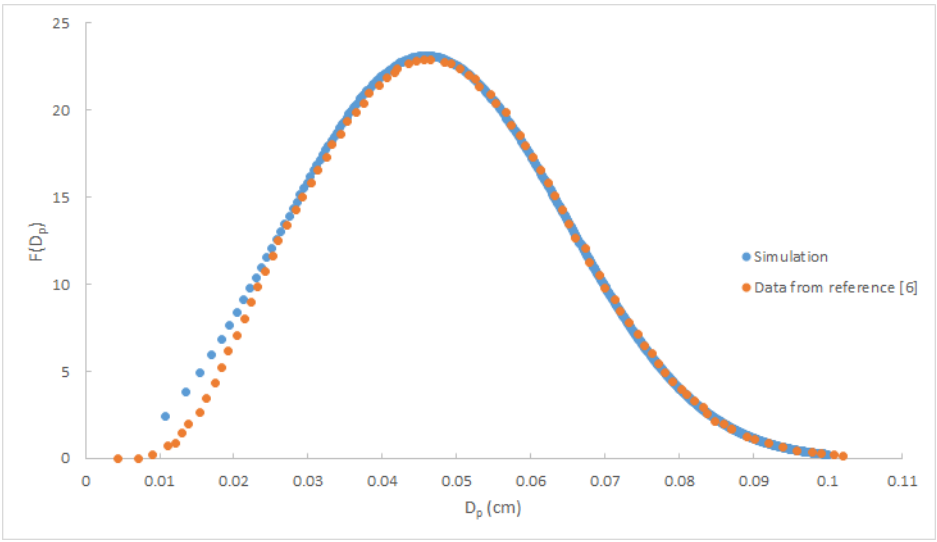

Figure 4.2: Simulation run to validate the developed model. Comparison of the PSD of the polymer exiting the second reactor to figure 4 of the literature[6].

By analyzing figure 4.2 it is possible to see that the model replicates the results presented in the literature[6] with a small deviation at the beginning of the curve. This difference can be explained by the numerical method employed in each circumstance. However, after a particle diameter of about 250 µm the difference between the simulation results and the model is negligible. It is important to mention, however, that the PSD presented in figure 4.2 describes the polymer exiting the **second** reactor in the reactor train. The following figure 4.3 establishes the same comparison based on the results of the simulation for the polymer exiting the **first** reactor and the results presented for the same case in figure

5 of the literature[6].

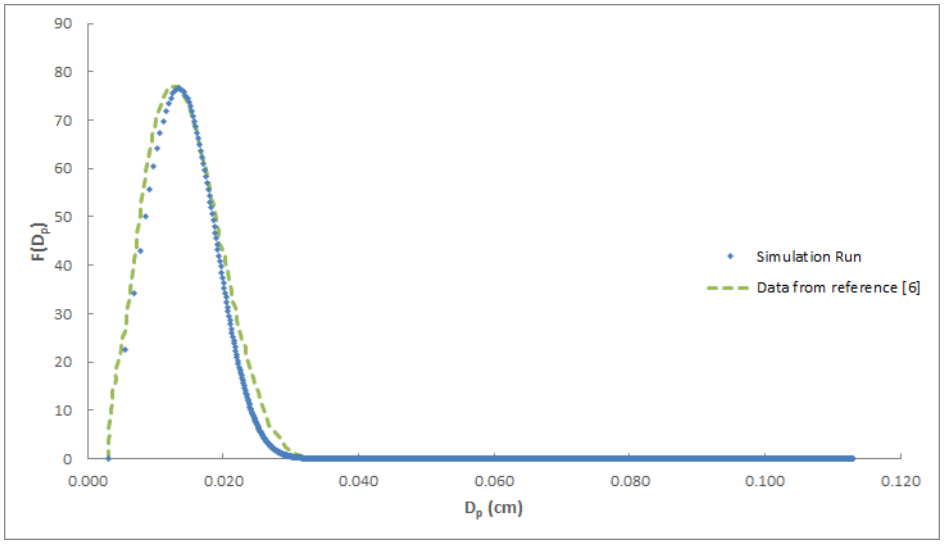

Figure 4.3: Simulation run to validate the developed model. Comparison of the PSD of the polymer exiting the first reactor to figure 5 of the literature[6].

It is possible to observe that for the first reactor deviations also occur, although less pronounced than the ones present in figure 4.2 and well within the error range.

With these results the model can be assumed as valid for the description of slurry phase ethylene polymerization in a CSTR battery.

4.1.2 Results

The results presented here are obtained solving equations 3.13 and 3.14 using a script developed in *Matlab*®. The results are then plotted and presented.

Simulation I

Simulation I intends to analyze the effect of catalyst particle diameter on the polymer's PSD. The data used for the simulation is summarized in table 4.2.

Table 4.2: Constant parameters for Simulation I using isobutane as a diluent.

i		2	
τ_1	60 min	τ_2	120 min
k_p^1	1.2 x 10^4 L/(mol.min)	k_p^2	2.4 x 10^5 L/(mol.min)
m	28.05 g/mol	C^*	1 x 10^{-3} mol/L
$[M]$	4 mol/L	ρ_{pol}	915 g/L

This simulation is based on an experiment conducted at LCPP - C2P2 [20], at **70 °C**, **3 bar** total reactor pressure, **5%** ethylene molar concentration in the gaseous inlet and using **isobutane** as the diluent. The concentration and density of the polymer were predicted using Sanchez-Lacombe EOS and corrected to simulate standard LLDPE, as shown by the density value in table 4.2. The initial catalyst particle diameter was varied from 30 µm to 100 µm and the PSD calculated.

As for the reactor setup, this simulation considers a cascade of 2 CSTR reactors with different polymerization conditions. The first reactor can be considered a prepolymerization reactor, as shown by its lower mean residence time (τ_1) and kinetic rate constant (k_p^1), while the second reactor presents more relevant polymerization conditions. The concentration of monomer is considered the same in both reactors.

The following figure (4.4) shows the result of the simulation.

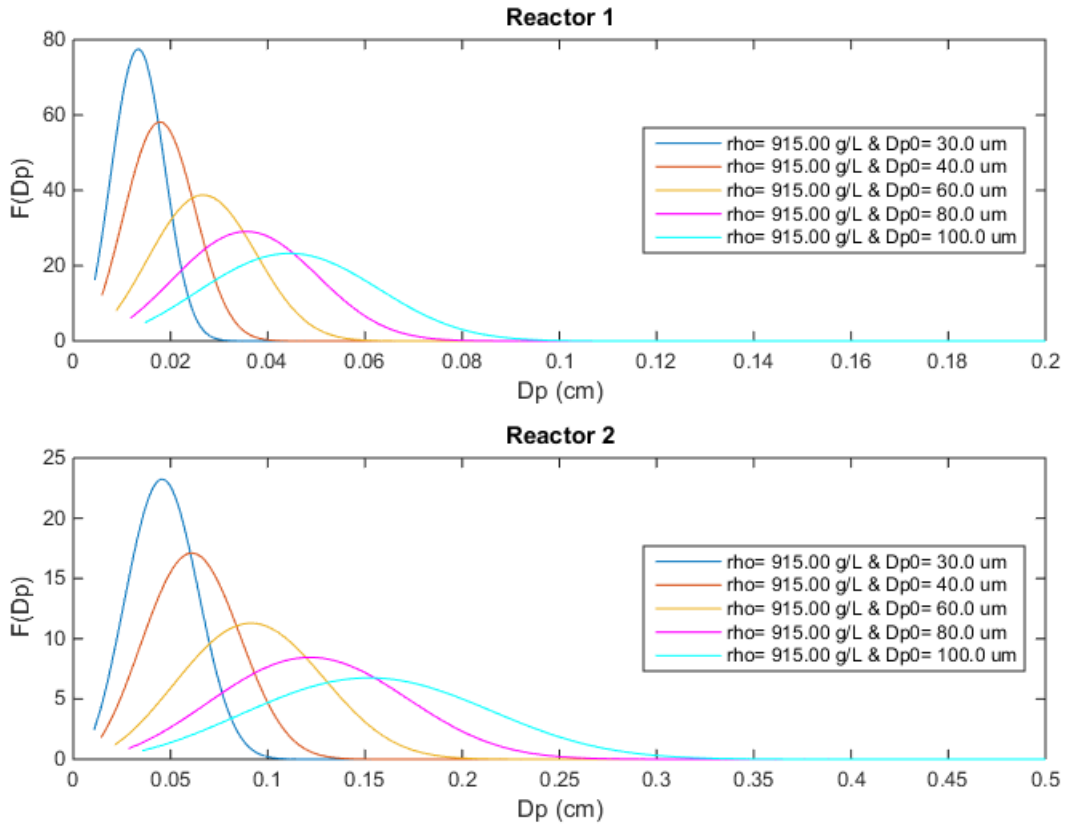

Figure 4.4: Simulation I polymer PSD results using isobutane as diluent.

A significant difference is detected when varying the catalyst particle diameter (D_p^0). As the diameter increases a broadening of the PSD is observed. This entails an increase in mean particle diameter, as is expected, due to the fact that the polymerization begins with a bigger particle.

However, simulation I does not take into account particle swelling which is the main analysis objective of this model but it does serve the benefit of another assurance that the model behaves as expected.

Simulation II

Simulation II analyses the effect of **polymer swelling** on polymer PSD. To this effect the simulation parameters are changed from those presented in table 4.2. In this simulation the total reaction pressure is changed. By varying the reaction pressure both the density of the polymer phase and the monomer concentration at the active sites change, due to the fact that they represent an equilibrium of the components in the reactor operating at a certain pressure. This results in polymer swelling, affecting the average particle diameter of the produced polymer.

The experiment represented by simulation II was also conducted at 70 ° C, 5% ethylene molar concentration, using isobutane as diluent but the various densities achieved correspond to total reactor pressures of 3, 5, 10, 15, 18 and 20 bar. With increasing reactor pressure the densities of the polymer phase decrease. In other words, bigger particles (swollen) are produced.

Table 4.3 contains the parameters used in this simulation.

Table 4.3: Constant parameters for Simulation II using isobutane as a diluent.

i	2	D_p^0	30 µm
τ_1	60 min	τ_2	120 min
k_p^1	1.2 x 10^4 L/(mol.min)	k_p^2	2.4 x 10^5 L/(mol.min)
m	28.05 g/mol	C^*	1 x 10^{-3} mol/L

Simulation II analyzes one of the main objectives of this model, the effect of particle swelling in polymer PSD. The various simulations were ran for different density and monomer concentration, each corresponding to a different experiment performed at different reaction pressures, as mentioned before. The following table shows the relationship between each reaction pressure and the respective density and concentration predicted by the Sanchez-Lacombe model.

Table 4.4: Simulation II relationship between total reactor pressure and polymer density and ethylene concentration.

P (bar)	3	5	10	15	18	20
ρ_{pol} (g/L)	823.25	818.96	807.05	792.43	781.46	772.48
$[M]$ (mol/L)	0.0120	0.0206	0.0403	0.0678	0.0892	0.1074

In table 4.4 the data presented concerns the Sanchez-Lacombe EOS predictions for polymer density and monomer concentration at the active sites for each reaction pressure. Predictions were made taking into account that the reaction temperature and monomer bulk concentration are, respectively, 70 ° C and 5% (molar). The results of the simulation are presented in the following figure 4.5.

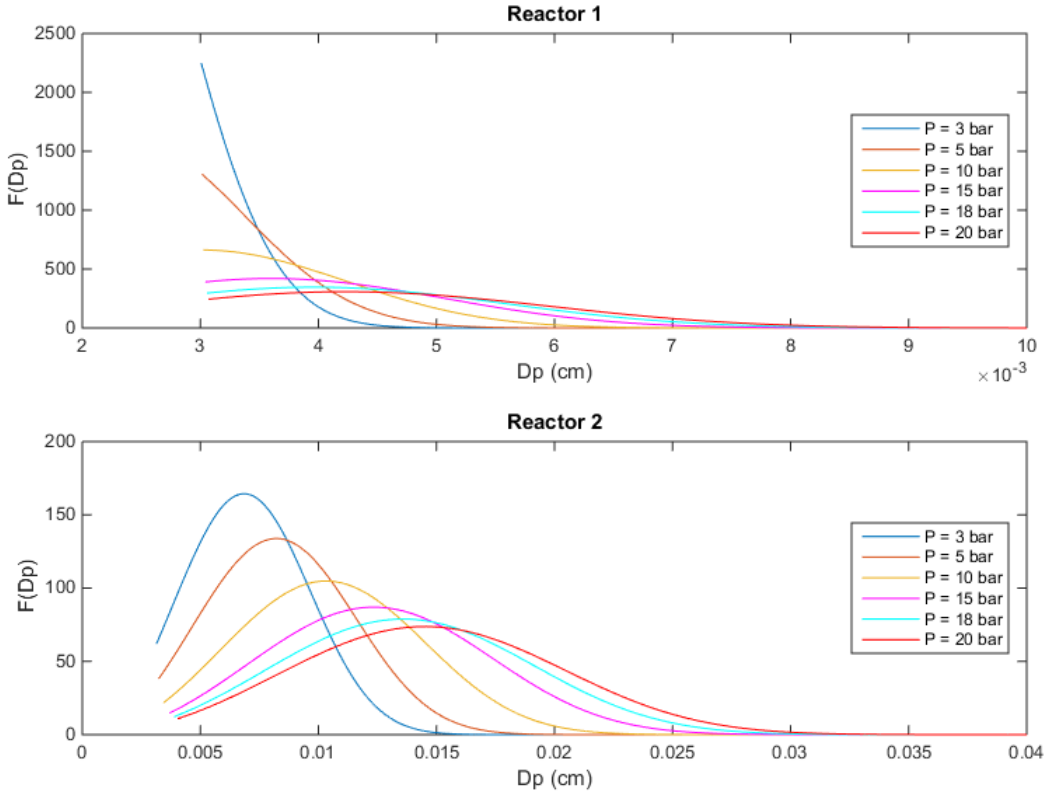

Figure 4.5: Simulation II polymer PSD results using isobutane as diluent.

The first difference noticed when comparing the results of Simulation II (figure 4.5) to the results of Simulation I (figure 4.4) is that the produced polymer particles are much smaller in Simulation II, as shown by the polymer diameter (D_p) axis. This is due to the fact that, in the second simulation, the monomer concentration (shown in table 4.4) is several times lower than the value of 4 mol/L assumed for the first simulation.

Analyzing now the results of this simulation it is possible to observe an increase in average particle diameter (swelling) with reaction pressure. Table 4.4 shows that by increasing total reactor pressure (with constant ethylene bulk concentration) from **3 bar** to **20 bar** the monomer concentration at the active sites increases nearly **ninefold**. This results in **lower** polymer density and, as figure 4.5 shows, **higher** average particle size, indicating greater productions.

Another notable result is that the PSD for the **first reactor** indicates that there is only a very small degree of polymerization occurring. There is a significant number of particles exiting the reactor with diameters very close to the initial catalyst particle diameter (D_p^0) of 30 µm (0.003 cm), which could indicate a **bypass** situation. However, this is once again due to the low concentrations of monomer in the active sites and due to the lower mean residence time (τ_1) of the first reactor.

Nonetheless, since the first reactor in the series is usually employed as a **prepolymerization** reactor, the PSD it presents does not constitute a worrying issue.

Analyzing the PSD of the second reactor the results reflect a longer polymerization, seen in the shape of the curves. It appears that an increase in reactor pressure (in other words, a decrease of polymer density combined with an increase of monomer concentration at the active sites) causes a **broadening of the PSD** resulting, expectedly, in the production of larger particles. In the case of the most swollen polymer (ρ_{pol} = 772.48 g/L) the average particle diameter is approximately 150 µm while for the case of the least swollen polymer (ρ_{pol} = 823.25 g/L) it is approximately 70 µm. To produce a polymer with bigger particles greater monomer concentrations must be achieved, however, the experiments on which these simulations were based were conducted in a laboratory environment rather than an industrial one.

However, it is clear that by changing reactor pressure, both polymer density (ρ_{pol}) and monomer concentration at the active sites ($[M]$) change and the effect that is seen in the results (figure 4.5) is the combined effect of density and monomer concentration change. Thus, it is interesting to analyze the effect of polymer density alone on the PSD.

To that effect the same simulation was ran with a constant **monomer concentration** $[\mathrm{M}]$ of **4 mol/L** and the results are shown in the following figure 4.6.

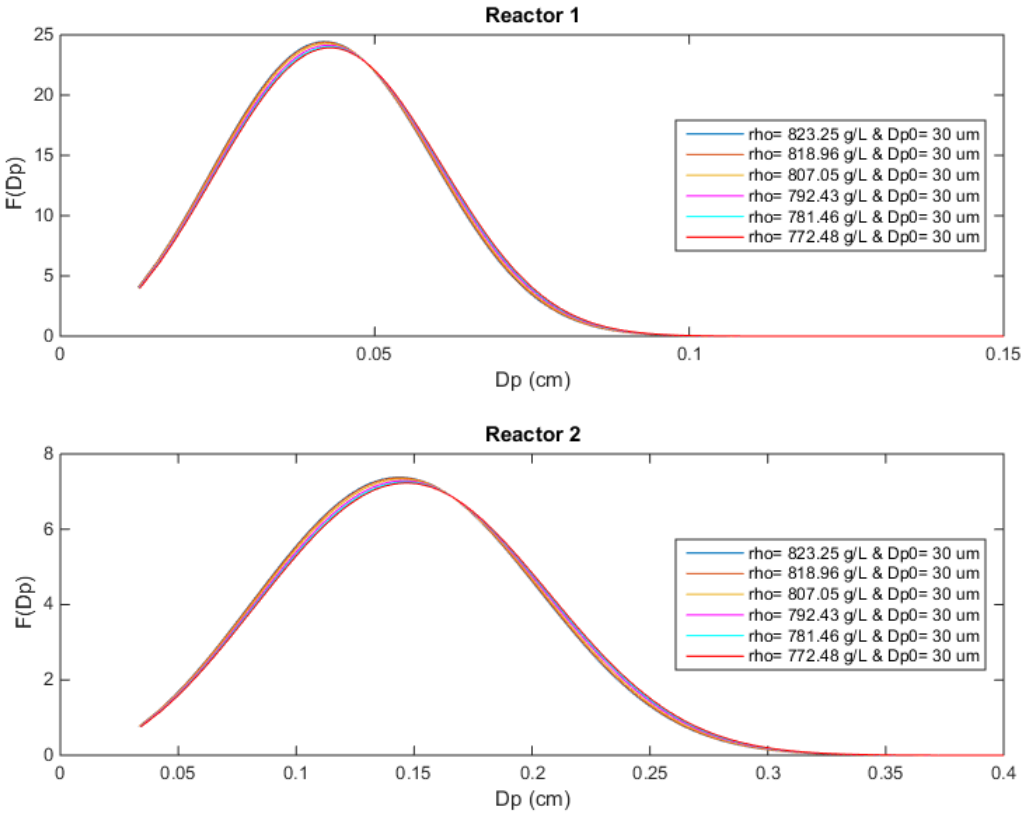

Figure 4.6: Simulation results varying only polymer density.

Figure 4.6 shows almost overlapping PSD curves, thus, a magnification is shown in the following figure. The number of curves is also reduced in order to better analyze the differences.

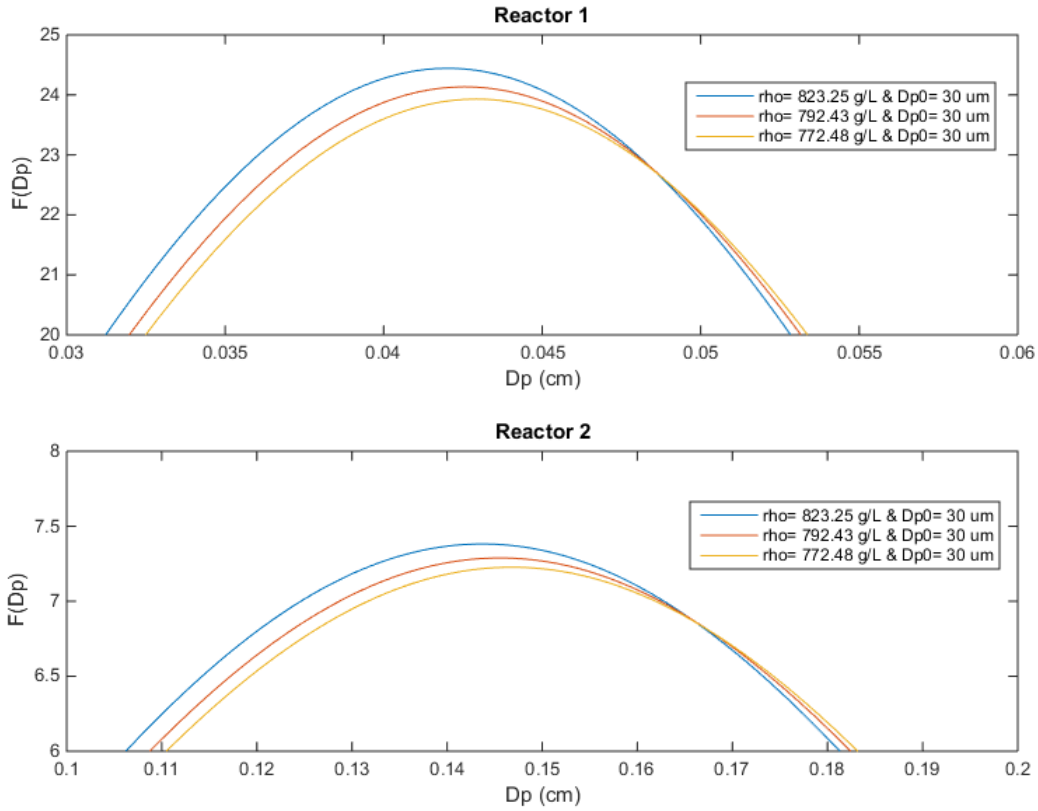

Figure 4.7: Magnification of the simulation results varying only polymer density.

The results show that a change in polymer density alone does not influence the polymer PSD significantly. It is possible to observe in figure 4.7 that by decreasing the polymer density from **823.25 g/L** to **772.48 g/L** the average particle diameter shows a very slight increase from approximately **1.437 mm** to **1.468 mm**. In other words, a decrease of 50.77 g in a dm^3 (or liter) of polymer only shows an increase of 2% in average particle diameter.

Simulation III

Simulation III analyzes the **effect of diluent type** on particle swelling and polymer PSD. As such, the simulation was ran based on experiments conducted at the same operating conditions. These conditions were: **90 ° C** temperature, **3 bar** total reactor pressure and **5 %** molar concentration of ethylene in the gas phase. The following table summarizes the parameters assumed for Simulation III.

Table 4.5: Constant parameters for Simulation III using isobutane and n-hexane as diluents.

i	2	D_p^0	30 µm
τ_1	60 min	τ_2	120 min
k_p^1	1.2 x 10^4 L/(mol.min)	k_p^2	2.4 x 10^5 L/(mol.min)
m	28.05 g/mol	C^*	1 x 10^{-3} mol/L

The parameters kept constant are the same as those used in Simulation II. The following table summarizes the different conditions obtained for each of the diluents.

Table 4.6: Parameters obtained for the diluents isobutane and n-hexane, in Simulation III.

Diluent	**isobutane**	**n-hexane**
P (bar)	3	3
T (° C	90	90
$[\mathrm{M}]$ **(mol/L)**	9.5 x 10^{-3}	3.86 x 10^{-2}
$\rho_{\mathbf{pol}}$ **(g/L)**	814.3	773.1

The following figure 4.8 shows the results of this simulation.

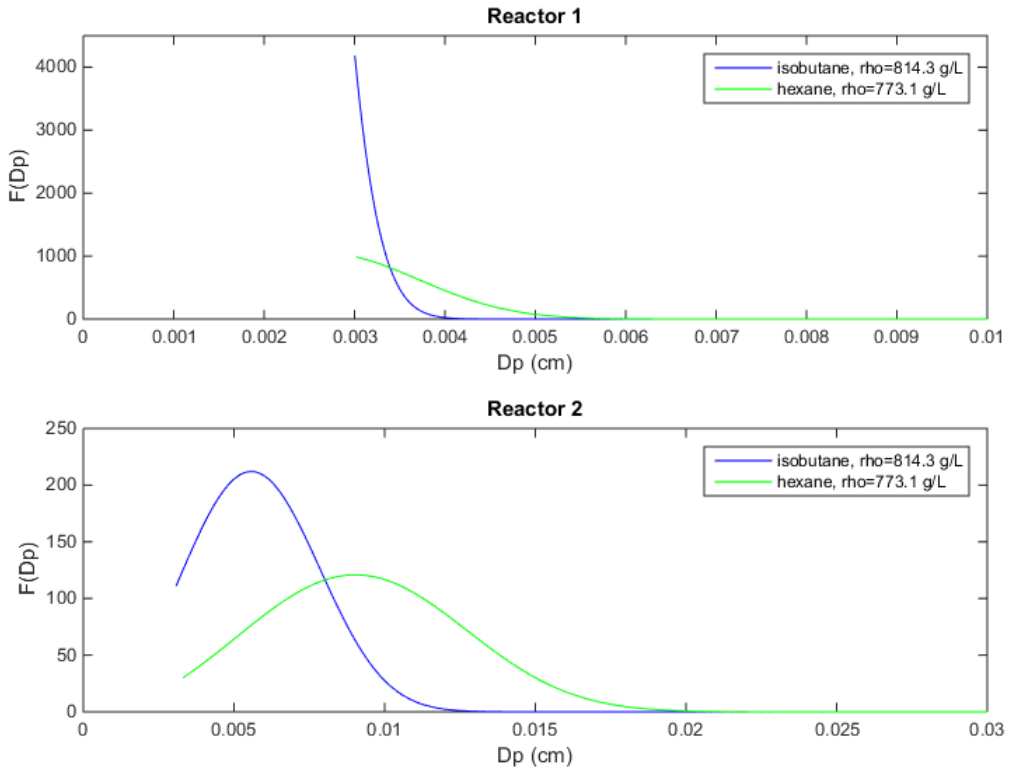

Figure 4.8: Simulation III results. Comparison between isobutane and n-hexane as diluents.

Similarly to what was observed in Simulation II, the low monomer concentrations in the first reactor combined with its lower mean residence time result in a lower productivity.

Yet it is clear that n-hexane presents a **much higher co-solubility effect** on ethylene, since the monomer concentration achieved with this diluent is significantly higher than the one obtained with isobutane.

Figure 4.8 shows that **n-hexane** causes significantly more swelling than isobutane as shown by the average particle diameter of the produced polyethylene: 56 µm for **isobutane** and 91 µm for **n-hexane**.

These results are expected due to the fact that the values predicted by Sanchez-Lacombe indicate a higher monomer concentration near the active sites for n-hexane. This entails a higher polymerization rate and thus, higher productivities (longer chains and bigger particles; more polymer). On the other hand, a higher monomer concentration means that more monomer will be solubilized in the growing polymer phase, further swelling the particles and decreasing the resulting polymer phase density.

4.2 Gas-Phase Reactor Model

In this section the results of the simulations ran for the gas-phase reactor model are discussed.

4.2.1 Summary of Data used in Simulation and Model Validation

The validation of the developed model is achieved by attempting to reproduce example 7 of US Patent 6864332 B2 [18]. Taking into account the model assumptions described earlier, the most important data assumed for the simulations is summarized in the following table 4.7.

Table 4.7: Data assumed for gas-phase reactor model simulation [5, 11, 10, 17, 19, 18, 21, 22, 23].

Parameter	Units	Value	Reference
Inlet Flow Temperature T_0	° C	35	[18, 23]
Inlet Molar Flowrate F	mol/s	11000	Assumed
Reactor Diameter d	m	4.75	[18, 21]
Reactor Bed Height h_b	m	13.3	[18, 23]
Catalyst Particle Diameter d_c	µm	50	[10]
Polymer Particle Diameter d_p	µm	500	[5]
Initial Catalyst Active Site Concentration C_0^*	mol/m^3_c	0.52	[11]
Heat Transfer Coefficient h	W/(m^2.K)	280	[17]
Catalyst Density ρ_c	kg/m^3	2300	[11]
Catalyst Heat Capacity $C_{p,c}$	J/(kg.K)	2000	[11]
Catalyst Mass Flowrate Q_c	kg/s	0.0019	Assumed
Polymer Heat Capacity $C_{p,p}$	J/(kg.K)	2000	[11]
Kinetic rate constant $k_p^{80^\circ C}$	m^3/(mol.s)	180	[11]
Catalyst deactivation rate constant $k_d^{80^\circ C}$	s^{-1}	1 x 10^{-4}	[11]
Reaction Activation Energy E_a	J/mol	42000	[11]
Catalyst Deactivation Energy E_d	J/mol	42000	[11]
Heat of Reaction ΔH_{pol}	J/mol	-107600	[11]
Fluidized Bed Porosity ε_f	-	0.55	[19]
Total Reactor Pressure P	bar	22.4	[18]
Ethylene Partial Pressure P_{Et}	bar	7	[11, 22]

The values presented in table 4.7 were taken from the presented references, with the exception of the total molar inlet flow F and catalyst flowrate Q_c. The inlet flowrate was adjusted so as to provide a value for superficial gas velocity in the adequate range (0.5 - 1 m/s), ensuring bed fluidization. The catalyst flowrate was also adjusted to obtain typical production values.

In the following table other important data taken from US Patent 6864332 B2 [18] is presented. This is the data specific to example 7, case b, in which the reactor is operated in dry mode using ethane.

The example used to validate the model was example 7b from US Patent 6864332 B2 [18]. In this case the reactor is operated in dry mode using ethane at **total reactor pressure** of **22.4 bar** and **35% ethylene molar composition**. The alkane chosen to run this simulation was **isobutane** (partial pressure of 1 bar) and an ethylene molar composition of 31.3 % was achieved under the same reactor pressure. The following table 4.8 shows the comparison between the results presented in [18] and the results obtained in the simulation.

Table 4.8: Comparison between results of example 7b of [18] and the results of the developed model simulation.

Parameter	Literature	Simulation	Variation (%)
HDPE Production (t/h)	21.6	21.4	-0.9
Reactor Temperature (° C)	88	88	0
Superficial gas velocity (m/s)	0.75	0.82	9.3

The developed model was simulated through two different methods. The **first** is a *Microsoft Excel*® workbook using the *Solver* function, where the selected solver must be the GRG Nonlinear solver, since the model is a non-linear system. The **second** method is a script developed using the software *Matlab*®, more specifically the *fsolve* function of Matlab's Optimization toolbox. The two methods' results were in agreement.

The main difference between the two methods is that while the Excel workbook solves the equations in order, thus only needing an initial approximation for the T_s variable, the Matlab *fsolve* function solves all equations simultaneously, thus needing initial approximations for all variables. This makes it a significantly sensitive method and great care must be taken when introducing the initial approximations.

Analyzing the results presented in table 4.8 it is evident that the developed model is an adequate approximation of reality. The slight difference in HDPE production can be explained by the fact that the reactor inlet compositions are very different in the two cases:

- The "real" case (example 7b of the patent) considers an inlet flow consisting of a mixture of Ethylene, Methane, Ethane, Nitrogen and Hydrogen;
- In the simulation only Ethylene, isobutane and nitrogen can be considered due to the assumptions made during the development of the model;

The difference of 9.3 % in superficial gas velocity can also be explained by the difference in inlet composition. By considering components with lower heat capacity in the model, the result is that, to achieve the same reactor temperature of 88 ° C it is necessary to increase the total molar inlet flowrate F, thus resulting in a higher superficial gas velocity, albeit within the limits of FBR operation.

Considering that a significant number of parameters presented in the literature were imposed to the model (such as reactor diameter, bed height, total reaction pressure), the developed model presents sufficiently similar results for it to be considered valid.

4.2.2 Results

In this section the results obtained with the developed model will be presented according to the following sequence:

1. A comparison will be made between **n-hexane** and **isobutane**, regarding their cosolubility effect on ethylene;
2. A series of simulations with **n-hexane** will be presented considering partial pressures of 0.1, 0.5, 0.8 and 1 bar of the alkane;
3. A series of simulations with **isobutane** will be presented considering partial pressures of 1, 3, 7 and 13 bar of the alkane;
4. A comparison between **n-hexane** and **isobutane** will be made, in terms of **polyethylene production** and **reactor behaviour**;

The results were obtained using the *Matlab*® script. They were then exported to the Excel Workbook and plotted.

Co-solubility Effect Comparison

In this section Sanchez-Lacombe predictions will be presented for two different ternary systems: **n-hexane/ethylene/HDPE** and **isobutane/ethylene/HDPE**. To analyze the alkanes' co-solubility effect on ethylene it is necessary to consider **fixed reactor pressure and fixed ethylene pressure**, and to vary the alkanes' and nitrogen pressure to keep total pressure fixed.

The first results presented here compare both n-hexane and isobutane in 10 bar reactor pressure, 7 bar ethylene pressure and alkane partial pressures varying from 0.1 to 1 bar. The results are summarized in table 4.9:

Table 4.9: Sanchez-Lacombe ethylene solubility predictions for n-hexane/ethylene/HDPE and isobutane/ethylene/HDPE ternary systems.

Alkane	Temperature (° C)	Reactor Pressure (bar)	Ethylene Pressure (bar)	Alkane Pressure (bar)	Ethylene mass fraction in HDPE (g_{Et}/g_{HDPE})
n-hexane	80	10	7	0.1	4.50×10^{-3}
				0.5	4.70×10^{-3}
				0.8	4.80×10^{-3}
				1	5.00×10^{-3}
isobutane	80	10	7	0.1	4.48×10^{-3}
				0.5	4.53×10^{-3}
				0.8	4.57×10^{-3}
				1	4.60×10^{-3}

These results are plotted in the following figure 4.9:

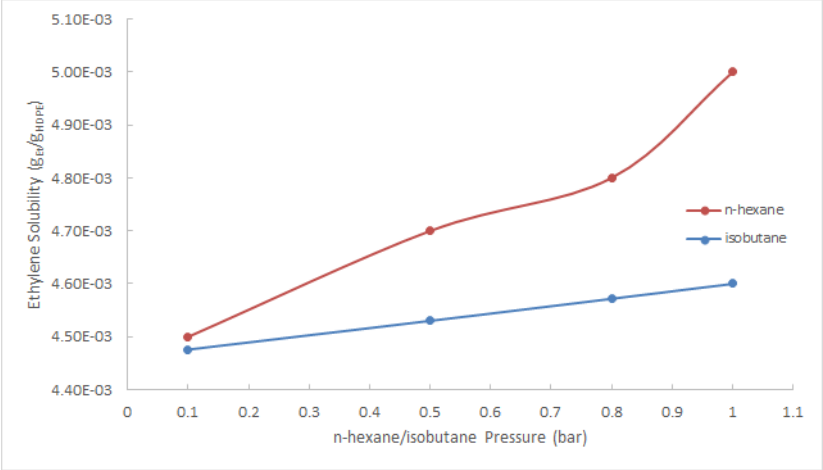

Figure 4.9: Sanchez-Lacombe ethylene solubility predictions for n-hexane/ethylene/HDPE and isobutane/ethylene/HDPE ternary systems.

Through the analysis of figure 4.9 it is possible to observe that ethylene solubility in HDPE increases using either n-hexane or isobutane and its increase accompanies the increase in partial alkane pressure. However there is an observable difference favoring n-hexane over isobutane since the solubility value achieved with n-hexane is slightly higher.

However, considering that the reactor is operated in dry mode, it is necessary to take into account the **vapor pressure** of n-hexane/isobutane. This parameter was estimated using Antoine's Equation and the following figure summarizes the difference in vapor pressure for the two alkanes in a range of common polymerization reaction temperatures (80-100 ° C).

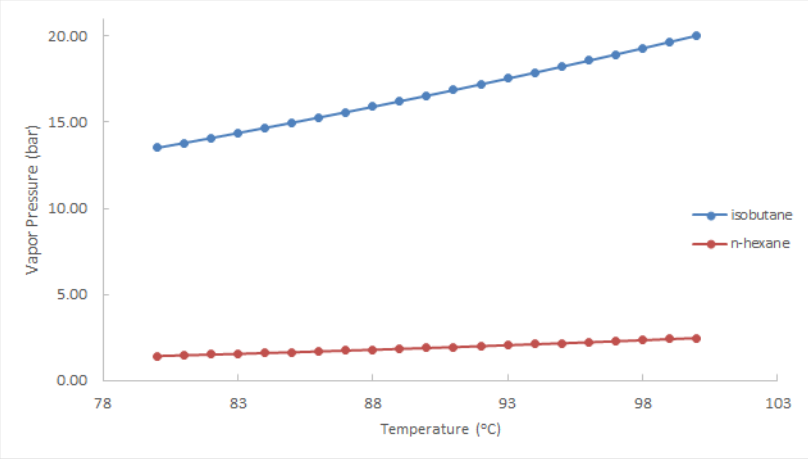

Figure 4.10: Variation of vapor pressure for n-hexane and isobutane (data obtained from [24, 25]).

In figure 4.10 the difference between the vapor pressures of n-hexane and isobutane is evident. While for n-hexane its pressure varies from 1.42 bar at 80° C to 2.47 bar at 100° C, for isobutane the values vary from 13.51 bar to 20.03 bar for the same temperature range.

This implies that it is possible to introduce a much greater quantity of isobutane in the reactor than n-hexane, while still maintaining dry mode operation.

On another note, the values presented here are the basis for the partial pressures of n-hexane/isobutane chosen for the following simulations.

Simulation I

Simulation I analyzes the effect of increasing **n-hexane partial pressure** in polyethylene production and reactor behaviour. The parameters used for the simulation were the same ones described in table 4.7.

The following table summarizes the results obtained from simulation I.

Table 4.10: Reactor model simulation results for n-hexane partial pressure of 0.1, 0.5, 0.8 and 1 bar and constant ethylene partial pressure of 7 bar.

$\mathbf{P_{hex}}$ (bar)	$\mathbf{Q_{PE}}$ (t/h)	$\mathbf{T_b}$ (° C)	$\mathbf{T_s}$ (° C)	Productivity (g PE/g cat)	Per Pass Conversion (%)	$\mathbf{u_g}$ (m/s)
0.1	21.2	92.3	98.6	3095	6.1	0.824
0.5	21.9	90.7	97.3	3206	6.3	0.820
0.8	22.2	89.0	95.7	3247	6.4	0.816
1	23.2	89.7	96.6	3385	6.7	0.818

The following figures represent the plotted results shown in table 4.10.

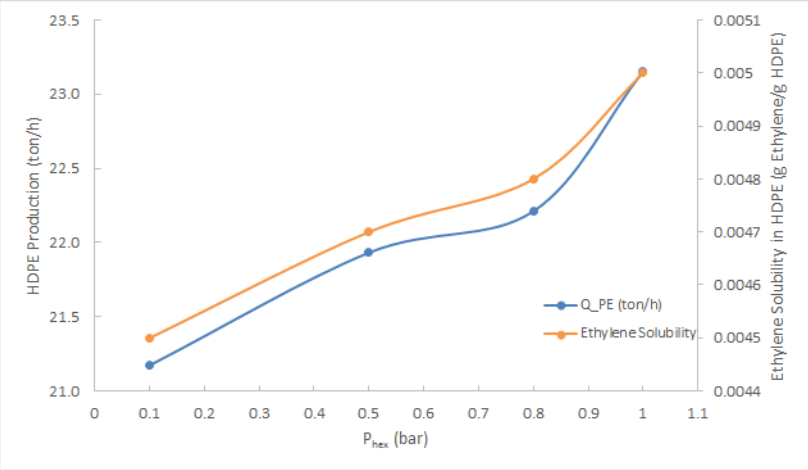

Figure 4.11: Simulation I HDPE production flowrate results.

In figure 4.11 it is possible to observe an evident increase in HDPE production with the addition of more n-hexane.

The presence of more n-hexane inside the reactor increases the solubility of ethylene in HDPE and, thus, the ethylene concentration near the catalyst active sites. Additionally, by increasing the partial pressure of n-hexane, the molar composition of the gaseous inlet stream is being changed and, since n-hexane possesses a higher molecular weight and heat capacity than both ethylene and nitrogen, the gaseous inlet mass flowrate increases and it removes more heat (as shown in the following figure 4.12).

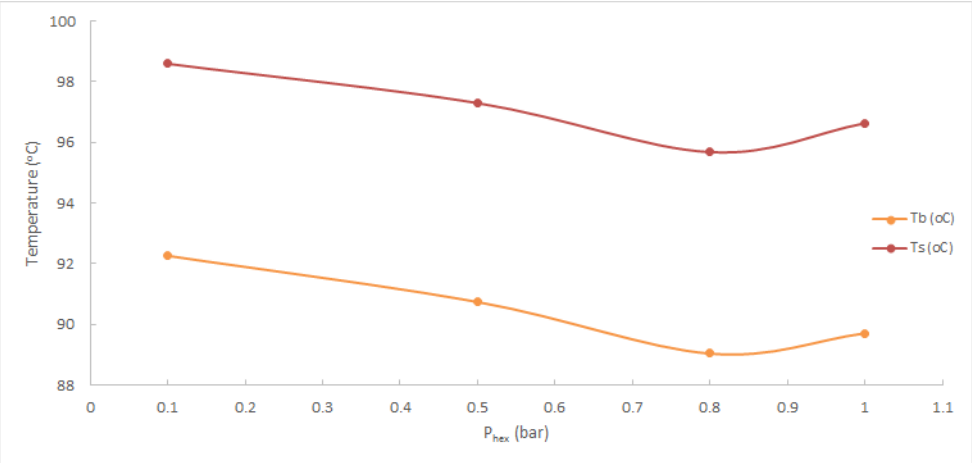

Figure 4.12: Simulation I bulk and solids temperature results.

In this figure a tendency to **decrease both bulk and solids temperature** (T_b and T_s, respectively) is expectedly observed, due to the fact that the increase in n-hexane partial pressure also increases the gas stream heat capacity.

However a slight temperature increase is observed from 0.8 bar to 1 bar. This increase is explained by the **ethylene solubility values** predicted by Sanchez-Lacombe EOS (shown in figure 4.11). Changing n-hexane partial pressure from 0.8 bar to 1 bar Sanchez-Lacombe predicts a steeper increase in ethylene solubility than the ones observed in lower n-hexane pressures. This leads to an value of HDPE production of such an order that **the increase in gas mass flowrate is not enough** to further decrease the reactor temperature.

Nevertheless, the reactor bulk gas phase temperature for 1 bar n-hexane partial pressure (87.8° C) is still lower than the temperature for 0.1 or 0.5 bar (89.1 and 88.2° C, respectively) and the HDPE production is significantly greater (21 ton/h to 23 ton/h).

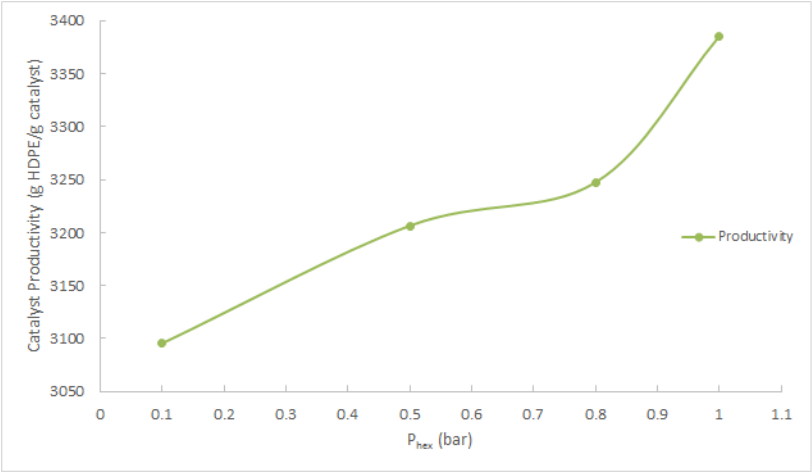

Figure 4.13: Simulation I catalyst productivity results.

Regarding catalyst productivity, it is possible to observe that a general **increase** is observed with greater n-hexane partial pressure. This increase can once again be explained by the values of ethylene solubility predicted by Sanchez-Lacombe EOS.

It is interesting, however, to compare the trend of catalyst productivity with the trend observed in temperature (figure 4.12), indicating that heat removal is essential for good reactor operation but other aspects exist that affect production and productivity.

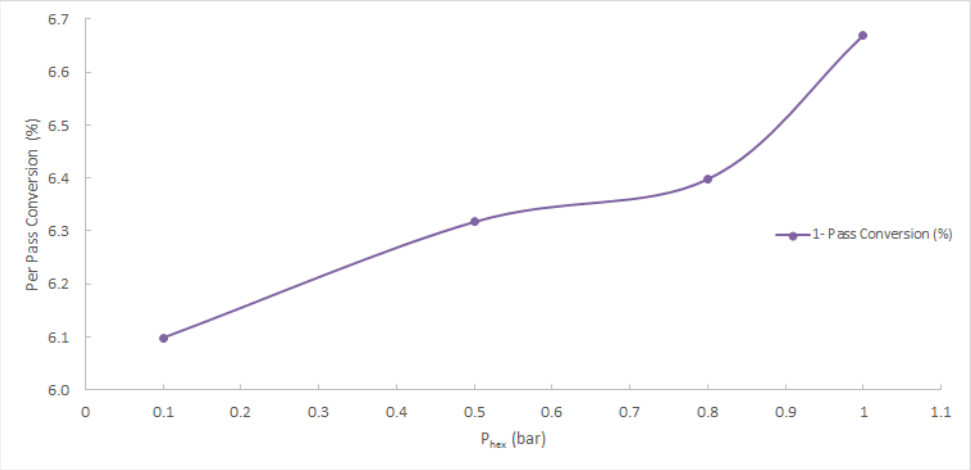

Figure 4.14: Simulation I reaction per pass conversion results.

Figure 4.14 shows, as expected, a general increase in monomer conversion per pass with greater n-hexane partial pressures.

In terms of superficial gas velocity (u_g) it is possible to observe that the difference in values is negligible and that the values are well within the typical range to ensure bed fluidization (0.5 - 1 m/s). This is due to the fact that, while mass flowrate is chaging in a significant order, the change in reactor temperature causes the volumetric flowrate to remain almost constant.

Simulation II

For this simulation the parameters assumed are the same as in simulation I (subsection 4.2.2), with the exception of the addition of **isobutane** instead of n-hexane and the isobutane partial pressures considered being 1, 3, 7 and 13 bar.

The results of the simulation are summarized in the following table:

Table 4.11: Reactor model simulation results for isobutane partial pressure of 1, 3, 7 and 13 bar, and constant ethylene partial pressure of 7 bar.

$\mathbf{P_{isobut}}$ **(bar)**	$\mathbf{Q_{PE}}$ **(t/h)**	$\mathbf{T_b}$ **(° C)**	$\mathbf{T_s}$ **(° C)**	**Productivity (g PE/g cat)**	**Per Pass Conversion (%)**	$\mathbf{u_g}$ **(m/s)**
1	21.4	88.4	94.8	3122	6.2	0.815
3	22.0	81.9	88.4	3220	6.3	0.800
7	23.9	74.2	81.4	3495	6.9	0.783
13	28.1	69.3	77.7	4107	8.1	0.772

The first observation to take out of table 4.11 is that, due to the higher pressures of isobutane added to the gaseous stream, the difference of values is more evident when compared with Simulation I.

One crucial aspect is that the **vapor pressure** of isobutane for the temperature of 69.3° C is 10.7 bar and the simulation is considering 13 bar of isobutane partial pressure. In these conditions a vapor-liquid equilibrium is established and the reactor can not be considered in dry mode operation. As such, the simulation was ran once more with a different value of F (total gaseous inlet molar flowrate). Instead of the initially assumed 11000 mol/s, a value of 8000 mol/s was assumed.

The following table 4.12 shows the new results.

Table 4.12: Reactor model simulation results for isobutane partial pressure of 1, 3, 7 and 13 bar, constant ethylene partial pressure of 7 bar and total inlet molar flowrate of 8000 mol/s.

$\mathbf{P_{isobut}}$ **(bar)**	$\mathbf{Q_{PE}}$ **(t/h)**	$\mathbf{T_b}$ **(° C)**	$\mathbf{T_s}$ **(° C)**	**Productivity (g PE/g cat)**	**Per Pass Conversion (%)**	$\mathbf{u_g}$ **(m/s)**
1	22.5	111.2	117.9	3285	8.9	0.630
3	23.4	102.4	109.4	3424	9.3	0.616
7	25.8	92.0	99.7	3766	10.2	0.599
13	30.5	85.1	94.2	4452	12.1	0.587

The results presented in table 4.12 now **allow** for 13 bar of isobutane partial pressure while maintaining dry mode operation, due to the temperature increase to 85.1 ° C, effectively raising the isobutane vapor pressure to 15 bar.

The following figures represent the plotted results described in table 4.12.

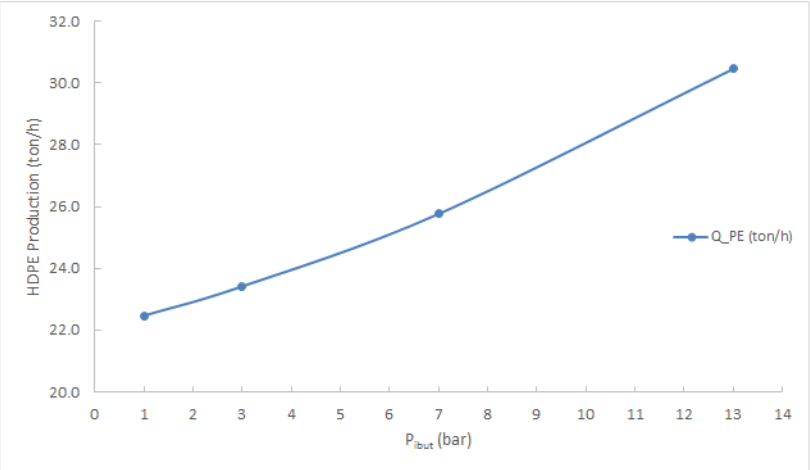

Figure 4.15: Simulation II HDPE production flowrate results.

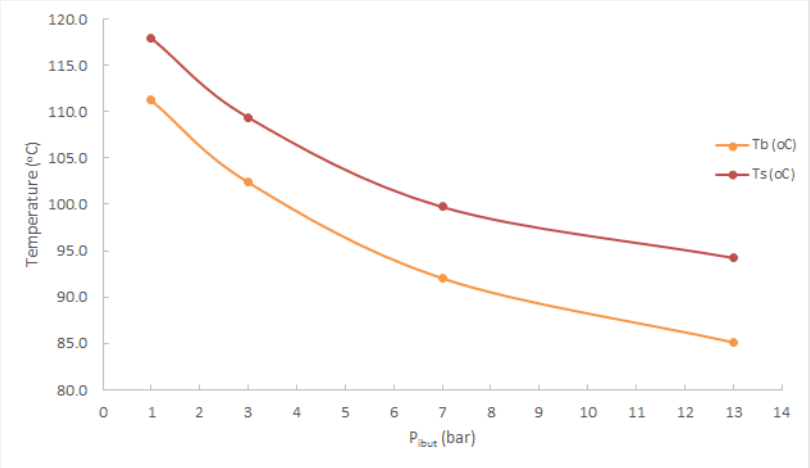

Figure 4.16: Simulation II bulk and solids temperature results.

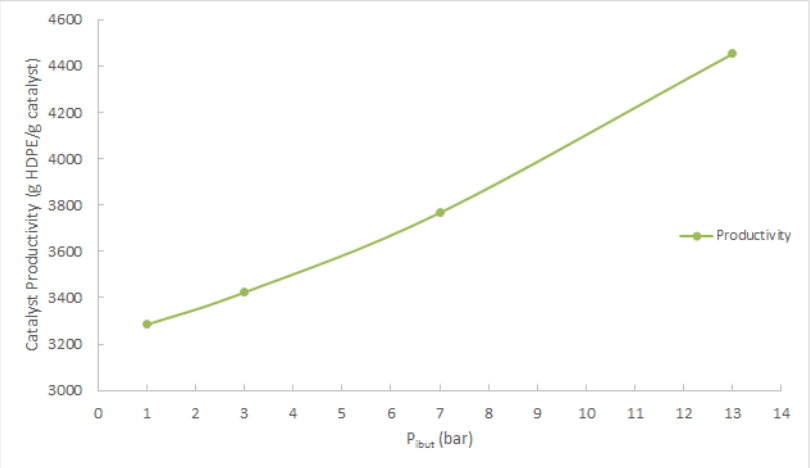

Figure 4.17: Simulation II catalyst productivity results.

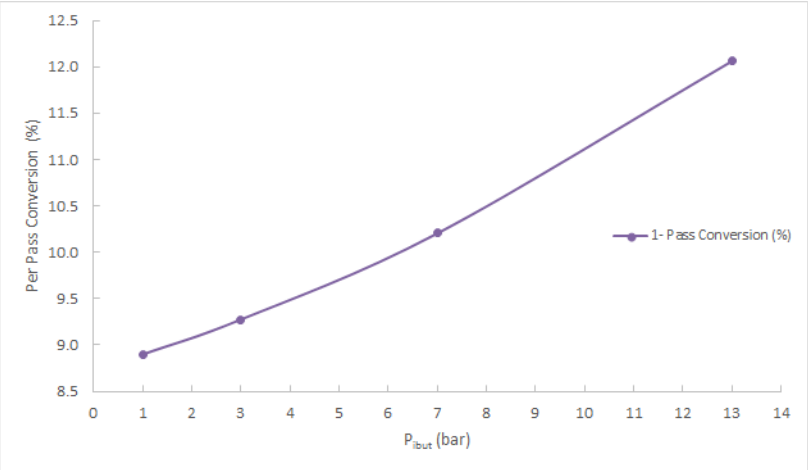

Figure 4.18: Simulation II reaction per pass conversion results.

The overall trends observed in this simulation are similar to those observed in Simulation I. The differences between the two are the higher values of production obtained using isobutane, essentially due to its higher vapor pressure, thus allowing to introduce a greater quantity of alkane while still guaranteeing dry mode operation.

The following figures analyze the effect of inlet molar flowrate in HDPE production and reactor temperature, as analyzed in tables 4.11 and 4.12. The parameters assumed were the same, the isobutane partial pressure was kept constant at 7 bar and molar inlet flowrate was varied between 8000 and 11000 mol/s.

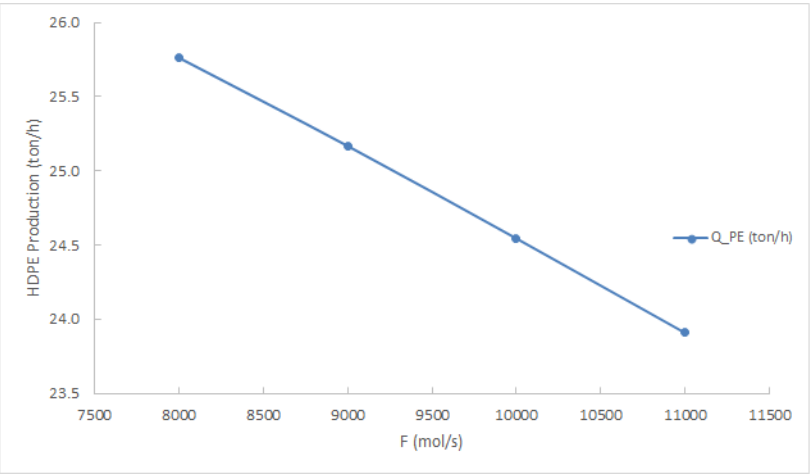

Figure 4.19: Simulation results for HDPE Production dependence on inlet molar flowrate.

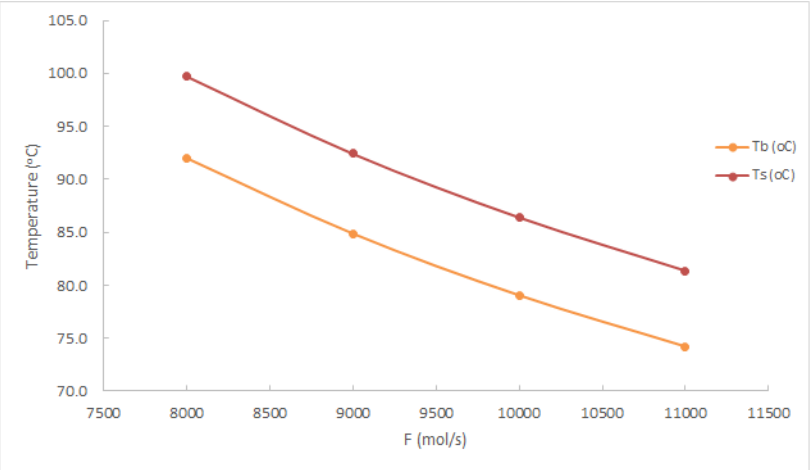

Figure 4.20: Simulation results for reactor temperature dependence on inlet molar flowrate.

One other relevant aspect is the increase in production (Q_{PE}), temperature (T_b and T_s), productivity and per pass conversion, when comparing tables 4.11 and 4.12. This aspect can be observed in figures 4.19 and 4.20. The trend shows an **increase** of HDPE production (and therefore, productivity and conversion as well) with the **decrease** in inlet molar flowrate F.

This increase of such values is expected, essentially due to two reasons: the **first** is the increase of the particle's residence time in the reactor and the **second** is the strong dependence of kinetic parameters on temperature.

With lower values of gas inlet flowrate the gaseous stream removes less heat and both the solids temperature T_s and the bulk phase temperature T_b increase. This in turn increases the polymerization rate and, thus, the values of production, productivity and conversion.

However, in terms of industrial applications, it is necessary to take other aspects into account such as the superficial gas velocity u_g, the polymer melt temperature (approximately 135° C for HDPE) and the formation of hotspots that can lead to particle agglomeration and poor reactor performance.

Therefore, while it seems intuitive (considering this model) to decrease the inlet molar flowrate F in order to achieve higher production values, there are certain constraints that must be respected in order to guarantee a safe reactor operation. For instance, the lowest value of F that is possible to assume in this simulation is approximately 6500 mol/s because, while the polymer phase temperature is still 107° C), the superficial gas velocity is 0.50 m/s which is the lowest acceptable velocity to ensure bed fluidization.

N-hexane and Isobutane Results Comparison

Rather than running an altogether new simulation, this section **compares** the results for **isobutane** and **n-hexane** in simulations I and II ran under the same conditions. These conditions are summarized in the following table:

Table 4.13: Data assumed for simulation III.

Parameter	Units	Value
Reaction Pressure P	bar	22.4
n-hexane/isobutane Pressure	bar	1
Inlet Molar Flowrate F	mol/s	8000

The data not specified in previous table 4.13 is assumed according to table 4.7.

The results comparison is summarized in the following table:

Table 4.14: Simulation III results. Comparison between n-hexane and isobutane.

Parameter	Units	n-hexane	isobutane
HDPE Production $\mathbf{Q_{PE}}$	ton/h	24.3	22.5
Bulk Temperature $\mathbf{T_b}$	$^\circ$ C	112.7	111.2
Solids Temperature $\mathbf{T_b}$	$^\circ$ C	120.0	117.9
Productivity	$g_{HDPE}/g_{catalyst}$	3550	3285
Per Pass Conversion	%	9.6	8.9
Superficial gas velocity $\mathbf{u_g}$	m/s	0.633	0.630

Analyzing the results presented in table 4.14 it is evident that for the same operating conditions (including component partial pressure) n-hexane presents better production results than isobutane, due to a stronger co-solubility effect, as was observed in subsection 4.2.2.

In terms of temperature (T_b and T_s), however, isobutane is able to achieve slightly lower temperatures than n-hexane. Although n-hexane presents higher molecular weight and heat capacity than isobutane, these results are once again related to the Sanchez-Lacombe predictions of ethylene solubility in HDPE.

Ethylene presents a higher solubility in the presence of n-hexane, thus increasing polymerization rate and the amount of heat released. Despite the higher heat capacity, the gaseous stream is not able to absorb enough heat to achieve lower temperatures than isobutane, although the difference of 1.5° C is not relevant.

The differences in productivity and per pass conversion are consistent with the difference in production and the values of superficial gas velocity (u_g) are very similar.

4.2.3 Sensitivity Analysis

A sensitivity analysis was conducted in order to determine the parameters that most influence the model outputs (Q_{PE}, T_b, T_s, Productivity, Per Pass Conversion and u_g). In this section five parameters analysis will be presented and discussed. More sensitivity analysis results can be consulted in Appendix B.

The data assumed for the simulation will be the one considered in simulation I (section 4.2.2) with an n-hexane partial pressure of 0.5 bar. The reason for this choice was so that it would be possible to vary the parameter in the sensitivity analysis to higher or lower values. The parameters discussed here will be:

- Catalyst activity, varying $k_p^{T_{ref}}$;
- Alkane heat capacity C_p;
- Ethylene solubility in HDPE, varying C_{Et}^P;
- Alkane partial pressure, varying P_{hex};
- Inlet Flow Temperature, varying T_0;

The catalyst activity is an important parameter to analyze. Not only is catalyst activity directly relate to HDPE production but it is also related to the reactor and solids temperature due to the change in polymerization heat released. Catalyst activity may vary depending on the type of catalyst used, so variations of $\pm$ 10 and 50 % to $k_p^{T_{ref}}$ were considered.

The alkane's heat capacity is also an essential parameter for the model. In reactor operation it is possible to change the composition of the inlet feed to allow for more or less heat absorption, by changing the the introduced alkane or even a mixture of alkanes (though in such case an analysis must be conducted to predict the co-solubility and anti-solubility effects in question). Variations of $\pm$ 10 and 50 % to C_p based on n-hexane heat capacity ($C_{p,hex}$) were considered.

Ethylene solubility in the growing polymer phase is, as discussed before, one of the most important parameters in the kinetic equations. It defines the effective concentration of monomer that is available near the catalyst active sites for polymerization. Variations of $\pm$ 10 and 20 % were considered to C_{Et}^p.

Another parameter to analyze will be the n-hexane partial pressure. Considering the objectives of this work this as crucial paremeter. The quantity of n-hexane present in the reactor has effect on heat absorption, ethylene solubility in HDPE and, therefore, HDPE production, productivity and conversion. Variations of 100 % and - 80 % were considered due to the fact that Sanchez-Lacombe EOS data is needed and is only available for the n-hexane pressures of 0.1, 0.5, 0.8 and 1 bar.

The final analyzed parameter will be inlet flow temperature T_0. It is interesting to observe how a difference in the temperature of the inlet stream will affect the production and temperature of the reactor. Variations of $\pm$ 5 and 10 $^\circ$C will be considered.

The following table presents the sensitivity analysis results for catalyst activity:

Table 4.15: Sensitivity analysis results for the variation of $k_p^{T_{tref}}$.

Parameter Varied: $k_p^{T_{tref}}$						
Variation	$\mathbf{\Delta Q_{PE}}$ **(%)**	$\mathbf{\Delta T_b}$ **(%)**	$\mathbf{\Delta T_s}$ **(%)**	**ΔProductivity (%)**	**Δ1-P. Conv. (%)**	$\mathbf{\Delta u_g}$ **(%)**
+ 10 %	12.1	7.2	7.5	12.1	12.1	1.8
+ 50 %	58.9	34.3	35.9	58.9	58.9	8.5
- 10 %	-12.3	-7.3	-7.7	-12.3	-12.3	-1.8
- 50 %	-62.1	-37.6	-39.2	-62.1	-62.1	-9.4

In table 4.15 it is possible to observe that a variation in catalyst activity influences the results in a significant manner. A variation of + 10 % in $k_p^{T_{tref}}$ produces an increase of 12.1 % in production, productivity and conversion, an increase of 7.2 and 7.5 % in T_b and T_s, respectively, and an increase of 1.8% in superficial gas velocity.

The increase in production is related to the increase in kinetic propagation rate at the reference temperature of 80° C. Since the k_p presents an Arrhenius Law dependence on temperature, the production and related parameters are very sensitive to a variation in $k_p^{T_{tref}}$.

The variation in both temperatures is essentially related to the increase in production. With higher production there is a higher ammount of polymerization heat being released but since there is no exponential dependence of the heat balance parameters on temperature, the observed variation in T_b and T_s is lower than the one observed in production.

As for the variation in superficial gas velocity, the difference is not relevant due to the fact that the main cause is the change in temperature and, therefore, the volumetric flowrate.

When changing the value variation from + 10% to + 50 % the variations of the output parameters changes five fold, expectedly. Negative variations (-10 and -50 %), however, appear to have a stronger effect on the output parameters. This is due to the fact that the developed model is not linear.

The next table 4.16 shows the results for the sensitivity analysis varying the alkane's C_p:

Table 4.16: Sensitivity analysis results for the variation of the alkane's C_p.

Parameter Varied: $C_{p,hex}$						
Variation	$\mathbf{\Delta Q_{PE}}$ **(%)**	$\mathbf{\Delta T_b}$ **(%)**	$\mathbf{\Delta T_s}$ **(%)**	**ΔProductivity (%)**	**Δ1-P. Conv. (%)**	$\mathbf{\Delta u_g}$ **(%)**
+ 10 %	-0.2	-0.7	-0.6	-0.2	-0.2	-0.2
+ 50 %	-0.9	-3.2	-3.0	-0.9	-0.9	-0.8
- 10 %	0.2	0.7	0.6	0.2	0.2	0.2
- 50 %	0.9	3.5	3.3	0.9	0.9	0.9

The results of table 4.16 show that a change of even $\pm$ 50% in the heavy alkane's C_p does not originate significant differences in most parameters.

As expected the bulk gas phase temperature T_b and the polymer phase temperature T_s are the most influenced parameters (-3.2% and -3.0% respectively for a + 50% variation in C_p) due to the immediate

change in heat capacity, conditioning heat absorption. This change in temperatures is then related to the slight changes in production, productivity and conversion. The superficial gas velocity u_g also presents very slight differences resulting from the alteration of volumetric flowrate.

As observed in table 4.15 a change of +10 % to +50% in C_p also changes the parameters five fold and the negative variations (- 10% and - 50%) also appear to generate more difference in output variables.

The following table 4.17 presents the results of the sensitivity analysis by changing ethylene solubility as seen in C_{Et}^P:

Table 4.17: Sensitivity analysis results for the variation of ethylene solubility in HDPE, as seen in C_{Et}^P.

Parameter Varied: C_{Et}^P						
Variation	$\mathbf{\Delta Q_{PE}}$ **(%)**	$\mathbf{\Delta T_b}$ **(%)**	$\mathbf{\Delta T_s}$ **(%)**	**ΔProductivity (%)**	**Δ1-P. Conv. (%)**	$\mathbf{\Delta u_g}$ **(%)**
+ 10 %	12.1	7.2	7.5	12.1	12.1	1.8
+ 20 %	58.9	34.3	36.0	58.9	58.9	8.6
- 10 %	-12.3	-7.3	-7.7	-12.3	-12.3	-1.8
- 20 %	-62.1	-37.6	-39.2	-62.1	-62.1	-9.4

In the first place it is important to mention that the maximum variation was changed from $\pm$ 50% in the previous parameters to $\pm$ 20% in ethylene solubility to account for more realistic situations.

It is possible to observe in table 4.17 that a variation of 10% in C_{Et}^P causes the same differences in output values as a variation of 10% in $k_p^{T_{ref}}$. This is to be expected since the polymerization rate defined by equation 3.24 presents first order dependence on both terms.

The next table (4.18) summarizes the results of the sensitivity analysis while varying the alkane's partial pressure, as seen in P_{hex}:

Table 4.18: Sensitivity analysis results for the variation of n-hexane partial pressure P_{hex}.

Parameter Varied: P_{hex}						
Variation	$\mathbf{\Delta Q_{PE}}$ **(%)**	$\mathbf{\Delta T_b}$ **(%)**	$\mathbf{\Delta T_s}$ **(%)**	**ΔProductivity (%)**	**Δ1-P. Conv. (%)**	$\mathbf{\Delta u_g}$ **(%)**
+ 100 %	5.6	-1.1	-0.7	5.6	5.6	-0.3
- 80 %	-3.5	1.7	1.3	-3.5	-3.5	0.4

Table 4.18 shows that a variation in P_{hex} causes a significant difference in production, productivity and conversion values. This is due to the difference in ethylene solubility that increases or decreases depending on the amount of n-hexane in the reactor.

The two temperatures, however, are less affected by the change in n-hexane partial pressure. The bulk gas phase temperature T_b presents a slightly difference than T_s due to the fact that the amount of n-hexane present in the gas-phase directly modifies the average heat capacity and therefore changes the temperature, albeit slightly. The difference in superficial gas velocity u_g arises from the change in temperature and is negligible.

The following table 4.19 summarizes the results of the sensitivity analysis while varying the inlet flow temperature T_0:

Table 4.19: Sensitivity analysis results for the variation of inlet flow temperature T_0.

Parameter Varied: T_0						
Variation	$\mathbf{\Delta Q_{PE}}$ **(%)**	$\mathbf{\Delta T_b}$ **(%)**	$\mathbf{\Delta T_s}$ **(%)**	**ΔProductivity (%)**	**Δ1-P. Conv. (%)**	$\mathbf{\Delta u_g}$ **(%)**
+ 5 ° C	1.5	6.1	5.8	1.5	1.5	1.5
+ 10 ° C	2.8	12.0	11.4	2.8	2.8	3.0
- 5 ° C	-2.0	-6.4	-6.1	-2.0	-2.0	-1.6
- 10 ° C	-4.7	-13.2	-12.6	-4.7	-4.7	-3.3

The results from table 4.19 show a moderate effect of inlet flow temperature in production, productivity and conversion and a more significant effect on T_s and T_b. However slight, the decrease/increase in production shown when decreasing/increasing the inlet flow temperature T_0 is once again related to the CSTR approach. A higher inlet temperature results in higher temperature increase within the reactor, which increases the rate of polymerization R_p. The superficial gas velocity u_g is affected due to the density changes of the gas phase inside the reactor, which in turn changes the volumetric flow of the gaseous stream fluidizing the bed.

Chapter 5

Conclusions

The production of polyethylene is one of the most important aspects of the modern polyolefin industry. Polyethylene is a commodity and, as such, generates large sales volumes worldwide. The increase of its production is a continuous work and mathematical models play an important role in such work. The following section contains the conclusions of the developed models and is divided into two sections.

5.1 Particle Size Distribution Model

The particle size distribution of a polymer is one of its most important defining properties. In industry it affects not only the most obvious parameters such as polymer volume but it also presents important ramifications in operations downstream of the reactor, such as polymer degassing. Therefore, the advantages of models such as the one developed are evident.

Regarding the analysis of the simulations it is possible to conclude that the polymer density does not significantly influence the polymer PSD (although lower densities lead to broader PSD), especially taking into account that usual density ranges for polyethylenes are in the 0.90 - 0.96 g/cm^3.

On the other hand, changing the initial catalyst particle diameter yields much more significant results. As expected the increase in catalyst particle diameter yields broader PSD with much higher polymer particle diameters. This is a significant conclusion due to the fact that industrial catalysts have various particle diameters and the developed model considers only a single value for said diameter. Thus considering various diameters allows for a simulation that provides results closer to a real situation.

The variation of total reactor pressure analyzed in simulation II shows that increasing the reaction pressure broadens the PSD and increases the mean particle diameter D_p. This happens due to the fact that, by increasing reactor pressure, the solubility of the monomer in the diluent and in the polymer phase increases and, thus, the polymerization rate as well.

However by changing the reactor pressure from **3 bar** to **20 bar**, the mean particle diameter only increases from about **70** µm to about **150** µm. Although this translates into more than twice the diameter,

the increase in reactor pressure is quite severe, as the final reactor pressure considered is almost **7 times** greater than the initial one.

In the final simulation it is possible to conclude that the type of diluent is crucial for the PSD. Considering a reaction conducted at **the same operating conditions** (pressure, temperature and feed composition) it was possible to observe that using **hexane** as a diluent, instead of isobutane, the result was a polyethylene presenting a 62.5% higher average polymer size. This is related to a **greater co-solubility effect** (as was shown in section 4.2.2) on ethylene, as predicted by the **Sanchez-Lacombe EOS** thermodynamic model.

5.2 Gas-Phase Reactor Model

The developed model contemplates one of the most common industrial situations for the production of polyethylene, the gas-phase fluidized bed reactor. It is able to predict polyethylene **production**, **reactor temperature** and other parameters such as productivity, per pass monomer conversion and superficial gas velocity for **steady-state dry mode operation** with different alkanes acting as induced condensing agents.

On a side note, since this work compares the model results obtained using two different alkanes, **n-hexane** and **isobutane**, a comparison between the two was made in order to determine their **co-solubility effect** on ethylene in high density polyethylene.

The alkane whose presence most increases ethylene solubility in HDPE was found to be **n-hexane**, considering the same moles of alkane in the system. However, the vapor pressure of isobutane is significantly higher than the one of n-hexane, thus allowing it to be introduced in much higher quantities in the reactor.

Regarding validation, the model was compared with the results of example 7b of US Patent 6864332 B2. The same reactor diameter (d), catalyst bed height (h_b) and reactor pressure were considered. The composition of the feed was adjusted.

The values predicted by the model deviated from the patent in **0.9%** for HDPE Production (Q_{PE}), **0%** for reactor temperature (T_b) and **1.4%** for superficial gas velocity. As such, the model can be considered **a good approximation** to reality.

Considering simulations I and II, it is possible to conclude that **increasing** the induced condensing agent's **partial pressure** increases polymer production and lowers the reactor temperature, in general. The exception was found for the case of **n-hexane**, in which from 0.8 bar to 1 bar the HDPE production flowrate increased abruptly and a slight increase in reactor temperature was observed. The increased temperature, however, is still lower than the simulation for 0.1 bar of n-hexane.

In the case of **isobutane** it was possible to introduce greater quantities of the alkane and achieve higher production values and lower temperatures than the n-hexane simulation, despite its lower heat capacity and co-solubility effect.

It was also found that reducing the inlet flowrate increases both production and temperatures. However, the conclusion is that there is a minimum value at which it is not possible to further decrease the inlet flowrate, as it would not respect essential constraints, such as polymer melt temperature and bed fluidization.

From the comparison between model results using n-hexane or isobutane it is possible to obtain the same conclusions that were taken from the alkane comparison regarding monomer solubility in the polymer phase. As expected, considering the same partial pressure and therefore the same number of moles, the model predicts higher production, productivity and conversion results for n-hexane. The temperatures, while higher than the isobutane simulation, are very similar as well as the values of superficial gas velocity.

In short it is possible to conclude that a higher ammount of each of the alkanes increases production and decreases temperature; for the same pressure of each alkane, n-hexane presents the best productivity results; in general, using isobutane is favorable since it allows for higher production.

By running a sensitivity analysis it is possible to conclude that the most influencial parameters for model output are the **catalyst's activity** ($k_p^{T_{ref}}$) and **ethylene solubility** in the polymer (C_{Et}^P). Contrary to what was expected, the alkane's **heat capacity** (C_p) did not have much influence on production, although it shows influence on the bulk reactor temperature (T_b). However, since the heat capacity also depends on temperature it is possible that greater variations are needed to observe a significant effect on production.

The alkane's **partial pressure** is a parameter than significantly influences reactor production, as opposed to tempeature.

The developed model is an extremely simplified one, only able to give simple information regarding the process. Future development of this model is of paramount importance in order to obtain more detailed information about the reactor and reaction environment. In the following section 5.3 suggestions will be made regarding the future perspectives of the model development.

5.3 Future Development

Regarding the PSD prediction model future development includes:

- The introduction of catalyst deactivation;
- The introduction of real reactor residence time distributions;
- The introduction of catalyst PSD as input instead of a single catalyst particle diameter;
- The application of the model for processes other than slurry phase;

For the case of the gas-phase reactor model the future development of the model is related to:

- The adaptation of the model to transient state;
- The incorporation of a thermodynamic model that allows the user to consider more components in the reactor;
- The introduction of a more complex thermodynamic model to predict the properties of the gas phase;
- Modeling of condensed mode operation;
- Modeling of polymer swelling in the reactor

There are many more advances that can be made in either model. However, a cost-benefit analysis must be made in order to determine whether the effort required to add more features to the models results in meaningful and beneficial information.

Bibliography

[1] A. J. Peacock. *Handbook of Polyethylene: Structures: Properties and Applications*. CRC Press, 1^{st} edition, 2000. ISBN-10: 0824795466.

[2] A. Azeem. Polyethylene maufacturing and its properties. Textile Chemical Processing. National Textile University.

[3] E. Sagel. Polyethylene global overview. Foro Pemex, June 2012.

[4] K. Yoshio. Global outlook of polyolefin business. Sumitomo Chemical (Asia Pacific) Pte Ltd, September 2011.

[5] J. B. P. Soares and T. F. L. McKenna. *Polyolefin Reaction Engineering*. Wiley-VCH, 1^{st} edition, 2012. Print ISBN: 978-3-527-31710-3.

[6] J. B. Soares and A. E. Hamielec. Effect of reactor residence time distribution on the size distribution of polymer particles made with heterogeneous ziegler-natta and supported metallocene catalysts. a generic mathematical model. *Macromolecular Theory and Simulations*, 4(6):1085–1104, November 1995.

[7] Chemical reactors. `http://www.essentialchemicalindustry.org/processes/chemical-reactors.html`, March 2013. Online; Accessed 28-08-2015.

[8] H. HOKANNEN. Process for manufacture lldpe polymers, Nov. 1999. URL `https://www.lens.org/lens/patent/US_5986021_A`.

[9] T. C. Mun. Production of polyethylene using gas fluidized bed reactor. *National University of Singapore*, HT022626U:1–20, 2005.

[10] T. Xie, K. B. McAuley, J. C. C. Hsu, and D. W. Bacon. Gas phase ethylene polymerization: Production processes, polymer properties, and reactor modeling. *Industrial & Engineering Chemistry Research*, 33(3):449–479, March 1994.

[11] A. Alizadeh. *Study of Sorption, Heat and Mass Transfer During Condensed Mode Operation of Gas Phase Ethylene Polymerization on Supported Catalyst*. PhD thesis, Queen's University, July 2014.

[12] M. A. Bashir, M. A.-h. Ali, V. Kanellopoulos, and J. Seppala. Modelling of multicomponent olefins solubility in polyolefins using sanchez–lacombe equation of state. *Fluid Phase Equilibria*, 358: 83–90, November 2013.

[13] W. Ray and R. Hutchinson. Polymerization of olefins through heterogeneous catalysis. viii. monomer sorption effects. *Journal of Applied Polymer Science*, pages 51–81, 1990.

[14] J. Kosek and Z. G. Dynamics of particle growth and overheating in gas-phase polymerization reactors. *Chemical Engineering Science*, pages 3951–3977, 2001.

[15] W. Yao, X. Hu, and Y. Yang. Modeling solubility of gases in semicrystalline polyethylene. *Journal of Applied Polymer Science*, pages 1737–1744, 2007.

[16] S. Floyd, K. Y. Choi, T. W. Taylor, and H. W. Ray. Polymerization of olefins through heterogeneous catalysis. iii. polymer particle modelling with an analysis of intraparticle heat and mass transfer effects. *Journal of Applied Polymer Science*, 32(1):2935–2960, July 1986.

[17] Y. S. Wong and P. K. Seville. Single-particle motion and heat transfer in fluidized beds. *AIChE Journal*, 52(12):4099–4109, December 2006.

[18] A. BRAGANCA. Process for the gas phase polymerization and copolymerization of olefin monomers. http://www.google.com.ar/patents/US6864332, Mar. 2005. Patent US 6864332 B2.

[19] H. Farag, M. Ossman, M. Mansour, and Y. Farid. Modeling of fluidized bed reactor for ethylene polymerization: effect of parameters on the single-pass ethylene conversion. *International Journal of Industrial Chemistry*, 4(1), December 2013.

[20] M. A. Bashir. Sanchez-lacombe eos data. Unpublished Data.

[21] Y. BANAT. Olefin gas phase polymerisation. https://www.google.com.ar/patents/US8669334, Mar. 2014. Patent US 8669334 B2.

[22] F. PON. Increased space-time yields in gas phase polymerization. https://patents.google.com/patent/US6541578B2, Apr. 2003. Patent US 6541578 B2.

[23] D. BRAGANCA. Process for the gas phase polymerization and copolymerization of olefin monomers. https://patents.google.com/patent/EP1246853B1/en, Nov. 2004. Patent EP 1246853 B1.

[24] D. Gmbh. Dortmund data bank. http://ddbonline.ddbst.com/AntoineCalculation/AntoineCalculationCGI.exe. Consulted in September 19 2015.

[25] N. I. of Standards and Technology. Isobutane. http://webbook.nist.gov/cgi/cbook.cgi&ID=C75285&Mask=4. Consulted in September 19 2015.

[26] R. C. Reid, J. M. Prausnitz, and B. E. Poling. *The Properties of Gases & Liquids*. McGraw-Hill, 4^{th} edition, 1987. ISBN: 0070517991.

Appendix A

Thermodynamic Properties

In this appendix some auxiliary data is described, pertaining to thermodynamic calculations necessary for the gas-phase polyethylene reactor model.

The ideal gas equation was used to predict the the mass of the components inside the reactor.

A.1 Gaseous Component Heat Capacity

In this section the calculation of heat capacity for the various components in the gas phase is described according to the reference [26].

The equation that describes the heat capacity of a gaseous component at a given temperature T is described by the following equation:

$$C_p(T) = A + B \cdot T + C \cdot T^2 + D \cdot T^3 \tag{A.1}$$

In the developed model, it is necessary to consider a mean heat capacity, calculated between the inlet flow temperature (T_0) and the bulk phase reactor temperature (T_b). This is achieved by integrating equation A.1 between T_0 and T_b:

$$\overline{C_p} = \int_{T_0}^{T_b} \left(A + B \cdot T + C \cdot T^2 + D \cdot T^3\right) dT \tag{A.2}$$

The result is described in the following equation A.3:

$$\overline{C_p} = \left[A(T_b - T_0) + \frac{B}{2}\left(T_b^2 - T_0^2\right) + \frac{C}{3}\left(T_b^3 - T_0^3\right) + \frac{D}{4}\left(T_b^4 - T_0^4\right)\right] / (T_b - T_0) \tag{A.3}$$

The following table summarizes the parameters (A, B, C and D) assumed for each of the gaseous components. The parameters were taken from [26] and the calculated C_p units are J/(mol.K).

Table A.1: Component Parameters for heat capacity calculations [26].

Component	Ethylene	n-hexane	isobutane	Nitrogen
A	3.806	-4.413	-1.39	31.15
B	1.57 x 10^{-1}	5.82 x 10^{-1}	3.85 x 10^{-1}	-1.36 x 10^{-2}
C	-8.35 x 10^{-5}	-3.12 x 10^{-4}	-1.85 x 10^{-4}	2.68 x 10^{-5}
D	1.76 x 10^{-8}	6.49 x 10^{-8}	2.90 x 10^{-8}	-1.17 x 10^{-8}

A.2 Solubility and Polymer Density Correlations

In order to be able to introduce the solubility data from Sanchez-Lacombe EOS into the models, correlations were made. These establish the relationship between the desired parameter (ethylene and alkane solubility in HDPE or HDPE density) with the introduced alkane partial pressure.

The following tables summarizes the solubility data at 80 ° C and 7 bar ethylene partial pressure, varying the alkane's partial pressure.

Table A.2: Sanchez-Lacombe EOS data for an ethylene/n-hexane/HDPE ternary system at 80° C and 7 bar ethylene partial pressure.

$\mathbf{P_{hex}}$ (bar)	Ethylene mass fraction	n-hexane mass fraction	Ethylene solubility	n-hexane solubility	HDPE phase density (kg/m^3)
0.1	0.96	0.04	0.0045	0.0036	823.97
0.5	0.82	0.18	0.0047	0.018	820.37
0.8	0.74	0.26	0.0048	0.0286	817.72
1	0.69	0.31	0.005	0.0366	815.72

Table A.3: Sanchez-Lacombe EOS data for an ethylene/isobutane/HDPE ternary system at 80° C and 7 bar ethylene partial pressure.

$\mathbf{P_{ibut}}$ (bar)	Ethylene mass fraction	isobutane mass fraction	Ethylene solubility	isobutane solubility	HDPE phase density (kg/m^3)
1	0.77	0.23	0.0046	0.0086	821.81
3	0.53	0.47	0.0049	0.0244	816.21
7	0.33	0.67	0.0056	0.0571	804.58
13	0.21	0.79	0.069	0.1186	782.74

It is important to mention that the dependence of solubility on temperature was neglected due to the fact that it can only be completely considered by integrating the Sanchez-Lacombe thermodynamic model into the reactor model. As such, the temperature of 80 ° C was used as reference in the simulations.

The resulting correlations using n-hexane are described in the following expressions:

$$Solubility_{Et} = 0.0017 \cdot P_{hex}^3 - 0.0027 \cdot P_{hex}^2 + 0.0016 \cdot P_{hex} + 0.0044 \tag{A.4}$$

where the n-hexane pressure is introduced in bar units and the correlation coefficient (R^2) was 1.

$$Solubility_{hex} = 0.0362 \cdot P_{hex} \tag{A.5}$$

with a value of R^2 of 0.9995.

$$\rho_{HDPE} = 824.92 - 9.1177 \cdot P_{hex} \tag{A.6}$$

with a R^2 of 0.9995.

For the case of isobutane the correlations are presented as follows.

$$Solubility_{Et} = 4 \times 10^{-6} \cdot P_{ibut}^2 + 0.0001 \cdot P_{ibut} + 0.0045 \tag{A.7}$$

where the isobutane pressure is introduced in bar units and the correlation coefficient (R^2) was 1.

$$Solubility_{ibut} = 0.0092 \cdot P_{ibut} - 0.0029 \tag{A.8}$$

with a value of R^2 of 0.996.

$$\rho_{HDPE} = 825.9 - 3.2611 \cdot P_{ibut} \tag{A.9}$$

with a R^2 of 0.996.

With the obtained solubility values it is possible to calculate the concentration values using the following expressions:

$$C_{Et}^P = Solubility_{Et} \frac{MW_{Et}}{\rho_{HDPE}} \tag{A.10}$$

$$C_{ICA}^P = Solubility_{ICA} \frac{MW_{ICA}}{\rho_{HDPE}} \tag{A.11}$$

The obtained values of C_{Et}^P and C_{ICA}^P are then applied to the model. It is important to mention that although the correlations are theoretically capable of predicting solubility values for intermediate partial pressures, the only values considered for the simulations were the ones resultant from the SL EOS data available. This is due to the fact that predictions for intermediate partial pressures are inaccurate and can result in unrealistic data.

A.3 Pure Component Vapor Pressure

In order to guarantee dry mode operation it is necessary to know how the vapor pressure of each of the components varies with temperature. By maintaining the component's partial pressure below the vapor pressure at the reactor temperature T_b it is possible to assume that no condensation occurs without significant error.

During the model assumptions it was said that ethylene and nitrogen condensation was neglected. Considering nitrogen this is understandable, whereas for the case of ethylene it requires some explanation. According to NIST [25], the vapor pressure for ethylene was calculated in temperatures ranging from 149 to 188 K assuming the maximum value of 2.8 bar approximately for the highest temperature. Since the temperatures considered in the model are closer to 400 K, the condensation of ethylene was neglected.

Antoine's Equation assumes the following form:

$$\log_{10}(P_v) = A - \frac{B}{C+T} \tag{A.12}$$

The following table summarizes the equation coefficients for n-hexane and isobutane. The data was collected from NIST [25] for the case of isobutane and Dortmund Database [24] for n-hexane.

Table A.4: Antoine equation coefficients for n-hexane and isobutane [25, 24].

Component	**n-hexane**	**isobutane**
A	7.01051	4.3281
B	1246.33	1132.108
C	232.988	0.918

The temperature input must be in $^\circ$C for n-hexane and K for isobutane. The resulting vapor pressure units are mm Hg and bar, respectively.

Appendix B

Simulation Data

In this appendix the data tables for the simulations will be presented. The data tables regarding the slurry phase PSD model will not be presented due to their excessive size.

Simulation I - Addition of n-hexane

Table B.1: Parameters assumed for gas-phase reactor model simulation I.

Parameter	Value	Units	Parameter	Value	Units
T_0	35	° C	F	11000	mol/s
P	22.4	bar	P_{Et}	7	bar
P_{hex}	0.1 - 1	bar	P_{N_2}	14.4 - 15.3	bar
$k_p^{T_{ref}}$	180	m^3/(mol.s)	$k_d^{T_{ref}}$	1 x 10^{-4}	s^{-1}
T_{ref}	80	° C	E_a, E_d	42000	J/mol
ΔH_{pol}	-107600	J/mol	ρ_c	2300	kg/m^3
Q_c	1.9 x 10^{-3}	kg/s	$C_{p,c}, C_{p,pol}$	2000	J/(kg.K)
C_0^*	0.52	mol/m^3	$\varepsilon_{fluidization}$	0.55	-
d_c	50	µm	d_p	500	µm
d	4.75	m	h_b	13.3	m

Table B.2: Results for gas-phase reactor model simulation I.

Parameter	Units				
P_{hex}	bar	**0.1**	**0.5**	**0.8**	**1**
T_s	° C	98.6	97.3	95.7	96.6
T_b	° C	92.3	90.7	89.0	89.7
$C_{p,Et}$	J/(mol.K)	48	48	48	48
$C_{p,hex}$	J/(mol.K)	159	158	158	158
C_{p,N_2}	J/(mol.K)	29	29	29	29
$Q_{Et,in}$	kg/s	96.4	96.4	96.4	96.4
$Q_{ICA,in}$	kg/s	4.2	21.2	33.9	42.3
$Q_{N_2,in}$	kg/s	210.5	205.0	200.9	198.1
$Q_{Et,d}$	kg/s	0.03	0.03	0.03	0.03
$Q_{ICA,d}$	kg/s	0.02	0.11	0.18	0.23
$Q_{Et,out}$	kg/s	90.5	90.3	90.2	90.0
$Q_{ICA,out}$	kg/s	4.2	21.1	33.8	42.2
$Q_{N_2,out}$	kg/s	210.5	205.0	200.9	198.1
k_p	m^3/(mol.s)	374.0	356.2	335.1	347.4
k_d	s^{-1}	2 x 10^{-4}	2 x 10^{-4}	2 x 10^{-4}	2 x 10^{-4}
C^*	mol/m^3	0.040	0.042	0.044	0.043
R_p	mol/(m^3.s)	1977	2048	2074	2162
Q_{PE}	kg/s	5.9	6.1	6.2	6.4
	ton/h	21.2	21.9	22.2	23.2
$Productivity$	$g_{PE}/g_{Catalyst}$	3095	3206	3247	3385
$1 - PassConversion$	%	6.1	6.3	6.4	6.7
u_g	m/s	0.824	0.820	0.816	0.818

Simulation II - Addition of isobutane

Table B.3: Parameters assumed for gas-phase reactor model simulation II.

Parameter	Value	Units	Parameter	Value	Units
T_0	35	° C	F	11000 - 8000	mol/s
P	22.4	bar	P_{Et}	7	bar
P_{ibut}	1 - 13	bar	P_{N_2}	2.4 - 14.4	bar
$k_p^{T_{ref}}$	180	m^3/(mol.s)	$k_d^{T_{ref}}$	1 x 10^{-4}	s^{-1}
T_{ref}	80	° C	E_a, E_d	42000	J/mol
ΔH_{pol}	-107600	J/mol	ρ_c	2300	kg/m^3
Q_c	1.9 x 10^{-3}	kg/s	$C_{p,c}, C_{p,pol}$	2000	J/(kg.K)
C_0^*	0.52	mol/m^3	$\varepsilon_{fluidization}$	0.55	-
d_c	50	µm	d_p	500	µm
d	4.75	m	h_b	13.3	m

Table B.4: Results for gas-phase reactor model simulation II with F = 11000 mol/s.

Parameter	Units	F = 11000 mol/s			
P_{ibut}	bar	**1**	**3**	**7**	**13**
T_s	° C	94.8	88.4	81.4	77.7
T_b	° C	88.4	81.9	74.2	69.3
$C_{p,Et}$	J/(mol.K)	48	47	47	47
$C_{p,ibut}$	J/(mol.K)	108	107	106	105
C_{p,N_2}	J/(mol.K)	29	29	29	29
$Q_{Et,in}$	kg/s	96.4	96.4	96.4	96.4
$Q_{ICA,in}$	kg/s	28.5	85.6	199.8	371.0
$Q_{N_2,in}$	kg/s	198.1	170.6	115.6	33.0
$Q_{Et,d}$	kg/s	0.03	0.03	0.04	0.05
$Q_{ICA,d}$	kg/s	0.04	0.15	0.41	0.91
$Q_{Et,out}$	kg/s	90.5	90.3	89.8	88.6
$Q_{ICA,out}$	kg/s	28.5	85.5	199.4	370.0
$Q_{N_2,out}$	kg/s	198.1	170.6	115.6	33.0
k_p	m^3/(mol.s)	324.5	253.2	190.4	163.7
k_d	s^{-1}	2 x 10^{-4}	1 x 10^{-4}	1 x 10^{-4}	1 x 10^{-4}
C^*	mol/m^3	0.046	0.057	0.073	0.083
R_p	mol/(m^3.s)	1994	2056	2232	2623
Q_{PE}	kg/s	5.9	6.1	6.6	7.8
	ton/h	21.4	22.0	23.9	28.1
$Productivity$	$g_{PE}/g_{Catalyst}$	3122	3220	3495	4107
$1 - PassConversion$	%	6.2	6.3	6.9	8.1
u_g	m/s	0.815	0.800	0.783	0.772

Table B.5: Results for gas-phase reactor model simulation II with F = 8000 mol/s.

Parameter	Units	F = 8000 mol/s			
P_{ibut}	bar	**1**	**3**	**7**	**13**
T_s	° C	117.9	109.4	99.7	94.2
T_b	° C	111.2	102.4	92.0	85.1
$C_{p,Et}$	J/(mol.K)	49	48	48	47
$C_{p,ibut}$	J/(mol.K)	111	110	108	107
C_{p,N_2}	J/(mol.K)	29	29	29	29
$Q_{Et,in}$	kg/s	70.1	70.1	70.1	70.1
$Q_{ICA,in}$	kg/s	20.8	62.3	145.3	269.8
$Q_{N_2,in}$	kg/s	144.1	124.1	84.0	24.0
$Q_{Et,d}$	kg/s	0.03	0.03	0.04	0.06
$Q_{ICA,d}$	kg/s	0.04	0.16	0.44	0.98
$Q_{Et,out}$	kg/s	63.9	63.6	62.9	61.6
$Q_{ICA,out}$	kg/s	20.8	62.1	144.9	268.8
$Q_{N_2,out}$	kg/s	144.1	124.1	84.0	24.0
k_p	m^3/(mol.s)	743.2	553.0	390.0	317.2
k_d	s^{-1}	4 x 10^{-4}	3 x 10^{-3}	2 x 10^{-3}	2 x 10^{-3}
C^*	mol/m^3	0.021	0.028	0.038	0.047
R_p	mol/(m^3.s)	2097	2186	2405	2843
Q_{PE}	kg/s	6.2	6.5	7.2	8.5
	ton/h	22.5	23.4	25.8	30.5
$Productivity$	$g_{PE}/g_{Catalyst}$	3285	3424	3766	4452
$1 - PassConversion$	%	8.9	9.3	10.2	12.1
u_g	m/s	0.630	0.616	0.599	0.587

Table B.6: Results for gas-phase reactor model simulation II with P_{ibut} = 7 bar.

Parameter	**Units**	$\mathbf{P_{ibut}}$ **= 7 bar**			
F	mol/s	**11000**	**10000**	**9000**	**8000**
T_s	° C	81.4	86.4	92.4	99.7
T_b	° C	74.2	79.1	84.9	92.0
$C_{p,Et}$	J/(mol.K)	47	47	47	48
$C_{p,ibut}$	J/(mol.K)	106	107	107	108
C_{p,N_2}	J/(mol.K)	29	29	29	29
$Q_{Et,in}$	kg/s	96.4	87.7	78.9	70.1
$Q_{ICA,in}$	kg/s	199.8	181.6	163.5	145.3
$Q_{N_2,in}$	kg/s	115.6	105.1	94.5	84.0
$Q_{Et,d}$	kg/s	0.04	0.04	0.04	0.04
$Q_{ICA,d}$	kg/s	0.41	0.42	0.43	0.44
$Q_{Et,out}$	kg/s	89.8	80.8	71.9	62.9
$Q_{ICA,out}$	kg/s	199.4	181.2	163.1	144.9
$Q_{N_2,out}$	kg/s	115.6	105.1	94.5	84.0
k_p	m^3/(mol.s)	190.4	233.5	295.7	390.0
k_d	s^{-1}	1 x 10^{-4}	1 x 10^{-4}	2 x 10^{-4}	2 x 10^{-3}
C^*	mol/m^3	0.073	0.061	0.050	0.038
R_p	mol/(m^3.s)	2232	2291	2350	2405
Q_{PE}	kg/s	6.6	6.8	7.0	7.2
	ton/h	23.9	24.5	25.2	25.8
$Productivity$	$g_{PE}/g_{Catalyst}$	3495	3588	3679	3766
$1 - PassConversion$	%	6.9	7.8	8.9	10.2
u_g	m/s	0.783	0.722	0.660	0.599

Sensitivity Analysis

Table B.7: Results for the sensitivity analysis varying F.

		Variation			
Parameter	**Units**	**+10%**	**+20%**	**-10%**	**-20%**
ΔQ_{PE}	ton/h	-0.5	-0.9	0.4	0.8
	%	-2.1	-4.2	1.9	3.7
ΔT_b	° C	-5.9	-10.9	7.1	15.8
	%	-6.5	-12.1	7.8	17.4
ΔT_s	° C	-6.1	-11.2	7.2	16.1
	%	-6.2	-11.5	7.4	16.5
$\Delta Productivity$	$g_{PE}/g_{Catalyst}$	-65.9	-134.7	61.6	117.5
	%	-2.1	-4.2	1.9	3.7
$\Delta Conversion$	-	-0.7	-1.3	0.8	1.9
	%	-11.0	-20.2	13.2	29.6
Δu_g	m/s	0.07	0.13	-0.07	-0.14
	%	8.2	16.4	-8.2	-16.5

Table B.8: Results for the sensitivity analysis varying $C_{p,ICA}$.

		Variation			
Parameter	**Units**	**+10%**	**+50%**	**-10%**	**-50%**
ΔQ_{PE}	ton/h	0.0	-0.2	0.0	0.2
	%	-0.2	-0.9	0.2	0.9
ΔT_b	° C	-0.6	-2.9	0.6	3.1
	%	-0.7	-3.2	0.7	3.5
ΔT_s	° C	-0.6	-2.9	0.6	3.2
	%	-0.6	-3.0	0.6	3.3
$\Delta Productivity$	$g_{PE}/g_{Catalyst}$	-6.0	-30.2	5.9	29.3
	%	-0.2	-0.9	0.2	0.9
$\Delta Conversion$	-	0.0	-0.1	0.0	0.1
	%	-0.2	-0.9	0.2	0.9
Δu_g	m/s	0.00	-0.01	0.00	0.01
	%	-0.2	-0.8	0.2	0.9

Table B.9: Results for the sensitivity analysis varying $k_p^{T_{ref}}$.

		Variation			
Parameter	**Units**	**+10%**	**+50%**	**-10%**	**-50%**
ΔQ_{PE}	ton/h	2.7	12.9	-2.7	-13.6
	%	12.1	58.9	-12.3	-62.1
ΔT_b	° C	6.5	31.1	-6.7	-34.1
	%	7.2	34.3	-7.3	-37.6
ΔT_s	° C	7.3	35.0	-7.5	-38.2
	%	7.5	35.9	-7.7	-39.2
$\Delta Productivity$	$g_{PE}/g_{Catalyst}$	388.8	1889.9	-395.8	-1990.3
	%	12.1	58.9	-12.3	-62.1
$\Delta Conversion$	-	0.8	3.7	-0.8	-3.9
	%	12.1	58.9	-12.3	-62.1
Δu_g	m/s	0.01	0.07	-0.02	-0.08
	%	1.8	8.5	-1.8	-9.4

Table B.10: Results for the sensitivity analysis varying Q_c.

		Variation			
Parameter	**Units**	**+10%**	**+50%**	**-10%**	**-50%**
ΔQ_{PE}	ton/h	2.5	12.4	-2.5	-11.7
	%	11.3	56.7	-11.2	-53.5
ΔT_b	°C	6.0	29.9	-6.0	-29.3
	%	6.7	33.0	-6.7	-32.3
ΔT_s	°C	6.8	33.7	-6.8	-32.8
	%	7.0	34.6	-7.0	-33.7
$\Delta Productivity$	$g_{PE}/g_{Catalyst}$	37.6	142.8	-42.4	-224.7
	%	1.2	4.5	-1.3	-7.0
$\Delta Conversion$	-	0.7	3.6	-0.7	-3.4
	%	11.3	56.7	-11.2	-53.5
Δu_g	m/s	0.01	0.07	-0.01	-0.07
	%	1.7	8.2	-1.7	-8.1

Table B.11: Results for the sensitivity analysis varying P_{ICA}.

		Variation	
Parameter	**Units**	**+100%**	**-80%**
ΔQ_{PE}	ton/h	1.2	-0.8
	%	5.6	-3.5
ΔT_b	°C	-1.0	1.5
	%	-1.1	1.7
ΔT_s	°C	-0.7	1.3
	%	-0.7	1.3
$\Delta Productivity$	$g_{PE}/g_{Catalyst}$	178.8	-111.0
	%	5.6	-3.5
$\Delta Conversion$	-	0.4	-0.2
	%	5.6	-3.5
Δu_g	m/s	-0.002	0.003
	%	-0.3	0.4

Table B.12: Results for the sensitivity analysis varying C_{Et}^P.

		Variation			
Parameter	**Units**	**+10%**	**+50%**	**-10%**	**-50%**
ΔQ_{PE}	ton/h	2.7	12.9	-2.7	-13.6
	%	12.1	58.9	-12.3	-62.1
ΔT_b	°C	6.5	31.1	-6.7	-34.1
	%	7.2	34.3	-7.3	-37.6
ΔT_s	°C	7.3	35.0	-7.5	-38.2
	%	7.5	35.9	-7.7	-39.2
$\Delta Productivity$	$g_{PE}/g_{Catalyst}$	388.8	1890.1	-395.8	-1990.4
	%	12.1	58.9	-12.3	-62.1
$\Delta Conversion$	-	0.8	3.7	-0.8	-3.9
	%	12.1	58.9	-12.3	-62.1
Δu_g	m/s	0.01	0.07	-0.02	-0.08
	%	1.8	8.5	-1.8	-9.4

Table B.13: Results for the sensitivity analysis varying T_0.

		Variation			
Parameter	**Units**	**+5° C**	**+10° C**	**-5° C**	**-10° C**
ΔQ_{PE}	ton/h	0.3	0.6	-0.4	-1.0
	%	1.5	2.8	-2.0	-4.7
ΔT_b	° C	5.5	10.9	-5.8	-12.0
	%	6.1	12.0	-6.4	-13.2
ΔT_s	° C	5.6	11.1	-5.9	-12.3
	%	5.8	11.4	-6.1	-12.6
$\Delta Productivity$	$g_{PE}/g_{Catalyst}$	49.4	88.2	-64.3	-150.5
	%	1.5	2.8	-2.0	-4.7
$\Delta Conversion$	-	0.1	0.2	-0.2	-0.3
	%	1.5	2.8	-2.0	-4.7
Δu_g	m/s	0.01	0.02	-0.01	-0.03
	%	1.5	3.0	-1.6	-3.3

Appendix C

Model Code in MATLAB

In this appendix the code for each model in MATLAB will be presented.

Slurry Phase Particle Size Distribution Model

The following text is an example segment of code for the model that performs the necessary calculations for the PSD model.

```
for j=1:length(rho_ic4)
    for a=1
            for i=1:length(tau);
                alfa(j,i)=kp(i)*M_ic4(j)*cstar*m/rho_ic4(j);
                for t=1:30000
                    if i==1
                        Dp_ic4(t,j,i,a)=Dp0(a)*(1+alfa(j,i)*t)^(1/3);
                        F_ic4(t,j,i,a)=3*(1+alfa(j,i)*t)^(2/3)/(alfa(j,i)*Dp0(a))
                        *exp(-t/tau(i))/tau(i);
                    else
                        Dp_ic4(t,j,i,a)=Dp0(a)*((Dp_ic4(t,j,i-1)/Dp0(a))+alfa(j,i)*t)^(1/3);
                        F_ic4(t,j,i,a)=3*((Dp_ic4(t,j,i-1)/Dp0(a))^3+alfa(j,i)*t)^(2/3)
                        /(alfa(j,i)*Dp0(a))*exp(-t/tau(i))/tau(i);
                    end
                end
                figure(1), hold on
                    subplot(length(tau),1,i),plot(Dp_ic4(:,j,i,a),F_ic4(:,j,i,a),color(j)), hold on
            end
    end
    leg_ic4{j}=sprintf('P = %0.0f bar',Pressure(j));
end
```

Gas-Phase Reactor Model

The code for the gas-phase reactor model is split into two files. The first file runs the solver and the second file contains the definition of the necessary equations and variables.

The following code contains the solver section:

```
clc
clear all
close all

%% %%%%%%%%%%%%%%%%%%%%%%%%%%%%%%%%%%%%%%%%%%%%%%%%%%%%%%%%%%%%%%%%%%%%%%%%%%%%%%%
%%%%%%%%%%%%%%%%%%%%%%%%% SYSTEM DESCRIPTION %%%%%%%%%%%%%%%%%%%%%%%%%%%%%%%%%%%%
%
% Q - Mass Flowrate
% MW - Molecular Weight
% rho - Specific Weight (kg.m-3)
% kp - Kinetic Propagation Constant
% Ea - Activation Energy
% kd - Kinetic Deactivation Constant
% Ed - Deactivation Energy
% C0star - Initial  active sites concentration
% Cstar - Active sites concentrations
% ReactHeat - Heat of Reaction
%
%%%%%%%%%%%%%%%%%%%%%%%%%%%%%%%%%%%%%%%%%%%%%%%%%%%%%%%%%%%%%%%%%%%%%%%%%%%%%%%
%
global R P Ts T0 Tref Tb F A_Et B_Et C_Et D_Et Cpg_Et A_ICA B_ICA C_ICA D_ICA A_N2 B_N2 C_N2 D_N2
Cpg_ICA Cpg_N2 Cp_c P_Et P_ICA P_N2 Q_Et_in Q_Et_d Q_Et_out m_Et m_ICA Q_ICA_in Q_ICA_d Q_ICA_out
Q_N2_in Q_PE Qc rho_b Vc Apc Vb h kp_Tref kd_Tref kp kd Rp C0star Cstar C_Et_P C_ICA_P ReactHeat
Ea Ed MW_Et MW_ICA MW_N2 MW_PE rho_PE Cp_PE
%
%% AUXILIARY CALCULATIONS  %%%%%%%%%%%%%%%%%%%%%%%%%%%%%%%%%%%%%%%%%%%%%%%%%%%%
%% Variable Initialization %
%
R = 8.3145;             % Perfect Gas Constant in (J/mol.K)
T0 = 35+273.15;         % Inlet Flow Temperature (K)
%
MW_Et = 28.054/1000;    % Ethylene Molecular Weight (kg.mol-1)
MW_ICA = 86.178/1000;   % ICA Molecular Weight (kg.mol-1)
MW_PE = 2;              % PE Molecular Weight (kg.mol-1)
MW_N2 = 28.014/1000;    % N2 Molecular Weight (kg.mol-1)
%
%%% Gaseous Component Heat Capacity %%%
%% Empyrical Parameters %%
% Ethylene %
A_Et = 3.806;
B_Et = 1.566e-01;
C_Et = -8.348e-05;
```

```
D_Et = 1.755e-08;
%
% n-ICAane %
A_ICA = -4.413;
B_ICA = 5.82e-01;
C_ICA = -3.119e-04;
D_ICA = 6.494e-08;
%
% Nitrogen
A_N2 = 3.115e1;
B_N2 = -1.357e-2;
C_N2 = 2.680e-5;
D_N2 = -1.168e-8;

%% %%%%%%%%%%%%%%%%%%%%OPERATING CONDITIONS %%%%%%%%%%%%%%%%%%%%%%%%%%%%%%%%
% Reactor Parameters %
%
P_Et = 7;                                          % Ethylene Partial Pressure in Reactor (Bar)
P_ICA = 0.5;                                       % ICA Partial Pressure in Reactor (Bar)
P = 22.4;                                          % Total Pressure (bar)
P_N2=P-P_Et-P_ICA;                                 % N2 Partial Pressure in Reactor (Bar)
F = 10000;                                         % Total Inlet Flowrate (mol/s)
rho_PE = 824.919541304348-9.11765217391297*P_ICA;  % PE density (kg/m3)
kp_Tref = 180;                                     % kinetic propagation constant (m3.mol-1.s-1)
kd_Tref = 1e-04;                                   % kinetic deactivation constant (s-1)
Tref = 353.15;                                     % Reference temperature(K)
%
% Catalyst Parameters %
%
Cp_c = 2000;                          % Catalyst Heat Capacity (J.kg-1.K-1)
Cp_PE = 2000;                         % Polymer Particle Heat Capacity (J.kg-1.K-1)
rho_c = 2300;                         % Catalyst Specifig Weight (kg.m-3)
C0star = 0.52;                        % Catalyst Initial Active Sites Concentration (mol.m-3)
dc = 50e-06;                          % Catalyst Particle Diameter (m)
d = 4.75;                             % Reactor Diameter (m)
b = pi*0.25*d^2;                      % Reactor cross-section area (m2)
hb = 13.3;                            % Reactor height (m)
Vb = hb*b;                            % Bed Volume (m3)
fluid_porosity = 0.55;                % Fluidized bed porosity (-)
rho_b= rho_c*(1-fluid_porosity);      % Fluidizes bed density (kg/m3)
Vp = Vb*(1-fluid_porosity);           % Particle Volume in catalyst bed (m3)
dp = 500e-06;                         % Mean polymer particle diameter (m)
np = 6/pi*Vp*dp^(-3);                 % Number of particles in catalyst bed
Vc = np*pi/6*dc^3;                    % Catalyst Volume (m3)
Qc = 0.0019;                          % Catalyst Mass Flow (kg.s-1)
Apc = np*pi*(dc)^2;                   % Catalyst Heat Transfer Area (m2)
h = 280;                              % Convective Heat Transfer Coefficient (W/m2.K)
%
% Reaction Parameters %
```

```
%
Ea = 42000;                 % Activation Energy (J/mol)
Ed = 42000;                 % Catalyst Deactivation Energy (J/mol)
ReactHeat = -107600;        % Heat of Reaction (J/mol)
C_Et_P = (0.00174603174603175*(P_ICA^3)-0.0026825396825397*(P_ICA^2)
+0.00156825396825398*(P_ICA)+0.00436825396825397)*rho_PE/MW_Et;
C_ICA_P = (0.0362315789473684*(P_ICA))*rho_PE/MW_ICA;              %
%
%
% guess=[Q_Et_out  Q_Et_d  Q_ICA_out  Q_ICA_d  kp    Rp         Q_PE     kd    Cstar  Cpg_Et  Cpg_ICA
Cpg_N2   Tb   Ts    m_et   m_ICA    m_N2  Q_Et_in  Q_ICA_in  Q_N2_in];
  guess=[   82      0.03     19.1       0.11   323  2030.88    6.0426  0.0002  0.046   2362
1831     1041   361  368   1574.5  345.47  3346.6    88       19       186.3];
%
[result, fval, exit, output]=fsolve(@variables,guess);
result
fval
output
```

The following section contains the code of the variables file.

```
%%%%%%%%%%%%%%%%%%%%%%%%%% SYSTEM DESCRIPTION %%%%%%%%%%%%%%%%%%%%%%%%%%%%
%
% Q - Mass Flowrate
% MW - Molecular Weight
% rho - Specific Weight (kg.m-3)
% kp - Kinetic Propagation Constant
% Ea - Activation Energy
% kd - Kinetic Deactivation Constant
% Ed - Deactivation Energy
% C0star - Initial  active sites concentration
% Cstar - Active sites concentration
% ReactHeat - Heat of Reaction
%
%%%%%%%%%%%%%%%%%%%%%%%%%%%%%%%%%%%%%%%%%%%%%%%%%%%%%%%%%%%%%%%%%%%%%%%%
%% REACTION SYSTEM %%
%
function eqs = variables(v)
%
global R Ts T0 Tref Tb F P_Et P_ICA P_N2 A_Et B_Et C_Et D_Et Cpg_Et Cpg_N2 A_ICA B_ICA C_ICA D_ICA
 A_N2 B_N2 C_N2 D_N2 Cpg_ICA Cp_c Q_Et_in Q_Et_d Q_Et_out Q_N2_in m_Et m_ICA m_N2 Q_ICA_in Q_ICA_d
 Q_ICA_out Q_PE Qc Apc Vb h rho_b Vc kp_Tref kd_Tref kp kd Rp C0star Cstar C_Et_P C_ICA_P ReactHeat
  Ea Ed MW_Et MW_ICA MW_PE MW_N2 rho_PE Cp_PE
%
%% OUTPUT VARIABLES %%%%%%%%%%%%%%%%%%%%%%%%
%
Q_Et_out = v(1);        % Ethylene Exit Flowrate (kg/s)
Q_Et_d = v(2);          % Dissolved Ethylene Flowrate (kg/s)
Q_ICA_out = v(3);       % ICA Exit Flowrate (kg/s)
```

```
Q_ICA_d = v(4);          % Dissolved ICA Flowrate (kg/s)
kp = v(5);               % Kinetic Propagation Constant (m3.mol-1s-1)
Rp = v(6);               % Reaction Rate (mol.m-3cat.s-1)
Q_PE = v(7);             % Polyethylene Production Flowrate (kg/s)
kd = v(8);               % Catalyst Kinetic Deactivation Constant (s-1)
Cstar = v(9);            % Catalyst Active Site Concentration (mol/m3)
Cpg_Et = v(10);          % Gaseous Ethylene Heat Capacity (J.kg-1.K-1)
Cpg_ICA = v(11);         % Gaseous ICAane Heat Capacity (J.kg-1.K-1)
Cpg_N2 = v(12);          % Gaseous N2 Heat Capacity (J.kg-1.K-1)
Tb = v(13);              % Bulk Temperature (K)
Ts = v(14);              % Reaction and Outlet Temperature (K)
m_Et = v(15)             % Mass of Ethylene inside the reactor (kg)
m_ICA = v(16)            % Mass of ICA inside the reactor (kg)
m_N2 = v(17)             % Mass of N2 inside the reactor (kg)
Q_Et_in = v(18)          % Ethylene Inletflowrate (kg/s)
Q_ICA_in = v(19)         % ICA Inletflowrate (kg/s)
Q_N2_in = v(20)          % N2 Inletflowrate (kg/s)

%
% MASS BALANCES %%%%%%%%%%%%%%%%%%%%%%%%%
%Ethylene Mass Balance (kg/s) %
eqs(1) = (Q_Et_in - Q_Et_d - Rp*Vc*MW_Et) - Q_Et_out;
%Dissolved Ethylene Mass Balance (kg/s) %
eqs(2) = MW_Et*C_Et_P*Q_PE/rho_PE - Q_Et_d;
%ICA Mass Balance%
eqs(3) = Q_ICA_in - Q_ICA_d - Q_ICA_out;
%Dissolved ICA Mass Balance (kg/s) %
eqs(4) = MW_ICA*C_ICA_P*Q_PE/rho_PE - Q_ICA_d;
%Arrhenius Law for kinetic constant (m3/mol.s) %
eqs(5) = kp_Tref*exp(Ea/R*(1/Tref-1/Ts))- kp;
%Kinetic Rate Law (mol/m3cat.s) %
eqs(6) = kp*Cstar*C_Et_P- Rp;
%Polyethylene Production Mass Balance (kg/s)%
eqs(7) = Rp*Vc*MW_PE/(MW_PE/MW_Et)- Q_PE;
%Arrhenius Law for deactivation constant (s-1) %
eqs(8) = kd_Tref*exp(Ed/R*(1/Tref-1/Ts))- kd;
%Active sites concentration Balance (mol/m3cat) %
eqs(9) = C0star/(1+kd*Vc/(Qc/rho_b))- Cstar;
%% Gaseous Component Heat Capacity (J/kg.K) %
%Ethylene
eqs(10) = ((A_Et*(Tb-T0)+B_Et/2*(Tb^2-T0^2)+C_Et/3*(Tb^3-T0^3)+D_Et/4*(Tb^4-T0^4)
)/(Tb-T0))/MW_Et- Cpg_Et;
%hexane/ ICA
eqs(11) = ((A_ICA*(Tb-T0)+B_ICA/2*(Tb^2-T0^2)+C_ICA/3*(Tb^3-T0^3)+D_ICA/4*(Tb^4-T0^4))
/(Tb-T0))/MW_ICA- Cpg_ICA;
%Nitrogen
eqs(12) = ((A_N2*(Tb-T0)+B_N2/2*(Tb^2-T0^2)+C_N2/3*(Tb^3-T0^3)+D_N2/4*(Tb^4-T0^4))
/(Tb-T0))/MW_N2- Cpg_N2;
%
```

```
%% HEAT BALANCE (T in K) %
eqs(13) = (ReactHeat*(Q_PE/MW_Et))/(Apc*h)+Ts- Tb;
eqs(14) = (T0*(Q_N2_in*Cpg_N2+Q_Et_out*Cpg_Et+Q_ICA_out*Cpg_ICA+Q_PE*Cp_PE+Qc*Cp_c)
/(Q_PE*Cp_PE+Qc*Cp_c))-(Tb*(Q_N2_in*Cpg_N2+Q_Et_out*Cpg_Et+Q_ICA_out*Cpg_ICA)
/(Q_PE*Cp_PE+Qc*Cp_c))-(ReactHeat*(Q_PE/MW_Et)/(Q_PE*Cp_PE+Qc*Cp_c))- Ts;
%
%% Mass of N2, Et and ICA inside the reactor (kg)
eqs(15) = ((P_Et*100000*Vb)/(R*Tb))- m_Et;
eqs(16) = ((P_ICA*100000*Vb)/(R*Tb))- m_ICA;
eqs(17) = ((P_N2*100000*Vb)/(R*Tb))- m_N2;
%Inlet Mass Flowrates (kg/s)
eqs(18) = F*m_Et/(m_Et+m_ICA+m_N2)*MW_Et- Q_Et_in;
eqs(19) = F*m_ICA/(m_Et+m_ICA+m_N2)*MW_ICA- Q_ICA_in;
eqs(20) = F*m_N2/(m_Et+m_ICA+m_N2)*MW_N2- Q_N2_in;
%
end
```

Variable Grouping

The following section contains tables that describe the variable groupings for the gas-phase reactor model. This allows for a better understanding of what each equation calculates, as well as its input variables.

Table C.1: Gaseous component heat capacity calculation variable grouping.

Variable	Description	Variable Type
A, B, C, D	Empyrical Parameters	Input
T_b	Bulk phase Temperature	Input
T_{in}	Reactor inlet Temperature	Input
$C_{p,component}$	Gaseous component heat capacity	Output

Table C.2: Component mass calculation variable grouping.

Variable	Description	Variable Type
$P_{component}$	Component partial pressure	Input
T_b	Bulk phase Temperature	Input
V_b	Reactor bed volume	Input
R	Perfect Gas Constant	Input
$m_{component}$	Component mass	Output

Table C.3: Component mass inlet flowrate calculation variable grouping.

Variable	Description	Variable Type
F	Total molar inlet flowrate	Input
$m_{component}$	Component mass	Input
$MW_{component}$	Component Molar Mass	Input
$Q_{component\_in}$	Component mass inlet flowrate	Output

Table C.4: Kinetic propagation constant calculation variable grouping.

Variable	Description	Variable Type
$k_p^{T_{ref}}$	kinetic propagation constant at reference temperature	Input
T_{ref}	Reference Temperature	Input
T_s	Solids Temperature	Input
E_a	Activation Energy	Input
R	Perfect Gas Constant	Input
k_p	Temperature corrected kinetic constant	Output

Table C.5: Kinetic deactivation constant calculation variable grouping.

Variable	Description	Variable Type
$k_d^{T_{ref}}$	kinetic propagation constant at reference temperature	Input
T_{ref}	Reference Temperature	Input
T_s	Solids Temperature	Input
E_d	Deactivation Energy	Input
R	Perfect Gas Constant	Input
k_d	Temperature corrected kinetic constant	Output

Table C.6: Dissolved ethylene/ICA flowrate calculation variable grouping.

Variable	Description	Variable Type
$MW_{Et/ICA}$	Component Molar Mass	Input
$C^P_{Et/ICA}$	Component concentration in the polymer phase	Input
Q_{PE}	Polyethylene Mass flowrate	Input
ρ_{PE}	Polymer phase density	Input
$Q_{Et/ICA,d}$	Dissolved component mass flowrate	Output

Table C.7: Catalyst deactivation calculation variable grouping.

Variable	Description	Variable Type
C_0^*	Initial Active sites concentration	Input
k_d	Temperature corrected deactivation constant	Input
V_c	Catalyst Volume	Input
Q_c	Catalyst mass flowrate	Input
ρ_b	Fluidized bed density	Input
C^*	Temperature corrected active sites concentration	Output

Table C.8: Kinetic rate calculation variable grouping.

Variable	Description	Variable Type
k_p	Temperature corrected propagation constant	Input
C^*	Temperature corrected active sites concentration	Input
C^P_{Et}	Ethylene concentration in the polymer phase	Input
R_p	Rate of polymerization	Output

Table C.9: Ethylene Mass Balance calculation variable grouping.

Variable	Description	Variable Type
$Q_{Et,in}$	Inlet Ethylene Mass Flowrate	Input
$Q_{Et,d}$	Dissolved Ethylene Mass Flowrate	Input
R_p	Rate of polymerization	Input
V_c	Catalyst volume	Input
MW_{Et}	Ethylene Molar Mass	Input
$Q_{Et,out}$	Outlet Ethylene Mass Flowrate	Output

Table C.10: ICA Mass Balance calculation variable grouping.

Variable	Description	Variable Type
$Q_{ICA,in}$	Inlet ICA Mass Flowrate	Input
$Q_{ICA,d}$	Dissolved ICA Mass Flowrate	Input
$Q_{ICA,out}$	Outlet ICA Mass Flowrate	Output

Table C.11: Polyethylene Mass Balance calculation variable grouping.

Variable	Description	Variable Type
R_p	Rate of polymerization	Input
V_c	Catalyst volume	Input
MW_{Et}	Ethylene Molar Mass	Input
Q_{PE}	Polyethylene Mass Flowrate	Output

Table C.12: Catalyst Heat Balance calculation variable grouping.

Variable	Description	Variable Type
A_p	Particle heat transfer area	Input
h	Convective heat transfer coefficient	Input
ΔH_{polym}	Polymerization heat	Input
T_s	Solids Temperature	Input
T_b	Bulk phase Temperature	Output

Table C.13: Reactor Heat Balance calculation variable grouping.

Variable	Description	Variable Type
T_b	Bulk phase Temperature	Input
T_{in}	Reactor inlet Temperature	Input
$C_{p,component}$	Gaseous component heat capacity	Input
$C_{p,PE}$	Polyethylene heat capacity	Input
$C_{p,c}$	Catalyst heat capacity	Input
$Q_{component,out}$	Outlet Component Mass flowrate	Input
Q_{PE}	Polyethylene Mass Flowrate	Input
Q_c	Catalyst Mass Flowrate	Input
ΔH_{polym}	Polymerization Heat	Input
MW_{Et}	Ethylene Molar Mass	Input
T_s	Solids Temperature	Output